Biomechanical design of an electrospun scaffold for in situ cardiovascular tissue engineering

Document Version:

Publisher's PDF, also known as Version of Record (includes final page, issue and volume numbers)

Please check the document version of this publication:

• A submitted manuscript is the version of the article upon submission and before peer-review. There can be important differences between the submitted version and the official published version of record. People interested in the research are advised to contact the author for the final version of the publication, or visit the DOI to the publisher's website.
• The final author version and the galley proof are versions of the publication after peer review.
• The final published version features the final layout of the paper including the volume, issue and page numbers.

Link to publication

Biomechanical design of an electrospun scaffold for *in situ* cardiovascular tissue engineering

Financial support by the Dutch Heart Foundation for the pubblication of this thesis is gratefully acknowledged

funded by the
dutch heart foundation

Hartstichting

A catalogue record is available from the Eindhoven University of Technology Library

ISBN: 978-90-386-3617-7

Cover design: Michele Fabiano

Original picture Tsanislav Hristov © All rights reserved

Biomechanical design of an electrospun scaffold for *in situ* cardiovascular tissue engineering

PROEFSCHRIFT

ter verkrijging van de graad van doctor aan de
Technische Universiteit Eindhoven, op gezag van de
rector magnificus prof.dr.ir. C.J. van Duijn, voor een
commissie aangewezen door het College voor
Promoties, in het openbaar te verdedigen
op dinsdag 20 mei 2014 om 16:00 uur

door

Giulia Argento

geboren te Potenza, Italië

Dit proefschrift is goedgekeurd door de promotiecommissie:

voorzitter:	prof.dr. F.N. van de Vosse
1e promotor:	prof.dr. F.P.T. Baaijens
2e promotor:	prof.dr. C.V.C. Bouten
co-promotor:	dr.ir. C.W.J. Oomens
leden:	prof.dr. L. Geris (Université de Liège)
	prof.dr. K. Ito
	prof.dr. N. Verdonschot (St. Radboud University Hospital)

Dedicated to Michele and my family

Contents

Summary

Biomechanical design of an electrospun scaffold for *in situ* cardiovascular tissue engineering

End-stage valvular diseases commonly require valve replacement. Currently available heart valve replacements are either mechanical or bioprosthetic valves. Despite their excellent durability mechanical valves induce non-physiological flow profiles and may cause thromboembolic complications, necessitating lifelong anticoagulation treatment. Bioprosthetic valves, instead, are prone to calcification. None of these valves can fully restore the native valve function because they are unable to grow and repair, and in particular in young patients may require multiple surgical interventions during a lifetime. A living heart valve replacement might overcome these limitations and may be created at the site of destination via *in situ* tissue engineering. This approach employs a synthetic biodegradable scaffold that recruits endogenous cells from the bloodstream, which synthesize new tissue while the scaffold gradually degrades creating a living, functional heart valve replacement.

Electrospinning is a popular technique for the production of scaffolds for cardiovascular tissue replacements. The aim of this thesis was to investigate the relation between the micro-scale scaffold architecture (e.g. material properties, fiber orientation, fiber diameter, fiber density and fiber interconnections) and the macroscopic mechanical properties of the scaffold. In addition, the effect of collagen deposition on the evolving mechanical properties of the construct was examined. Next, the cell traction mediated remodeling of the collagen architecture was investigated using a discrete microstructural model.

We developed a computational micro-scale model of a representative volume element of the scaffold, incorporating the microstructural features of the electrospun material, to predict its macroscopic mechanical behavior. We validated the model against experiments showing that it is able to describe the mechanical behavior of electrospun scaffolds with different microstructural features. In addition, we investigated the mechanical behavior of valve-shaped scaffolds with different microstructures when subjected to transvalvular pulmonary pressure.

The results indicated that a high degree of scaffold anisotropy was required to reproduce the deformation patterns observed in native valve leaflets.

The cells recruited in the scaffold produce collagen, the main load-bearing component of cardiovascular tissues. In order to understand and predict how the scaffold influences the collagen architecture and how the synthesized collagen changes the mechanical properties of the initial construct, we extended the microstructural model by including collagen synthesis and remodeling. We hypothesized that the microstructure of the scaffold and the loading conditions dictate collagen synthesis and degradation. In the presence of an electrospun scaffold, cells feel the topology of the substrate (contact guidance) and secrete collagen along the scaffold fibers, independently of the externally applied load. As a result, the initial quasi-linear mechanical behavior of the scaffold gradually changes into an exponential tissue-like stress-strain mechanical behavior. We validated our model against biaxial mechanical tests performed on tissue engineered constructs cultured for two weeks in static and dynamic loading conditions using isotropic and anisotropic electrospun substrates.

Finally, when the scaffold degrades, the cells apply tension to the collagen fibers in the direction of their main orientation. After the scaffold has degraded, the applied load dictates the collagen remodeling. We investigated collagen remodeling in tissue engineered strips using a discrete microstructural model that includes cell traction and collagen synthesis and degradation. Results showed that the discrete model can reproduce the tissue compaction predicted by a continuum model, and that the amount of compaction occurring in the engineered strip is independent of the initial collagen distribution and tissue size.

The work described in this thesis provides tools to study the biomechanics of tissue engineered constructs made from electrospun fibrous scaffolds over time. We have shown how the microscopic architecture of the scaffold relates to the macroscopic mechanical behavior of the scaffold and of the evolving tissue construct.

Chapter 1

Introduction

1.1   The human heart

The human heart is a muscle that pumps blood through the vascular system by repeated, rhythmic contractions. The heart works as two pumps, one on the right and one on the left side. The right side pumps the blood through the lungs and the pulmonary circulation where the blood is oxygenated, while the left side pumps blood through the systemic circulation to deliver oxygen to the organs. The de-oxygenated blood from the systemic circulation enters the right atrium, where the cycle starts again. In the heart, both atria contract at the same time to allow the blood to flow into the ventricles, and both ventricles contract at the same time to force the blood into the circulation. The unidirectional blood flow is guaranteed by the presence of four heart valves. The atrioventricular tricuspid and mitral valves prevent reverse flow from the ventricles to the atria during systole (pumping phase of the heart cycle). The pulmonary and the aortic semilunar valves prohibit backflow from the pulmonary and the aortic arteries into the ventricles during diastole (relaxing phase of the heart cycle), respectively. The semilunar valves are trileaflets valves (Fig. 1.1), and can withstand high hemodynamic loads. The aortic valve has a mean diameter of 28±5 mm (Perrino and Reeves, 2008). In healthy subjects the transvalvular pressure difference is on average 10 mmHg (1.3 kPa) for the pulmonary valve and approximately 80 mmHg (10.6 kPa) for the aortic valve (Silverthorn and Garrison, 2004). The valve typically undergoes 3 billion cycles over a 75-year lifetime.

1.1.1   The semilunar heart valve leaflets

The semilunar heart valve leaflets are composed of three layers: the fibrosa, the spongiosa and the ventricularis (Figure 1.2).

The fibrosa is located at the outflow side and is composed of densely packed organized collagen fibers. The collagen fibers are mainly oriented in the circumferential direction at the commisures and become more branched in the belly region. The collagen fibers are largely responsible for the mechanical behavior of the leaflets, in particular at large strains.

The spongiosa forms the middle layer and is predominantely composed of glycosaminoglycans (GAGs). GAGs are characterized by a high water binding

capacity (Culav et al., 1999), and therefore the main role of the spongiosa is to absorb the shear stresses and the compressive forces (Vesely, 1997).

The ventricularis, at the inflow surface, is mainly composed of radially aligned elastin fibers. These elastic fibers ensure flexibility of the leaflet and recoil during systole (Vesely, 1997).
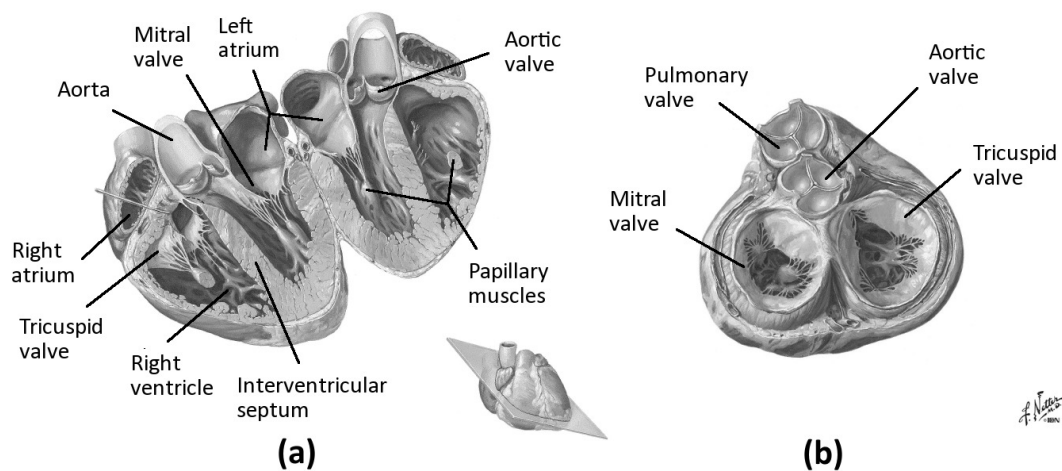
FIGURE 1.1: (a) Cross-sectional view of the human heart. Tricuspid and mitral valve are positioned between atrium and ventricle on the right and the left side respectively. The pulmonary valve is situated between the right ventricle and the inlet of the pulmonary artery, and the aortic valve between the left ventricle and the inlet of the aorta. (b) Top cross-sectional view of the heart, showing the four heart valves (modified from http://www.cicmd.com/images/cicmd/anatomy%20images/ANATOMY.htm)
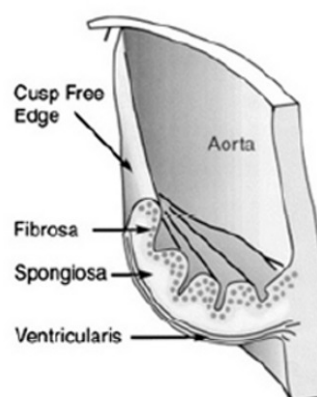
FIGURE 1.2: Schematic cross section of the aortic valve leaflet. The picture indicates the three valve's three layers: fibrosa, spongiosa and ventricularis (adapted from Vesely (1997))

1.2   Heart valve replacements

Heart valve disease is a significant health burden (Schoen and Levy, 1999). End-stage valvular diseases are commonly treated with valve replacement. Currently used heart valve replacements include mechanical and bioprosthetic valves. Each of these valves has its own advantages and disadvantages. Mechanical valves are readily available off-the-shelf and durable. However, the prostheses induce non-physiological flow profiles that may cause thromboembolic complications (Dasi et al., 2009, Senthilnathan et al., 1999), necessitating lifelong anticoagulation treatment. Bioprosthetic valves can have either human (homografts) or animal (xenografts) origin. These valves do not require anticoagulant treatment, but they are prone to calcification (Pibarot and Dumesnil, 2009, Siddiqui et al., 2009). Overall, for both kinds of replacement, the biggest limitation is their inability to grow, repair and remodel over time as native tissues do. This makes these valves suboptimal for use in pediatric and young patients, because multiple surgical interventions may be required to replace these prostheses. Tissue engineering (TE) aims to overcome these limitations by creating a living heart valve replacement.

1.3   Tissue engineering approach

In the last decade tissue engineers have made vast progress in developing functional living tissue replacements. The term "tissue engineering" was introduced for the first time in 1993 by Langer and Vacanti. It was defined as "an interdisciplinary field that applies the principles of engineering and life sciences toward the development of biological substitutes that restore, maintain, or improve tissue function or a whole organ" (Langer and Vacanti, 1993).

1.3.1   *In vitro* tissue engineering

According to the traditional *in vitro* tissue engineering paradigm, the development of a living tissue replacement typically requires the use of autologous cells. The patient's cells are harvested, expanded and then seeded onto a porous scaffold, which can be of biological or synthetic origin (decellularized xenograft or homograft

and polymeric saffolds respectively). The seeded scaffold is then placed in a bioreactor. Here cells are triggered to produce a new extracellular matrix (ECM) by the application of appropriate chemical and mechanical stimuli. The newly developed tissue construct can be implanted to replace the diseased native valve (Fig. 1.3 a) (Schenke-Layland et al., 2003, Knight et al., 2005, Mol et al., 2006).

For the *in vitro* tissue engineering approach a number of scaffold materials have been tested. Synthetic biodegradable materials are the main material choice because they allow a number of manufacturing possibilities and adjustable degradation kinetics (Shinoka et al., 1995, Kim et al., 2001, Stock et al., 2000, Sodian et al., 2002). Woven or non-woven fibrous scaffolds are typically used for cardiovascular tissue engineering (Van Lieshout et al., 2006), as the presence of pores in between the fibers easily allow cell infiltration. Fast degrading polymers (e.g. polyglycolic acid) typically degrade in a few weeks, while slowly degrading polymers (e.g. polycaprlactone) degrade over years (Henry et al., 2007, Niklason et al., 2010). Thermal or chemical processing of the polymer can induce changes in the degradation kinetics (La Carrubba et al., 2008, Hong et al., 2010). The choice of the proper degradation kinetics is crucial to provide the developing tissue support during maturation until it is able to take over the hemodynamic load.

1.3.2   *In situ* tissue engineering

In situ tissue engineering is a new and promising technology to produce living valve replacement in the human body itself. Decellularized xenografts can be used as *in situ* replacements, but they may cause a severe immunogenic response (Patience et al., 1998). As an alternative, a (polymeric) biodegradable scaffold can be used and implanted at the replacement site (Fig. 1.3 b). The scaffold can be functionalized with bioactives in order to guide the proliferation and the differentiation of the recruited cells and support the tissue formation. The scaffold may be pre-seeded with cells that have a paracrine signaling effect (Roh et al., 2010). The recruited cells will be responsible for new tissue formation.

This technology is clinically more attractive than the *in vitro* tissue engineering approach, as it does not require time consuming cell expansion and the use of complex bioreactor systems. In essence, it uses the patient's body as bioreactor for the development of new tissue. Recent in vivo studies show that, in response

to the implanted scaffold, an inflammatory cascade mediates the recruitment of the tissue forming cells (Roh et al., 2010).

1.4 Mechanical challenges of *in situ* tissue engineering: focus of this thesis

From a mechanical point of view, the implanted scaffold needs to satisfy a number of requirements:

- functionality at the time of implantation;

- capability to withstand the hemodynamic cyclic loads, with transvalvular pressures that can reach up to 80 mmHg for a heart valve in the aortic position;

- promote the maturation of the collagen network according to architectures that can be found in native valves;

- allow the neo-formed tissue to gradually take over the mechanical function to ensure long-term mechanical function;

The above scaffold properties are highly interconnected. The possibility to achieve the desired tissue microstructure depends on the structural organization of the scaffold (i.e. diameter of the scaffold fibers, scaffold porosity, orietation of the fibers). In turn, the architecture of the scaffold and the neo-tissue is responsible for the valve mechanical performance.

Given the central role of the scaffold in the *in situ* approach, it is necessary to optimize the scaffold's design in order to meet the requirements. A computational approach might help a systematic optimization of the scaffold properties. This thesis focuses on addressing these mechanical aspects of *in situ* TE.

1.4.1 Relation between structure and function in cardiovascular tissues

Native cardiovascular tissues consist of a network of collagen and elastin fibers dispersed in a matrix composed of glycosaminoglycans, water, and a cellular
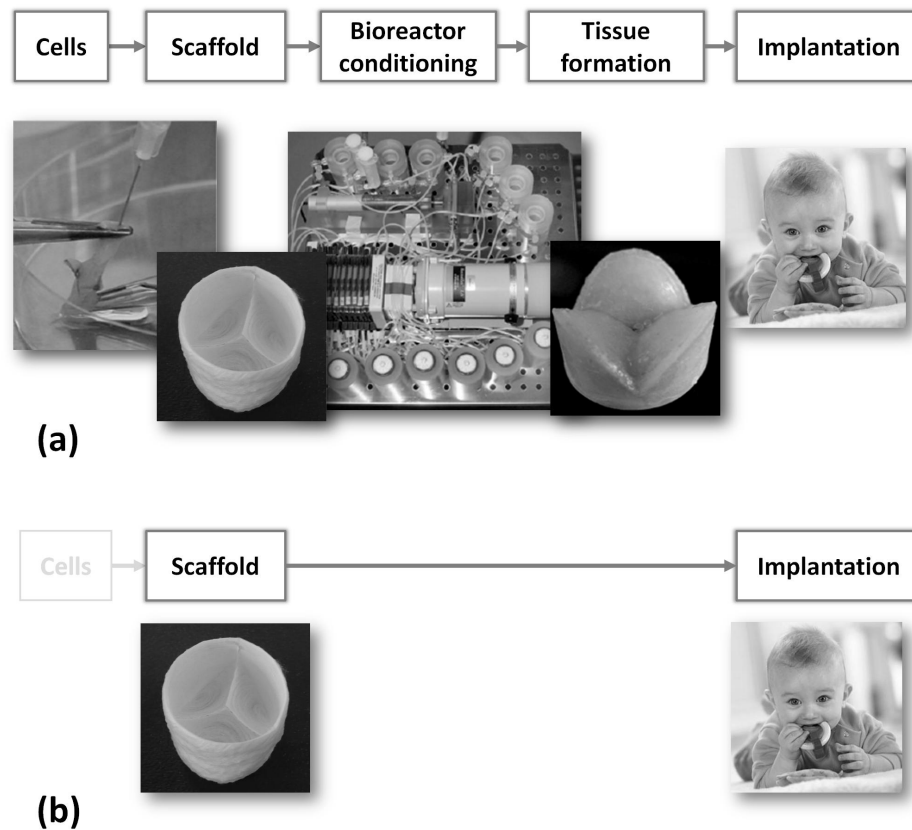
FIGURE 1.3: (a) Traditional tissue engineering approach. The cells, harvested from the patient, are seeded onto a scaffold. The scaffold is then placed in a bioreactor system, where tissue is triggered to grow. After tissue growth the construct is implanted in the human body. (b) *In situ* tissue engineering approach. A cell-free electrospun scaffold is implanted in the body, which serves as bioreactor (adapted from Mol et al. (2009)).

component. The collagen is the main load bearing component of a soft tissue (Alberts, 2000).

The aortic valve is characterized by a pronounced extensibility in the radial direction, and a higher stiffness in the circumferential direction (Billiar and Sacks, 2000a,b). This behavior reflects the structural arrangement of the fibrous components of the valve. In fact, as described in Section 1.1.1, the collagen network in a valve is mainly oriented in circumferential direction, whereas the elastin network is aligned in the radial direction (Thubrikar et al., 1986, Scott and Vesely, 1995, Vesely, 1997, Billiar and Sacks, 2000a, Lee et al., 2001) (Fig. 1.4).

The functionality that is resulting from this structure in the native valve has to be acquired and maintained over time in the *in situ* engineered valve.
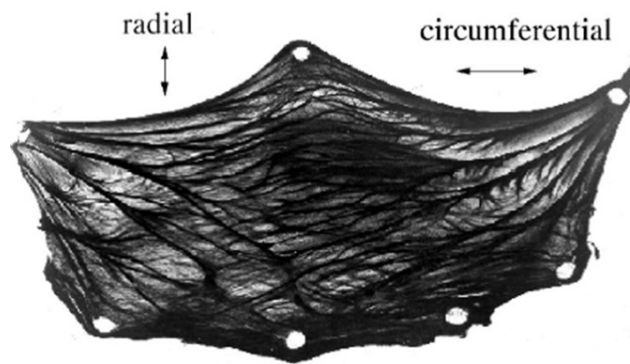
FIGURE 1.4: Aortic heart valve leaflet with circumferential collagen orientation (adapted from Sauren (1981)).

1.5   The electrospun scaffold

Electrospinning is an old technique (Cooley, 1902), which possibilities as a suitable technology to manufacture scaffolds for TE have been broadly investigated in recent years. In the electrospinning process, a polymeric solution is inserted in a syringe and a high voltage (5 to 50 kV) is applied between the syringe and a grounded collector which causes a jet of polymer erupt out of the syringe. This jet elongates forming a fiber that dries in the flight and is then collected on a (rotating) mandrel, resulting in a non woven network of polymer fibers (Fig. 1.5).
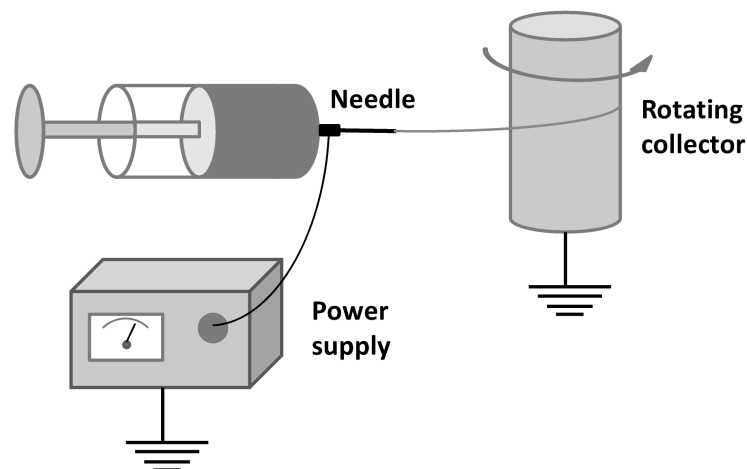
FIGURE 1.5: Electrospinning equipment provided with a syringe. The polymeric fibers are pulled out of the needle and collected on a (rotating) drum.

1.5.1   Design parameters of an electrospun scaffold

Electrospinning is a versatile technology, that offers a number of opportunities to control the architecture of the scaffold while a large number of materials can be processed. Several physical parameters (e.g. flow rate, electric voltage, distance between the syringe and the collector, collector rotational speed) control the spinning process (Li and Xia, 2004). In a typical electrospinning setup the fine tuning of these parameters is used to obtain the desired scaffold structure.

Previous studies have shown that an increased working distance (distance between syringe and collector) and an increased mandrel rotational speed lead to a decreased fiber diameter, and an increased fiber alignment. In contrast, an increase in flow rate determines an increased fiber diameter, and a decreased fiber alignment (Fridrikh et al., 2003, Beachley and Wen, 2009, Milleret et al., 2011). When the flow rate is low, or working distance is high, the solvent will evaporate significantly when travelling between the needle and the collector, increasing the stiffness of the fibers, making the fibers less prone to bending and resulting in more aligned fibers (Milleret et al., 2011). An increased rotational speed will straighten the fibers, so that they will be deposited in an aligned fashion. In addition, an increase of the electrical voltage (in the range 10 to 20 kV) can be used to decrease the fiber diameter (Chowdhury and Stylios, 2010). An increased humidity in the electropun chamber allows the wet deposited fibers to get easily fused, producing highly interconnected meshes (Raghavan and Coffin, 2011). Furthermore, the use of a very low temperature and controlled humidity is useful to increase the scaffold porosity (Simonet et al., 2007). The possibility of spinning meshes with large pore size is important, since it allows a better and desirable cell infiltration within the scaffold (Balguid et al., 2009), and finally the microstructural variations resulting from changing the spinning parameters is influenced by the type of spun material (Milleret et al., 2011).

Summarizing, the electropinning technology allows the production of scaffolds with a wide range of structural properties. Fiber diameter, fiber orientation, fiber interconnection, fiber material and fiber distance can all be adjusted and have an impact on the mechanical properties of the scaffold.

1.6   Microstructure versus macromechanical properties

In electrospun meshes, as well as in fibrous tissues, the arrangement of the fibrous components at the micro-scale (µm) determines the mechanical characteristics of the mesh on the macro-scale (cm). This thesis work aims to investigate

- the relation between the spatial arrangement of the fibrous components of the scaffold and the macromechanical properties of the scaffold and of the construct over time;

- impact of collagen synthesis and degradation on the mechanical properties of the construct;

- cell tension mediated collagen remodeling.

1.6.1   Modeling approach

The relation that occurs between microstructure and macromechanical properties indicates a connection between different length scales. To explore the mechanics of engineered constructs in a systematic way we described in detail in a finite element model the microstructural features of the scaffold and the construct as a network of 1D fibers. Next, we used an homogenization procedure to derive the macroscopic constitutive response of the given microstructural network (Smit et al., 1998) (Fig. 1.6).

In this thesis the micro- to macro-scale approach has been applied to understand and predict the relations between scaffold microstructure, tissue collagen structure and macroscopic mechanical function of the tissue.

1.7   Cell mediated extracellular matrix turnover

The *in situ* tissue engineering approach requires that cells that colonize the scaffold produce ECM. In particular, as the collagen is the main load-bearing component of a soft tissue, the architecture of the newly developed collagen network is crucial for
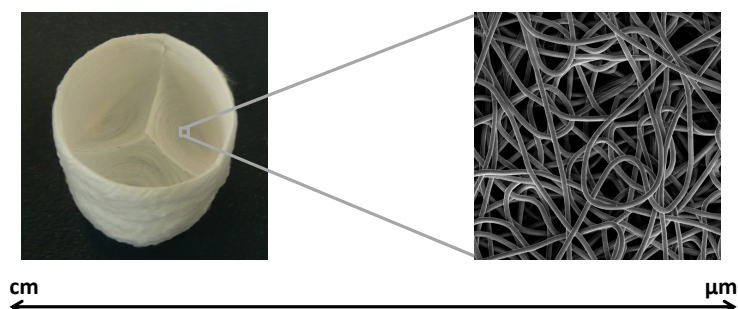
FIGURE 1.6:   Heart valve shaped (left) scaffold and scaffold microstructure
(right) with corresponding length scale.

the ultimate functionality of the tissue (Matsumoto and Hayashi, 1994, Humphrey, 1999, Niklason et al., 2001, Driessen et al., 2003, Driessen-Mol et al., 2003, Fridez et al., 2003, Driessen et al., 2004, Driessen-Mol et al., 2005). The mechanisms that are responsible for collagen deposition and therefore its architecture are currently subject of extensive studies. Controlling the collagen architecture is key for achieving mechanically well performing engineered tissues (Driessen et al., 2007).

A mechanical reciprocity between cells and collagen takes place in tissues (Fig. 1.7). On the one hand the collagen architecture is maintained by cells, as cells synthesize and reorient the collagen fibers (Trelstad et al., 1976, Paul and Bailey, 2003, Balguid et al., 2007, Soares et al., 2011). On the other hand cell orientation is also guided by the collagen fibers (contact guidance) (Foolen et al., 2012).

1.7.1   Cell-mediated collagen orientation

The cytoskeleton is a highly dynamic network that reorganizes itself in response to external stimuli. Actin filaments and myosin II filaments compose the cytoskeletal stress fibers. They generate tension within the cell (Ladoux and Nicolas, 2012).

The topography of the cell environment has been shown to be influence adherence and spreading of the cell, and therefore its final shape (Chen et al., 2003, Schwarz and Safran, 2013). Control of cell shape or orientation via substrate topography is called contact guidance. Next to this, biological and mechanical conditioning influence the cell orientation.
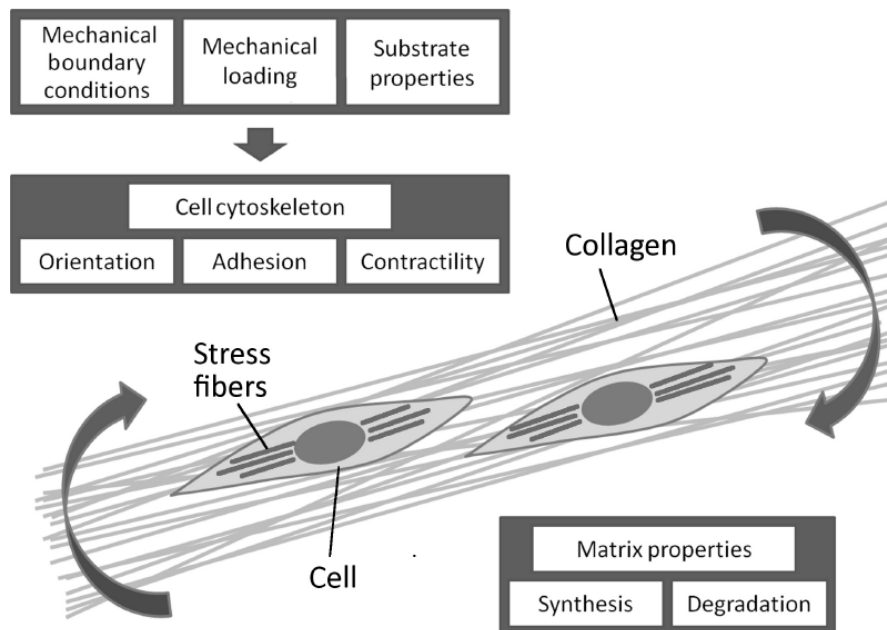
FIGURE 1.7: Schematic of the mechanisms of cell-mediated collagen turnover and remodeling mechanisms. The cells respond to their substrate and to the externally applied load. By doing that, the cells reorient the pre-existing collagen, while collagen synthesis and degradation take place (adapted from Soares et al. (2012)).

In many tissues, it has been shown that collagen aligns along the direction of the cell stress fibers. Collagen fibers grow in the vesicles at the base of the cytoplasmatic fibrils by addition of individual collagen molecules to the end of the fibrils (Holmes et al., 1994) or by end-to-end fusion (Graham et al., 2000, Kadler et al., 2000). Cell membrane protrusions co-aligned with the ECM fibrils serve as a delivery system for collagen secretion in the extracellular space (Canty et al., 2004, 2006). As in elongated cells the direction of the stress fibers coincide with the cell main direction (Greiner et al., 2013), the collagen will be produced along the cell main axis.

1.7.2 Tissue compaction

Cell sources that are typically used in cardiovascular tissue engineering are characterized by an activated remodeling phenotype. This means that the cells are able to respond to changes in stress in their environment by applying forces to it and remodeling their matrix (Rabkin-Aikawa et al., 2004). Inside the cell, this causes a reorganization of the cytoskeletal structure of the cells and the formation

of stress fibers, in order to reach the preferred cell stress balance (Brown et al., 1998). To achieve their stress equilibrium, cells exert forces on their surrounding, leading to tissue compaction.

Tissue compaction is currently one of the major concerns in heart valve TE. In vivo studies have reported the presence of leaflet retraction and consequent undesired valvular regurgitation (Hoerstrup et al., 2000, Sutherland et al., 2005, Flanagan et al., 2009, Gottlieb et al., 2010, Schmidt et al., 2010) (Fig. 1.8).

Van Vlimmeren et al. (2011) developed a model system to quantify the cell traction forces and the resulting amount of tissue compaction. Using PGA/P4HB scaffold strips, it was shown that the engineered constructs start to develop stress and compact after two weeks of culture (van Vlimmeren et al., 2010). They hypothesized that in the first two weeks the cell traction forces are counterbalanced by the scaffold stiffness. After two weeks the scaffold loses its mechanical integrity and the cells are able to compact the construct.

This thesis will numerically assess the effect of tissue compaction in engineered strips characterized by a discrete collagen structure.
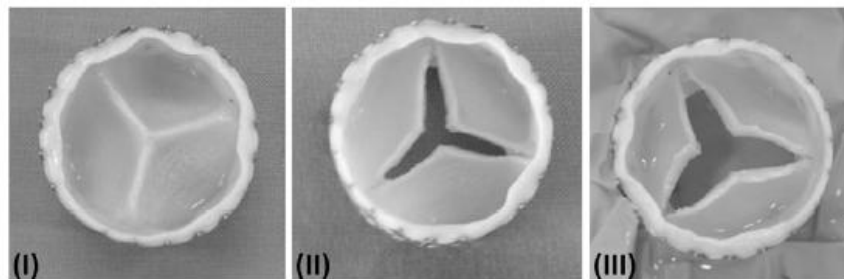
FIGURE 1.8: Compaction occurring in the engineered valve leaflets. The leaflets are separated after 4 weeks of culture. Compaction is shows immediately after leaflet separation (II) and after 3 hours (III) when the valve is kept on ice (adapted from van Vlimmeren (2011)).

1.8   Rationale and outline

The aim of the studies described in this thesis is to develop tools to describe the biomechanical properties of an electrospun scaffold for *in situ* tissue engineering, and the resulting engineered construct over time.

For this purpose a microstructural computational model is developed. This model describes in detail the microstructure of fibrous networks, in terms of spatial arrangement, fiber diameter and material of the constituent fibers. The macromechanical properties of such a network are evaluated via an homogenization procedure. Biaxial mechanical tests of electrospun meshes and tissue constructs are used to validate the model.

First a micro-scale model of a bare electrospun mesh is developed and used to investigate the relation between the scaffold microstructure and its macroscopic mechanical properties (Chapter 2). It is demonstrated that the model is able to successfully describe the mechanical behavior of scaffolds with different microstructures.

Next, the growth and degradation of collagen fibers in between the scaffold fibers is described for different external loading conditions, and included in the microstructural model. Chapter 3 concentrates on describing the mechanical properties of engineered constructs when tissue develops in the presence of an electrospun scaffold. Chapter 4 focuses on understanding the experimentally observed contact guidance provided by the electrospun fibers to recruited cells.

Finally, after tissue has matured and the scaffold has degraded, the effect of the cell traction on the collagen remodeling is investigated in a micro-scale framework (Chapter 5). The tissue compaction that occurs in tissue engineered strips due to the traction forces developed by the cells is described by means of the microstructural model.

The final Chapter 6 summarizes the obtained results and discusses the possibilities of future studies towards mechanically well performing engineered tissues.

In conclusion, the approach that is developed and exploited in the different studies relates different length scales. This approach is used to describe how the evolving microstructure relates to the mechanical properties of developing engineered constructs. Some indications on how the microstructural design of an electrospun scaffold are provided to improve the performance of engineered heart valve construct.

Chapter 2

Multi-scale mechanical characterization of scaffolds for heart valve tissue engineering

2.1   Abstract

Electrospinning is a promising technology to produce scaffolds for cardiovascular tissue engineering. Each electrospun scaffold is characterized by a complex micro-scale structure that is responsible for its macroscopic mechanical behavior. In this study, we focus on the development and the validation of a computational micro-scale model that takes into account the structural features of the electrospun material, and is suitable for studying the multi-scale scaffold mechanics. We show that the computational tool developed is able to describe and predict the mechanical behavior of electrospun scaffolds characterized by different microstructures. Moreover, we explore the global mechanical properties of valve-shaped scaffolds with different microstructural features, and compare the deformation of these scaffolds when submitted to diastolic pressures with a tissue engineered and a native valve. It is shown that a pronounced degree of anisotropy is necessary to reproduce the deformation patterns observed in the native heart valve.

2.2   Introduction

End stage heart valve diseases commonly result in valve replacement with either mechanical or biological prosthesis (Zilla et al., 2008). A critical limitation of these prosthesis is their inability to repair, to grow and to remodel in response to changes in their mechanical environment (Yacoub and Takkenberg, 2005). Therefore, in the last decade, considerable effort has been invested in the manufacturing of a living tissue engineered valve overcoming these limitations (Driessen-Mol et al., 2003). The concept of *in vitro* tissue engineering is based on seeding (autologous) cells on a biodegradable scaffold, and then providing the necessary biochemical and mechanical cues to culture a functional heart valve in a bioreactor system (Mol et al., 2009).

The local and global topological, structural and mechanical properties of the scaffold supporting the growth of autologous tissue strongly influence the properties of the engineered valve. For instance when using a non-woven fibrous mesh as starter matrix, the microstructure of the scaffold (e.g. fiber diameter, stiffness, interconnectivity and orientation, and the scaffold porosity) affects

cellular ingrowth, influences cell fate and extracellular matrix production (Balguid et al., 2009, Heath et al., 2010, Kai et al., 2011). On the larger scale (e.g., of the valve), the structural support of the scaffold enables mechanical stimulation of the developing tissue in pressure driven bioreactors (Mol, 2005), and may contribute to the in-vivo mechanical functionality of the construct when a slowly degrading scaffold material is used. Given the complex relation between the micro-structure of the scaffold and the macroscopic mechanical behavior of the construct, a computational model may support the design of the scaffold.

Electrospinning is a versatile and promising technique for manufacturing scaffolds for tissue engineering (Chen et al., 2007, Venugopal et al., 2008). In the electrospinning setup a high positive voltage power supply is responsible for the ejection of a polymeric jet from a needle connected to a syringe pump. The fiber is accelerated and collected on a grounded rotating and translating target (Cooley, 1902) (Fig. 2.1).
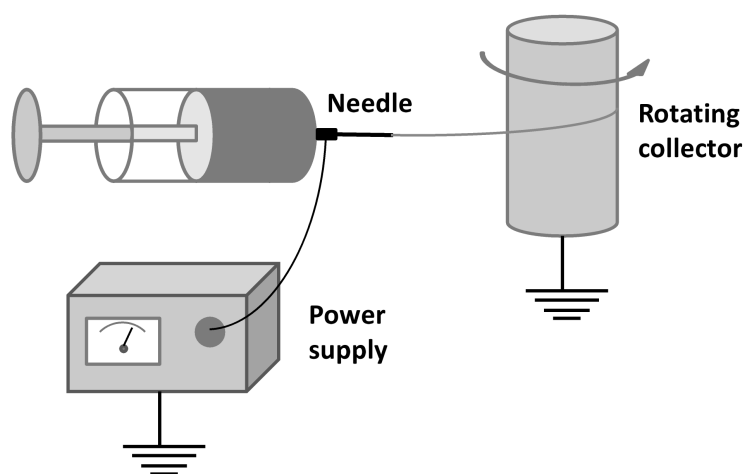
FIGURE 2.1: Electrospinning equipment provided with a syringe.The polymeric fibers are pulled out of the needle and collected on a rotating drum.

Electrospinning can be used to produce a wide range of microstructures depending on the parameters chosen. These include the type of polymer, the solvent, the flow rate, the voltage difference and the physical distance between the target and collector, and the rotational speed of the mandrel (Amoroso et al., 2011, Soliman et al., 2011). Only a few studies have made an effort to systematically investigate the influence of the microstructural features of fibrous scaffolds on the macroscopic mechanical properties (Stylianopoulos and Barocas, 2007, Stylianopoulos et al.,

2008). This work aims at developing a computational method to relate the microstructural properties of electrospun scaffolds to the macroscopic behavior, to enable the design of the scaffold.

Given the length scale difference between the fibrous microstructure (µm) and the scaffold macrostructure (cm), a multi-scale approach is required (Stella et al., 2010). Earlier finite element based multi-scale approaches (Kouznetsova et al., 2001, Breuls et al., 2002), assigned a representative area element (RAE) to each integration point of the macroscopic model. The macroscopic deformation was assigned to the RAE, and the area (or volume) averaged stress was extracted from the RAE and used on the macro scale. The advantage of this approach is that at the macro-scale no closed form constitutive model is needed, and therefore implicitly accounts for any evolution of the microstructure. Although conceptually attractive, the implementation in a finite element framework is computationally demanding. We present a different approach, which couples a detailed microscropic model to a closed form macroscopic constitutive model.This approach is computationally less demanding, and can be used effectively to design scaffolds when the micro-structure is assumed constant in time, but variations in the microstructure can be easily accommodated.

To demonstrate feasibility of the approach, the material properties are evaluated for an electrospun poly(ε-caprolactone) (PCL) scaffold. The micro-scale structural parameters were obtained using a numerical/experimental procedure (Meuwissen et al., 1996), and were subsequently used to analyze the deformation of heart valve shaped scaffolds. The deformation patterns were compared against those of a tissue engineered (Driessen et al., 2007) and a native porcine valve (Billiar and Sacks, 2000a).

2.3   Materials and Methods

2.3.1   Analysis of the problem: a multi-scale approach

The multi-scale approach is based on a discrete representation of the key micro structural features of an electrospun scaffold, i.e., the fiber diameter, the fiber interconnectivity, the fiber orientation, the fiber distance that accounts for the

scaffold porosity, and the intrinsic mechanical properties of the fiber material (
Fig. 2.2).
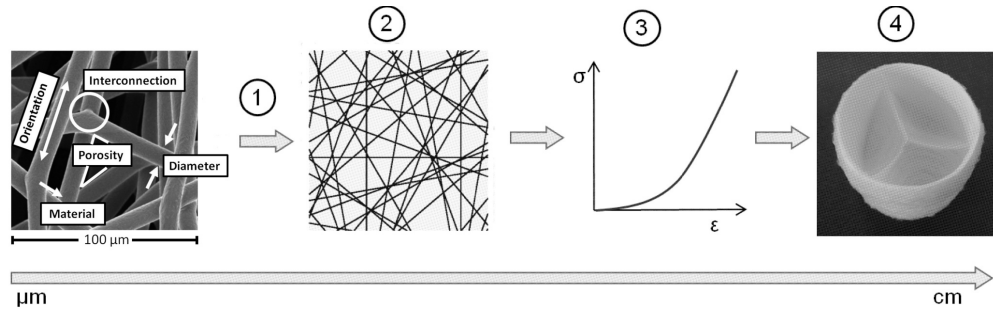
FIGURE 2.2: Schematic of a multi-scale approach of the mechanical behavior of
the scaffold. From the left, the first picture shows a SEM image of an electrospun
scaffold, the second picture represents the microstructural computational model
of the scaffold, the third picture depicts a possible mechanical behavior for the
model,and the fourth picture shows a valve-shaped scaffold characterized by the
computed material behavior.

The three dimensional electrospun scaffold is represented by a discrete two
dimensional fiber structure (2). The macroscopic in-plane deformation is
translated into appropriate boundary conditions on the RAE (2). The reaction
forces resulting from the inhomogeneous deformation of the RAE (2) are used to
extract an area averaged stress tensor, and is associated with the macroscopic
deformation tensor (3). Subsequently, the parameters of a macroscopic
constitutive model can be identified such that the mechanical behavior of the
RAE is captured accurately, and can be used in a regular finite element analysis
of the macroscopic structure (4).

2.3.2   Macro-scale constitutive model

The electrospun scaffold was assumed to be embedded in an incompressible
matrix, for instance a gel used as a sealant or for cell seeding (Mol, 2005). It is
macroscopically modeled as an incompressible fiber reinforced material, consisting
in an isotropic incompressible matrix surrounding an anisotropic fiber structure
(Driessen et al., 2005c). The total Cauchy stress ($\boldsymbol{\sigma}$) is split into a hydrostatic
pressure (p) and an extra stress ($\boldsymbol{\tau}$)

$$\boldsymbol{\sigma} = -p\boldsymbol{I} + \boldsymbol{\tau} \tag{2.1}$$

The extra stress is written as

$$\boldsymbol{\tau} = \hat{\boldsymbol{\tau}} + \sum_{i=1}^{N} \phi_{f,M}^i \left(\psi_{f,M}^i - \overrightarrow{e}_{f,M}^i \cdot \hat{\boldsymbol{\tau}} \cdot \overrightarrow{e}_{f,M}^i \right) \overrightarrow{e}_{f,M}^i \overrightarrow{e}_{f,M}^i \tag{2.2}$$

where $\hat{\boldsymbol{\tau}}$ is the isotropic matrix stress tensor, $\psi_{f,M}$ the (macroscopic) fiber stress, $\overrightarrow{e}_{f,M}$ the current fiber direction and N the number of fiber directions. When the macroscopic deformation gradient tensor $\boldsymbol{F}_M = \left[\vec{\nabla}_0 \vec{X} \right]^T$ is applied, the current fiber direction can be calculated from the fiber direction in the undeformed configuration $\vec{e}_{f0,M}$:

$$\lambda_{f,M} \vec{e}_{f,M} = \boldsymbol{F}_M \cdot \vec{e}_{f0,M} \tag{2.3}$$

where $\lambda_{f,M}$ is the fiber stretch:

$$\lambda_{f,M} = \sqrt{\vec{e}_{f0,M} \cdot \boldsymbol{C}_M \cdot \vec{e}_{f0,M}} \tag{2.4}$$

and $\boldsymbol{C}_M = \boldsymbol{F}_M^T \cdot \boldsymbol{F}_M$ the right Cauchy-Green deformation tensor. The angular fiber distribution is described by specifying an appropriate set of fiber contents $(\phi_{f,M})$ along a set of fiber directions $(\vec{e}_{f0,M})$. The fiber directions are defined in a coordinate system spanned by two vectors $\vec{v}_1$ and $\vec{v}_2$:

$$\vec{e}_{f0,M}(\gamma_i) = \cos(\gamma_i)\vec{v}_1 + \sin(\gamma_i)\vec{v}_2 \tag{2.5}$$

where γ_i is defined with respect to $\vec{v}_1$ in the plane spanned by $\vec{v}_1$ and $\vec{v}_2$.

The fiber volume fractions $\phi_{f,M}^i$ along the directions γ_i are described by the updated periodic distribution function introduced by Gasser et al. (2006) and used by Driessen et al. (2008):

$$\phi_{f,M}^i = A \, \exp \left[\frac{\cos\left(2\left(\frac{\gamma_i}{h}-\alpha\right)\right)+1}{\beta} \right] \tag{2.6}$$

The fiber volume fraction is function of the main orientation α, the dispersion parameter β, and the frequency scaling factor h. The fiber material law is assumed to be exponential for positive stretches:

$$\begin{cases} \psi_{f,M}^i = k_1 \lambda_{f,M}^2 \left[e^{k_2\left(\lambda_{f,M}^2-1\right)} - 1 \right], & \lambda_{f,M} \geq 0 \\ 0 & , \lambda_{f,M} \leq 0 \end{cases} \tag{2.7}$$

with $\psi_{f,M}$ and $\lambda_{f,M}$ macro-scale fiber stress and stretch respectively, and k_1 and k_2 are a stress-like and dimensionless parameter, respectively.

2.3.3   Micromodel

The micro-scale model mimics the fiber distribution that can be observed from a scanning electron microscopy (SEM) image of an electrospun scaffold. The distribution function of the discrete model is chosen in accordance with the fiber distribution function of the macro-scale model (Eq. 7). An exponential relationship is assumed to relate the micro-scale fiber stress $\psi_{f,m}$ and stretch $\lambda_{f,m}$ for positive stretches:

$$\begin{cases} \psi_{f,m}^i = h_1 \lambda_{f,m}^2 \left[e^{h_2\left(\lambda_{f,m}^2-1\right)} - 1 \right], & \lambda_{f,m} \geq 0 \\ 0 & , \lambda_{f,m} \leq 0 \end{cases} \tag{2.8}$$

where h_1 and h_2 are a stress-like and dimensionless parameter, respectively.

The nonlinearity of the material law is chosen to account of the undulations in the electrospun fiber that is otherwise not represented in the discrete model.

To generate a discrete representation of the measured fiber structure, an algorithm was developed by using the software Matlab (The Math-Works, Natik, MA). A discrete set of fiber directions was used, and the fiber volume fraction dictates the relative fiber spacing. The model (Fig. 2.3) is a network of one dimensional elements, and the RAE is chosen sufficiently big to ensure that it represents the mechanical properties of the macrostructure. All the microstructural properties of a scaffold can be varied. The sites of perfect bonding between two fibers, where the transmission of forces is allowed, are represented by nodes (pink dots in Fig. 2.3). The desired quantity of connected nodes can be randomly chosen among all the possible fiber intersections.
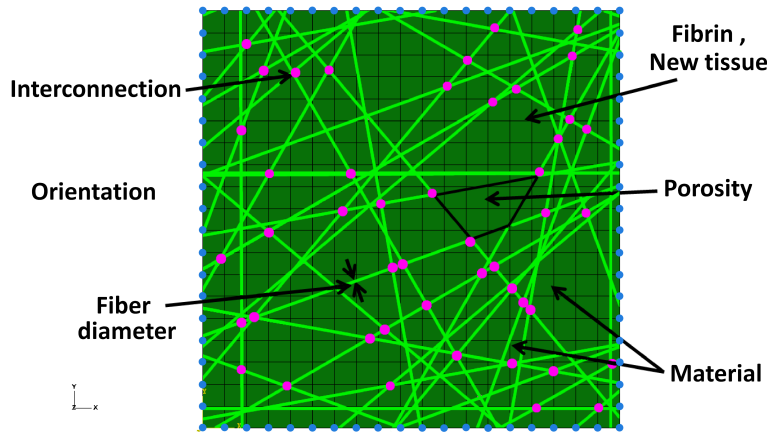
FIGURE 2.3: RAE scaffold model.

2.3.4 Boundary conditions

For a given macroscopic deformation tensor $\boldsymbol{F}_M$, a number of approaches can be used to impose the corresponding boundary conditions on the RAE. These include (Kouznetsova, 2002) (i) displacement boundary conditions that fully prescribe the deformation of all the boundary nodes of the RAE, (ii) periodic boundary conditions and (iii) minimal kinematic boundary conditions that prescribe the micro-fluctuation field (sum of the displacements of the boundary nodes) to be zero. Periodic boundary conditions are known to give the most precise solution. Yet, the complexity and non-periodicity of the scaffold microstructure raise questions about the possibility of getting similar results with different kind of

boundary conditions. A representative RAE was analyzed using the three different boundary condition options. The finite element code Abaqus/CAE was used to solve the microstructural problem. The microscopic quantities were coupled to the macroscopic quantities by using the averaging theorems proposed by Hill (1963, 1984) and Nemat-Nasser (1999), and used by Kouznetsova (2002) in the development of a full multi-scale framework. The sum of the resulting external forces $\overrightarrow{f_i}$ at the boundary nodes having initial position vectors $\overrightarrow{X_i}$ was averaged over the initial RAE volume V_0, whose thickness dimension is defined by the diameter of the fibers composing the RAE, to evaluate the macroscopic first Piola-Kirchhoff tensor $\boldsymbol{P}_M$:

$$\boldsymbol{P}_M = \frac{1}{V_0} \sum_{i=1}^{N} \overrightarrow{f_i} \, \overrightarrow{X_i} \tag{2.9}$$

and the Cauchy stress tensor $\boldsymbol{\sigma}_M$

$$\boldsymbol{\sigma}_M = \frac{1}{det \, \boldsymbol{F}_M} \cdot \boldsymbol{P}_M \cdot \boldsymbol{F}_M^T \tag{2.10}$$

Little difference was observed among the three cases analyzed. The use of displacement boundary conditions along the edges of the RAE proved to be the most robust approach, and was adopted throughout this work.

2.3.5   Parameter identification and model validation

Two electrospun scaffolds were produced to evaluate the parameters and test the predictive capabilities of the model. The scaffolds were electrospun in a climate-controlled electrospinning cabinet (IME Technology, Eindhoven, NL) equipped with a 0.6 mm diameter capillary and a distance of 15cm between the capillary and the 5 cm diameter rotating target drum. 20% (wt) PCL (Purac) was dissolved in Chloroform (CHCl3) and electrospun with a flow rate of 25 µL/min and a voltage of 18 kV applied. The first (scaffold 1) was spun with a rotational speed of 100 rpm (corresponding to a surface speed of 0.52 m/s), the second (scaffold 2) was composed of a thin layer spun at 50 rpm ensuring the integrity

of the scaffold and a thicker layer spun at 2000 rpm (10.47 m/s). Biaxial tests were conducted using the Biotester (CellScale Biomaterial Testing) to explore the mechanical properties of the scaffolds. Five samples per scaffold were soaked in ethanol to mimic the procedure used during tissue engineering, kept in water in the incubator for 24h, and tested in wet conditions at 37 °C. The samples were mechanically preconditioned by a sequence of uniaxial stretches in both directions in order to study the elastic behavior of the material. Subsequently an equibiaxial stretch was applied, followed by uniaxial stretches in both direction (Fig. 2.4). The strain pattern described allowed the study of the anisotropic mechanical behavior of the scaffold.
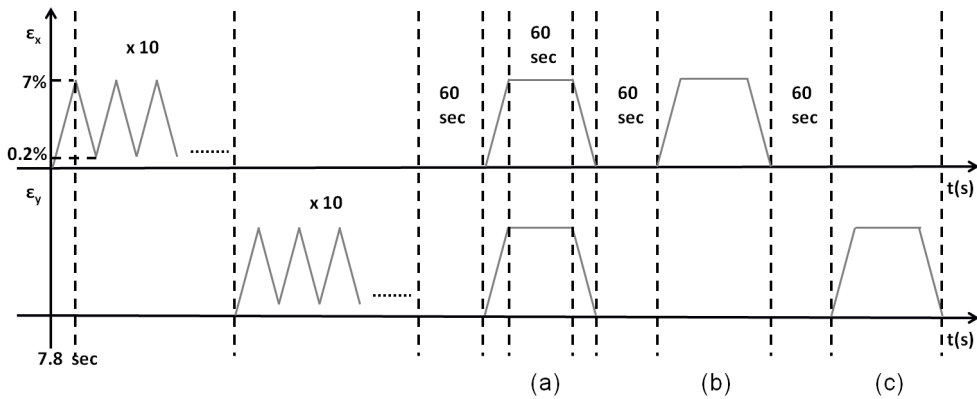
FIGURE 2.4: Strain pattern used for biaxial tests.The strain pattern consists in10 cycles of preconditioning along the x and y axis, followed by equibiaxial strain and uniaxial strain in the x and the y direction. A prestrain of 0.2% is applied, and the samples are strained up to 7%, with a strain rate of 100% strain/min.

The image processing software ImageJ was used to obtain the average fiber diameter and the fiber distribution from SEM images. The optimal microstructural fiber parameters h_1 and h_2 (Eq. 8) were identified using a least squares optimization of the biaxial stress-strain curves. These sets of h_1 and h_2 so calculated were used to predict the uniaxial behavior of the two scaffolds. In addition, the h_1 and h_2 associated with the anisotropic scaffold were used to predict the biaxial mechanical behavior of the isotropic scaffold.

Subsequently, a least squares optimization of both biaxial and uniaxial stress-strain curves provided by the multi-scale calculation was used to calculate the fiber parameters k_1 and k_2 (Eq. 7) of the macro-scale model.

2.3.6 Mechanical behavior of heart valve shaped scaffolds

For the two scaffolds, the parameters k_1 and k_2 (Eq. 7) and the fiber distributions were used to solve the macroscopic constitutive equations described in Section 2.2. Such equations were implemented in a computational framework on a valve-shaped geometry in the software package SEPRAN (Segal, 1984). Further details are described in Driessen et al. (2005c,a). A transvalvular pulmonary pressure of 2.8 kPa was applied.

2.3.7 Model predictions

The capabilities of the computational multi-scale framework were exploited. An orientation sensitivity analysis was carried out on a scaffold with the structural features and fiber properties of scaffold 1 used during the validation process. fiber standard deviations $\beta = 0.13$, $\beta = 0.42$ and $\beta = 2$ were used.

2.4   Results

Two scaffolds were analyzed. Scaffold 1 presents fibers with an average diameter of 10 μm, a fiber volume fraction of 17%, a high percentage of interconneted fibers ($\simeq 70\%$) and a nearly isotropic distribution ($\beta = 2$). Scaffold 2 presents fibers with average diameter of 5 μm, a fiber volume fraction of 16%, a few fiber connections ($\simeq 30\%$), due to a highly anisotropic fiber distribution ($\beta = 0.005$) (Fig. 2.5).

These parameters were used to build the micro-scale finite element model of the scaffolds. Using the biaxial stress-strain data (Fig. 2.6 a and 2.6 b), the parameters h_1 and h_2 (Eq. 8) were estimated for both scaffolds independently (Table 1). Using the parameter set of the anisotropic scaffold, the biaxial mechanical properties of the isotropic scaffold could be predicted well (Fig. 2.6 a), demonstrating the versatility of the approach. The optimal h_1 and h_2 were subsequently used to predict the uniaxial experiments (Fig. 2.6 c and 2.6 d), and good agreement was observed.

Using these scaffold parameters, the deformation patterns in a valve shaped scaffold were computed, and compared to the deformation in a tissue engineered heart valve (TEHV) (Driessen-Mol et al., 2003, Driessen et al., 2007), and
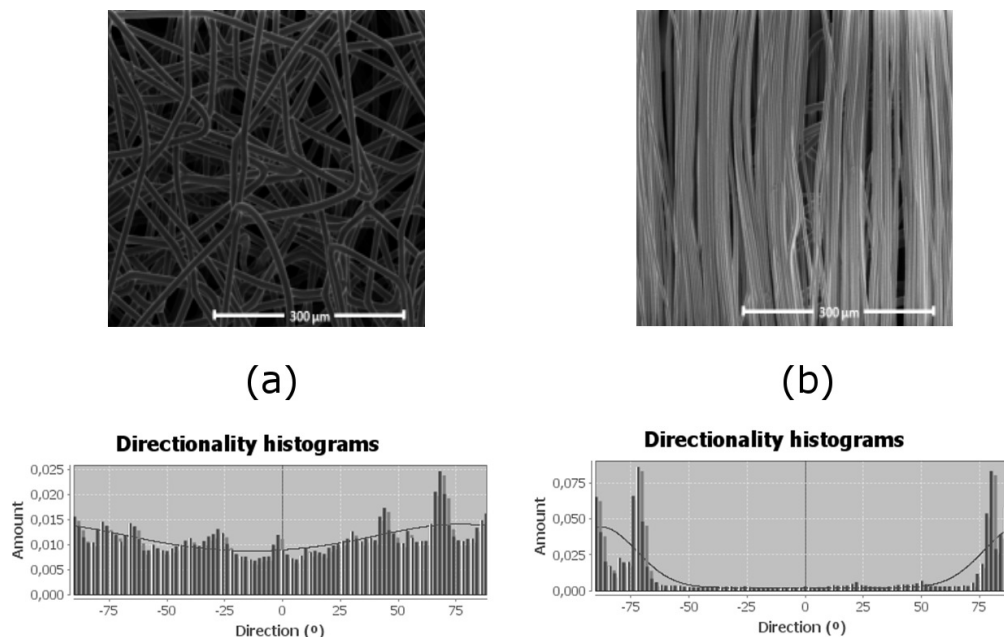
FIGURE 2.5: SEM image of scaffold 1(a) and scaffold 2(b) with respective fiber orientation.

to a native porcine heart valve (Billiar and Sacks, 2000a,b). The mechanical characterization of the engineered and native valves was previously performed by Driessen et al. (2007). The isotropic scaffold 1 ($\beta = 2$), behaves similarly to the tissue engineered leaflets ($\beta = 3.1$). This corresponds to the large values of the dispersity parameter. The anisotropic scaffold 2 has a much lower dispersity parameter ($\beta = 0.005$) compared to scaffold 1, and the deformation pattern resembles that of a native valve ($\beta = 0.13$) (Fig. 2.7), despite the fact that the intrinsic fiber stiffness of the PCL scaffold is much higher than the collagen fibers of the native leaflet (Table 1). These results suggest that the stiffness of the fibers plays an important role in the overall deformation of the construct, and the fiber distribution significantly influences the deformation pattern.

Simulations performed with different fiber distributions confirm that a pronounced anisotropy increases the strain in the belly region (Fig. 2.8) and improves the coaptation (Fig. 2.7 d).
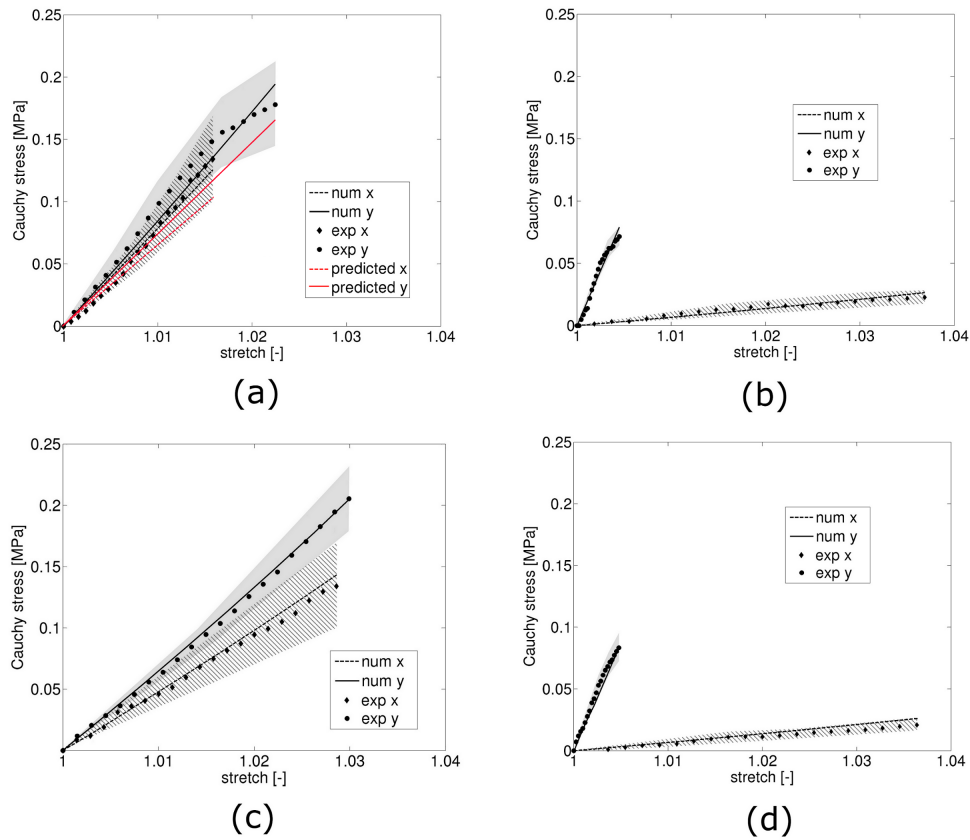
FIGURE 2.6: Fit of the experimental equibiaxial mechanical behavior for scaffold 1(a) and scaffold 2(b). Predicted biaxial mechanical behavior of scaffold 1 by using the optimal material parameters of scaffold 2 in red in(a). Predicted uniaxial behavior for scaffold 1(c)and scaffold 2(d) with the optimal parameters evaluated for the two scaffolds. The striped area and the gray area represent the experimental error around the average values.

2.5   Discussion

In the present study, a simplified and effective computational multi-scale analysis approach was presented to investigate the relation between the microstructure of an electrospun scaffold and the global mechanical properties of the scaffold. Feasibility of the approach was examined using two electrospun PCL scaffolds: an isotropic and a highly aligned, anisotropic scaffold. The microstructural parameters such as fiber diameter, fiber orientation, fiber spacing and fiber interconnectivity were obtained by analysis of SEM images. These structural parameters were subsequently used to build a two dimensional discrete representation of the scaffold. The mechanical parameters of the microstructural model were identified on the basis of equibiaxial extension tests. The predictive
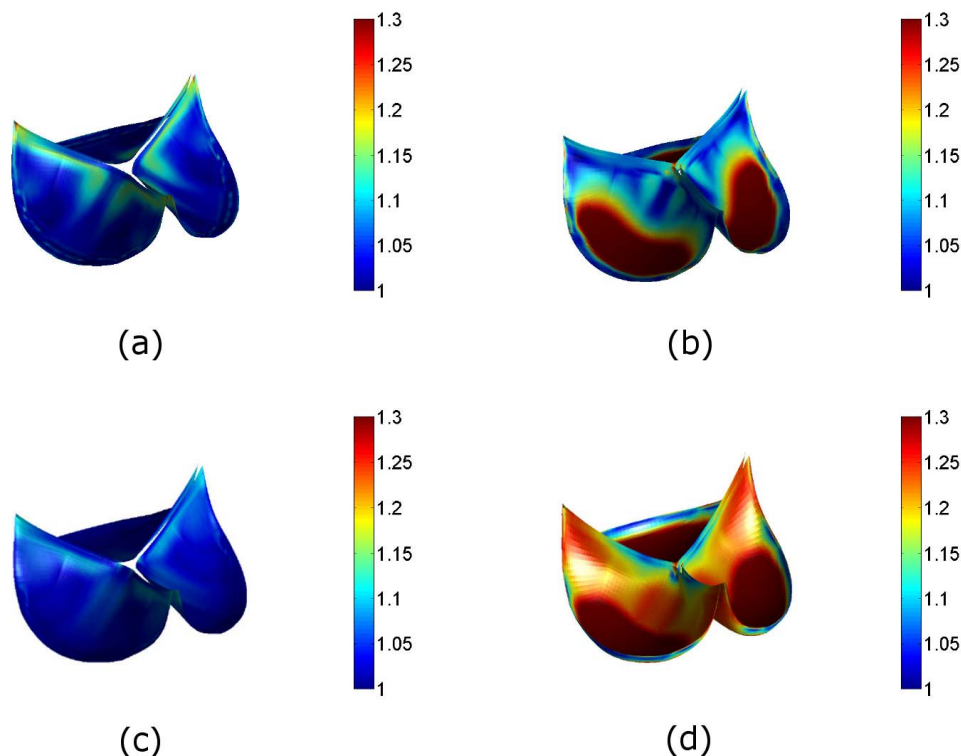
FIGURE 2.7: Principal stretch [-] distribution in valve-shaped electrospun constructs with microstructural features of scaffold 1 (a) and scaffold 2 (b),tissue engineered heart valve (c) and native heart valve (d).

capability of the model was examined using two orthogonal uniaxial tensile experiments and predicting the biaxial behavior of the isotropic scaffold using the material parameters estimated on the anisotropic one. Next to this, the scaffold parameters were used to analyze the deformation of heart valve shaped constructs, and these were compared to tissue engineered and native porcine heart valves.

The use of a closed-form constitutive model at the macro-scale reduces the computational cost to build the stiffness matrix proportional to the number of Gauss integration points used at the macroscopic scale, when compared to the full multi-scale coupling methods described previously (Kouznetsova et al., 2001, Breuls et al., 2002). The trade-off though, is a reduced flexibility. In the current approach the microstructure may not evolve as a function of time, it is less obvious how to account for spatial variations in the microstructure, and for each variation in the microstructure the macroscopic material parameters have to be identified independently. At the microstructural level a relatively simple fiber architecture was adopted, employing straight fibers. It accounts for fiber diameter, fiber orientation, fiber spacing and some of the mechanical properties,
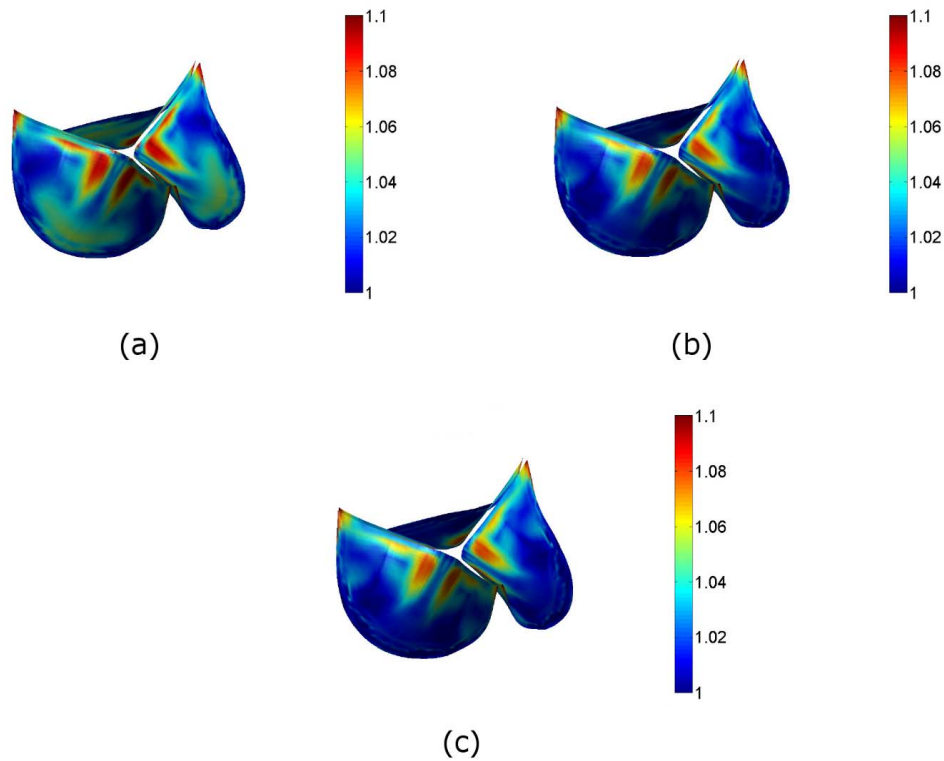
FIGURE 2.8: Predicted stretch distribution within the heart valve-shaped scaffolds with fiber standard deviation $\beta = 0.13$ (a), $\beta = 0.42$ (b) and $\beta = 2$ (c).

but the undulation of the fibers, typical for electrospinning, was not accounted for. Using the fiber mechanical properties identified using the anisotropic scaffold, the mechanical properties of the isotropic scaffold could be predicted with remarkable accuracy, despite the tortuosity of the fibers in the latter configuration. The fiber undulations were implicitly incorporated by choosing an exponential force-stretch relation for the fiber. Yet, the relative fragility of the PCL does not permit elastic deformation of the scaffold beyond 3-4%. At these low stretch levels successive fiber recruitment is less likely, and therefore an exponential stress-strain response of the scaffold is not observed. The actual fiber geometry may be incorporated by adopting the image-based approach developed by Amoroso et al. (2011).

The mechanics of heart valve tissue has been explored extensively (Billiar and Sacks, 2000a,b, Driessen et al., 2003, 2005c,a), and provides a good basis for the target properties of the tissue engineered heart valves. The design of an electrospun scaffold that mimics the mechanical properties of a native valve is not straight forward, because the microstructure has a significant impact on the macroscopic behavior. Hence, a discrete detailed model of the microstructure, that accounts

for the structural properties of each single fiber, the topology of the network, and the interactions between the fibers of the network is necessary to enable a rational design of such a scaffold (Stylianopoulos and Barocas, 2007, Stylianopoulos et al., 2008). For the design of a fibrous scaffold a network model that incorporates all the structural information of the network is more accurate than continuum models where fiber interaction is not accounted for (Billiar and Sacks, 2000a,b, Driessen et al., 2005a). It was shown that by adjusting the degree of fiber alignment, the deformation pattern in the scaffold has significant similarity with the deformations observed in a native porcine valve. This happens despite the large differences in the intrinsic fiber stiffness of the PCL fibers and the collagen fibers. Despite the limitations mentioned, the framework described is suitable to investigate the mechanics of a wide range of scaffolds. Therefore, it represents a powerful tool to assist the design of fibrous scaffolds for load bearing tissues.

Chapter 3

Modeling the impact of scaffold architecture and mechanical loading on collagen turnover in engineered cardiovascular tissues

3.1   Abstract

The anisotropic collagen architecture of an engineered cardiovascular tissue has a major impact on its in vivo mechanical performance. The initial scaffold microstructure and mechanical loading determine this evolving collagen architecture. Here we developed and validated a theoretical and computational micro-scale model to quantitatively describe the mechanical properties of engineered constructs when tissue develops in the presence of an electrospun scaffold. Using input from experimental studies we hypothesize that the interplay between scaffold microstructure and mechanical loading influence collagen synthesis and degradation. The mechanical and topological properties of in vitro engineered constructs cultured on isotropic and anisotropic electrospun substrate in static and dynamic loading conditions were evaluated. These results reveal that the formation of tissue layers on top of the scaffold surface influences the mechanical anisotropy on the tissue cultured on an anisotropic scaffold. Results show that the micro-scale model can successfully capture the collagen arrangement and the mechanical behavior of isotropic statically cultured constructs. Furthermore, it can predict the mechanical behavior of constructs cultured under static and cyclic loading conditions on isotropic and anisotropic scaffolds. Contact guidance by the scaffold, and not applied load, dominates the collagen architecture. Therefore, when the collagen grows inside the pores of the scaffold, pronounced scaffold anisotropy guarantees the development of a tissue that mimics the mechanical anisotropy of the native cardiovascular tissue.

3.2   Introduction

Tissue engineering is a promising technique to produce living replacements for biological tissues, able to repair, grow and remodel under biochemical and mechanical cues (Langer and Vacanti, 1993). Tissue engineering involves the seeding of cells onto a porous degradable scaffold and subsequent conditioning in a bioreactor system. The cells produce and organize the extracellular matrix that defines the load bearing properties of the tissue once the scaffold has degraded (Walters and Stegemann, 2013). Previous studies on native connective tissues have shown that the morphology of the collagen network is responsible for the mechanical properties in terms of stiffness and load bearing capability of the tissue

(Billiar and Sacks, 2000a, Driessen et al., 2005c). Analogously, the morphology of neo-formed tissue engineered collagenous networks is of fundamental importance, since it determines the mechanical properties and functionality of the constructs (Driessen et al., 2007).

The formation of collagen networks in tissue engineered constructs is a complex process. A number of load-driven remodeling mechanisms influence the reorganization of the collagen network over time. In cardiovascular tissues, the fibers mainly remodel along and in between the principal loading directions (Driessen et al., 2005c, Dahl et al., 2008) and the cells play an active role in the remodeling process (Soares et al., 2011, van Vlimmeren et al., 2012). When fibroblast-like cells are seeded onto a fibrous scaffold and cultured under pulsatile conditions, they align preferentially along the fibers of the scaffold, and produce collagen along the same direction (Hwang et al., 2009, Niklason et al., 2010). The neo-formed collagen fibers stay in close contact with the scaffold (Eckert et al., 2011), indicating that the contact guidance by the scaffold is a crucial factor in early stages of the development of the collagen network. Next to collagen synthesis, also enzymatic degradation of the collagen fibers takes place. The degradation of collagen fibers happens according to strain-dependent kinetics. When strain is applied to a collagen gel, the fibers that are oriented in the direction of the strain will degrade slower than the fibers in all the other directions (Bhole et al., 2009, Hadi et al., 2012).

Although the phenomena that drive the collagen reorganization in engineered tissues have been studied extensively, it is not known to what extent each of them influences the newly-formed tissue. Recently, de Jonge (2013) demonstrated that contact guidance by a microfiber electrospun scaffold dominates over strain-driven collagen formation under static as well as under cyclic loading conditions. In addition, due to collagen turnover, the mechanical properties of the neo-tissue will evolve over time. These findings indicate that the structure of the scaffold can be exploited to obtain anisotropic native-like load-bearing tissues. However, a systematic characterization of the morphology and the mechanics of the tissue engineered constructs resulting from scaffolds with different initial morphologies and subjected to different loading conditions (static and cyclic) is missing. The aim of the present paper is to investigate the mechanical properties of engineered tissues growing on fibrous substrates with different fiber distribution and subjected to static and cyclic loading conditions. This way the relative contribution of

substrate topology and (cyclic) strain to tissue turnover and tissue mechanical behavior is explored, with the ultimate aim to mimic the mechanical anisotropy that characterizes cardiovascular tissues.

We developed a micro-scale model describing the interaction between the scaffold architecture and the evolving collagen network, as well as the mechanical properties of the neo-tissue in response to dynamic loading conditions. The biaxial mechanical properties of the constructs were analyzed experimentally using both isotropic and anisotropic scaffolds. The scaffolds were composed of a biodegradable elastomer (PCL-bisurea) (Wisse et al., 2006), and were manufactured using electrospinning. The computational model captured the key experimental observations.

3.3 Materials and Methods

3.3.1 Micro-scale growth and degradation model

A representative area element (RAE) of a tissue engineered construct is built. The RAE is composed of a network of scaffold fibers and a network of collagen fibers. The initial fiber distributions are described by the fiber volume fractions $\phi_{f,c}^i$ and $\phi_{f,s}^i$ along the directions γ_i with the periodic version of the normal distribution function introduced by Gasser et al. (2006) and adapted by Driessen et al. (2008):

$$\phi_{f,c}^i = A_c \exp\left[\frac{\cos\left(2\left(\frac{\gamma_i}{h_c}-\alpha_c\right)\right)+1}{\beta_c}\right] \tag{3.1}$$

$$\phi_{f,s}^i = A_s \exp\left[\frac{\cos\left(2\left(\frac{\gamma_i}{h_s}-\alpha_s\right)\right)+1}{\beta_s}\right] \tag{3.2}$$

with α the main orientation, β the dispersion parameter, and h the frequency scaling factor. The subscripts c and s refer to collagen or scaffold parameters, respectively. The parameters A_s and A_c are calculated in order to equal the total volume fractions $\phi_{f,c}$ and $\phi_{f,s}$ respectively. The fibers are equally spaced in a

discrete way with an angular interval $\Delta\theta=10°$ between -90° and 90° -$\Delta\theta$. The initial collagen volume fraction is supposed to be low and isotropically distributed ($\alpha_c=0°$, $\beta_c=$3e+4), as in principle cells can produce collagen in every direction. Over time collagen fibers are developing through a combination of cell-mediated collagen synthesis and enzymatic degradation. Therefore, the turnover rate of the fiber radius $\frac{dr(t)}{dt}$ of a fiber in the direction γ_i is the difference of the radius growth rate $\mathcal{S}$ and the radius degradation rate $\mathcal{D}$

$$\left(\frac{dr(t)}{dt} (\gamma_i) \right) = \mathcal{S} - \mathcal{D}. \tag{3.3}$$

On the basis of previous experimental results, the growth of the fibers along the fiber direction γ_i is assumed to be ruled by the fiber radius growth rate, defined as

$$\mathcal{S} = k_1 \cdot \frac{\phi_s(\gamma_i)}{\phi_{tot,s}} \cdot \frac{(\phi_{max} - \phi_c(t))}{\phi_{max}} \cdot \frac{\exp\left(\frac{k_2}{\beta_s}\right)}{2\pi r(\gamma_i, t) \, l(\gamma_i)} \tag{3.4}$$

where $\phi_s(\gamma_i)$ represents the scaffold fiber volume fraction along the direction γ_i, $\phi_{tot,s}$ the total scaffold volume fraction. A linear function of the partial scaffold volume fraction, $\frac{\phi_s(\gamma_i)}{\phi_{tot,s}}$, indicates that the contact guidance with the fibers of the scaffold plays a major role in the distribution of the developing collagen fibers. This assumption is based on the work of Niklason et al. (2010), showing that, in the presence of a PGA electrospun scaffold, bundles of fibers grow along the direction of the fibers of the microfibrous scaffold. ϕ_{max} is the maximum collagen volume fraction, which is set to a value of 0.15 (estimated as possible collagen volume fraction after two weeks of tissue culture from the work of van Geemen et al. (2012) and Mol (2005)), and ϕ_c is the current total collagen volume fraction. The exponential of β_s indicates that the scaffold anisotropy influences the amount of collagen that is produced (Lee and al, 2005, Teh et al., 2013).

Furthermore, the inverse proportionality with the current radius $r(\gamma_i)$ and the fiber length $l(\gamma_i)$ indicates that the variation of fiber radius in each direction decreases with increasing radius. The constant value k_1 is intended to represent the mean synthetic activity of the cells.

TABLE 3.1: Model parameters.

parameter	value
k_1	8.3e-7 µm/h
k_2	0.33 [-]
k_3	3.78 µm/h
k_4	3.09e-6 µm/h
k_5	2.1e-2 [-]
ϕ_{max}	0.15

As long as the fiber has a positive radius, the enzymatic degradation rate along the direction γ_i is described by means of a strain-based Michaelis-Menten law (Menten and Michaelis, 1913), which is often used to describe enzyme kinetics. It is null when the radius becomes null.

$$\mathcal{D} = \begin{cases} k_3 - k_4 \cdot \frac{\left(\lambda_f(\gamma_i)-1\right)}{\left(k_5+\lambda_f(\gamma_i)-1\right)}, & r\left(\gamma_i\right) > 0 \\ 0, & r\left(\gamma_i\right) \leq 0 \end{cases} \tag{3.5}$$

where $\lambda_f\left(\gamma_i\right)$ represents the fiber stretch along the direction γ_i, and k_2, k_3 and k_4 are the parameters that rule the degradation kinetics.

The degradation that occurs when the strain is null (k_3) is defined on the basis of the experiments performed by Bhole et al. (2009) as described by Hadi et al. (2012). The parameters of the degradation law are defined in such a way that the curve reaches the quasi-plateau situation at 4% strain, as described by (Huang and Yannas, 1977).

All the model parameters that are used in the current work to describe collagen synthesis and degradation are reported in Table 3.1.

The growth and degradation rules described are implemented in a Forward Euler formulation over a total time interval of two weeks. At each time step the growth and degradation rate are calculated and the current radius of the j_{th} fiber along the i_{th} direction γ_i is updated

$$r_j\left(\gamma_i, t+1\right) = r_j\left(\gamma_i, t\right) + \left(dr\left(\gamma_i, t\right)\right)_g - \left(dr\left(\gamma_i, t\right)\right)_d. \tag{3.6}$$

The volume variation of the j_{th} fiber is

$$\frac{dV_j}{dt}\left(\gamma_i\right) = \pi \cdot \left(r_j\left(\gamma_i, t+1\right)^2 - r_j\left(\gamma_i, t\right)^2\right) \cdot l\left(\gamma_i\right). \tag{3.7}$$

The updated total collagen fiber volume takes into account the volume variation along each direction

$$V_c\left(t+1\right) = V_c\left(t\right) + \sum_{i=1}^{N} w_i \cdot dV_j\left(\gamma_i, t\right) \tag{3.8}$$

where w_i is the number of fibers in the i_{th} direction. Finally, the updated collagen volume fraction

$$\phi_c = \phi_c\left(t+1\right) = \frac{V_c\left(t+1\right)}{V_{RAE}} \tag{3.9}$$

is used to calculate the growth rate at the next step.

3.3.2   Finite element model

The micro-scale model is made of a RAE composed of two fibrous structures embedded in an isotropic matrix (Fig. 3.1). In the model one network mimics the fiber distribution that can be observed from a scanning electron microscopy (SEM) image of an electrospun scaffold. The other network represents a collagen network, which is supposed to be initially isotropic, as in principle collagen fibers can assemble in all directions. For both networks a discrete distribution function is chosen (Eq. 1 and 2). An exponential relationship is assumed to relate the micro-scale scaffold fiber stress $\psi_{f,s,m}$ and stretch $\lambda_{f,s,m}$ for positive stretches:

$$
\psi_{f,s,m}^i = \begin{cases} h_{1,s}\lambda_{f,s,m}^2 \left[e^{h_{2,s}\left(\lambda_{f,s,m}^2 - 1\right)} - 1 \right], & \lambda_{f,s,m} \geq 1 \\ 1, & \lambda_{f,s,m} < 1 \end{cases}.
\tag{3.10}
$$

The same is used to relate the micro-scale collagen fiber stress $\psi_{f,c,m}$ and stretch $\lambda_{f,c,m}$ for positive stretches:

$$
\psi_{f,c,m}^i = \begin{cases} h_{1,c}\lambda_{f,c,m}^2 \left[e^{h_{2,c}\left(\lambda_{f,c,m}^2 - 1\right)} - 1 \right], & \lambda_{f,c,m} \geq 1 \\ 1, & \lambda_{f,c,m} < 1 \end{cases}
\tag{3.11}
$$

where h_1 and h_2 are a stress-like and dimensionless parameter respectively and subscripts c and s refer to collagen or scaffold parameters respectively.

The nonlinearity of the material law is chosen to account for the undulations in the electrospun fibers and collagen fibers that is otherwise not represented in the model.

The discrete representation of the electrospun fibrous network was generated with the method previously developed by Argento et al. (2012). A similar method is used to describe the discrete collagen network. A Matlab (The Math-Works, Natick, MA) algorithm evaluates from the fiber volume fraction the number of fibers in each direction. In each direction, the collagen fibers are displaced along with the scaffold fibers. The remaining collagen fibers are displaced with a random distance from the others in the considered direction. All the microstructural properties of scaffold and collagen network (diameter, volume fraction, interconnectivity, orientation) can be varied. Connections between the elements of each network are set, to enable transmission of forces. An interconnection between elements is defined as a node placed at the intersection of the two fibers. A defined percentage of all the possible fiber intersections are randomly picked as fiber interconnections.

The finite element microscopic problem was solved by using the software Abaqus (Simulia, Providence, RI). A user material (UMAT) was developed to implement the growth and degradation laws described in Section 3.3.1.
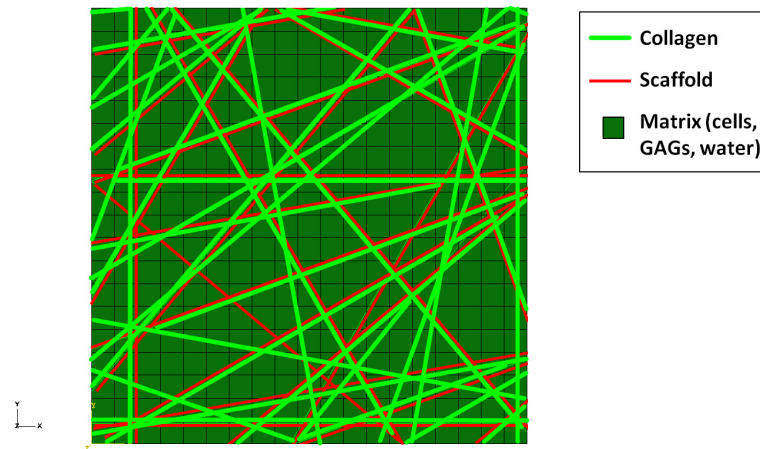
FIGURE 3.1: Schematic of a representative area element (RAE), composed of a network of scaffold fibers (red) and a network of collagen fibers (light green) embedded in a continuum matrix (dark green).

3.3.3   Engineered constructs

Two different PCL-bisurea (Wisse et al., 2006) scaffolds were produced to perform the model validation. The scaffolds were electrospun in a climate-controlled electrospinning cabinet (IME Technology, Eindhoven, NL) equipped with a 0.6 mm diameter capillary and a distance of 15 cm between the capillary and the 5 cm diameter rotating target drum. 20% (wt) PCL-bisurea was dissolved in chloroform (CHCl_3) and electrospun with a flow rate of 25 µL/min and a voltage of 18 kV applied. Scaffold 1 was spun with a rotational speed of 100 rpm (corresponding to a surface speed of 0.52 m/s), scaffold 2 was spun at 2500 rpm (corresponding to a surface speed of 13 m/s). The thickness of the two scaffolds was 135 µm and 125 µm, respectively. The image processing software ImageJ was used to obtain the average fiber diameter and the fiber distribution from SEM (FEI, Netherlands) images.

Samples of each of the two scaffolds were glued over a flexible membrane of Bioflex well plates (Flexcell International, Hillsborough, NC, USA) as described by de Jonge (2013). Each construct was seeded with myofibroblasts, and cultured for two weeks. We tested two different scaffold configurations, one with isotropic and one with anisotropic fiber distribution. Five experimental conditions were investigated: biaxial constrain applied to the isotropic scaffold (Fig. 3.2 a), biaxial constrain applied to the anisotropic scaffold (Fig. 3.2 b), uniaxial 10% dynamic strain at 1 Hz frequency applied to the isotropic scaffold (Fig. 3.2 c), uniaxial 10%

dynamic strain at 1 Hz frequency applied to the anisotropic scaffold (with uniaxial strain applied along and perpendicular to the fiber direction) (Fig. 3.2 d and e). Dynamic straining was started 30 minutes after seeding the cells into the scaffold, so that the cells could feel the strain immediately, before they start producing matrix.
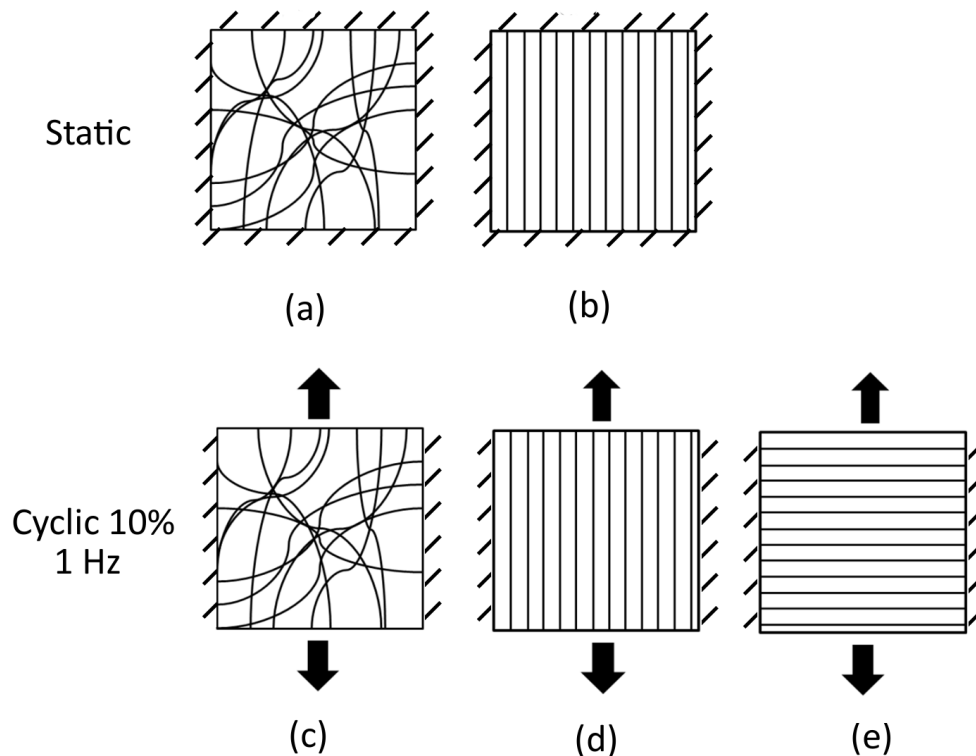
FIGURE 3.2: Schematic overview of the experimental design. a) Isotropic scaffold with biaxial constrain applied, b) anisotropic scaffold with biaxial constrain, c) isotropic scaffold with uniaxial 10% dynamic strain applied, d) anisotropic scaffold with uniaxial 10% dynamic strain applied parallel to the fiber direction, e) anisotropic scaffold with uniaxial 10% dynamic strain applied perpendicular to the fiber direction

After two weeks of culture, the tissue engineered samples were cut loose from the membranes and left to rest for half an hour. Before detaching the samples from the membrane, a rectangular shape was drawn on each statically cultured sample with a tissue felt pen (Fig. 3.3). After resting time, the change in size of the edges of the rectangle was measured, in order to quantify tissue compaction.

Chloramin-T assay (Huszar et al., 1980) was used to evaluate the hydroxiproline content, which was then converted to collagen content. The collagen distribution within the constructs was evaluated with a CNA staining technique (Krahn et al.,

2006) using a Confocal Laser Scanning Microscope (Carl Zeiss, Oberkochen, Germany) scanning from the top and from the bottom of the samples.

After culture, one sample for each group was soaked for ten minutes in a bleach product to remove the tissue, and then washed for three times in water. After drying, the scaffold samples were imaged with SEM.
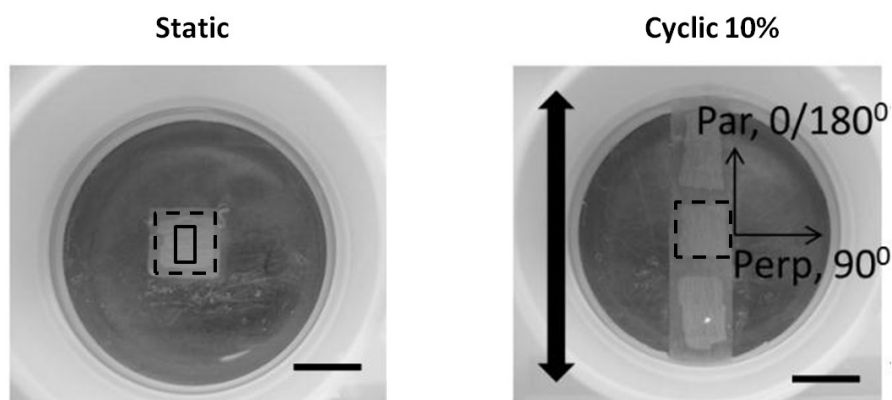
FIGURE 3.3: Experimental system. The constructs were cultured either statically (left) or cyclically (right). In the statically cultured samples the part in the black square with solid line was used to measure tissue compaction. In the statically and cyclically cultured samples the part in the black square with the dashed line was used for tissue analysis (Chloramin-T assay and mechanical testing). For the anisotropic scaffolds, the cyclic strain is applied in direction parallel and perpendicular to the scaffold fibers. Arrows indicate directions of applied cyclic strain. The scale bar indicates 1 cm.

3.3.4   Mechanical testing

Biaxial tests were conducted on cell-free scaffolds as well as engineered constructs at the end of the two week culture time using a Biotester (CellScale Biomaterial Testing).

Three samples per scaffold were soaked in ethanol, kept in water in the incubator for 24 h, and tested in wet conditions at 37°C. The samples were stretched with a biaxial and then uniaxial stretch in both directions at 10%-20%-30% (Fig. 3.4), and the results were averaged for each type of scaffold.

The same protocol was used to test the engineered samples. For each group two samples were tested.
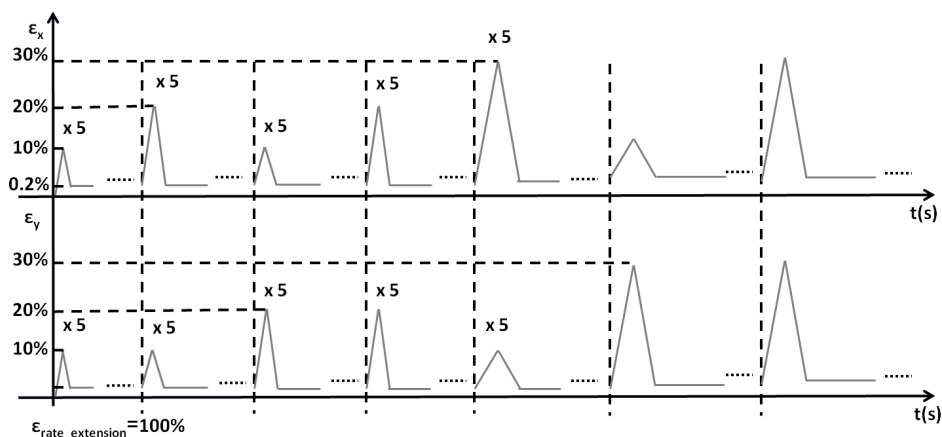
FIGURE 3.4: Strain pattern used for biaxial tests. The strain pattern consists in 5 cycles of equibiaxial strain and uniaxial strain in the x and the y direction at 10%, 20% and 30% strain. A prestrain of 0.2% is applied. A strain rate of 100% strain/min is used.

3.3.5   Scaffold and collagen computational characterization

Scaffold 1 shows fibers with an average diameter of 5.6 µm, a fiber volume fraction of 27% and an isotropic fiber distribution (β=13.7). Scaffold 2 is composed of fibers with an average diameter of 4.6 µm, a fiber volume fraction of 33% and an anisotropic fiber distribution (β=0.65) (Fig. 3.5).

The microstructural fiber parameters of the anisotropic scaffold $h_{1,s}$ and $h_{2,s}$ (Eq. 9) were identified using a least squares optimization of the stress-strain curves at 30% biaxial strain, evaluated by using an homogenization procedure (Kouznetsova, 2002) . The same parameters were used to predict the mechanical behavior of the isotropic scaffold.

The collagen volume fractions calculated by Chloramin-T assay (Huszar et al., 1980), in combination with the collagen orientation data from CNA staining, were used to evaluate the constants that describe the collagen turnover kinetics in Eq. 3, using a least square optimization procedure. Parameters k_1 and k_2, that describe the collagen growth, were evaluated on the mechanical data of the statically cultured isotropic and anisotropic constructs. Parameters k_3, k_4 and k_5 , describing the collagen degradation, were estimated using the experimental mechanical data of the biaxial isotropic statically loaded constructs and uniaxial cyclically loaded constructs, with strain applied along the scaffold fibers. All the

TABLE 3.2: Parameters of the fibers constitutive behavior and prestress.

parameter	value
$h_{1,s}$	804.77 kPa/mm^2
$h_{2,s}$	2.77 [-]
$h_{1,c}$	4027.95 kPa/mm^2
$h_{2,s}$	13.54 [-]
E	1 kPa
$\sigma_{prestress}$	116.84 kPa

parameters used in the synthesis and degradation model to simulate the described experiments are summarized in Table 3.1.

The compaction was measured for the constructs cultured with static strain. To account for the compaction, in the finite element framework a prestress was assigned to each collagen fiber. The collagen prestress represents the stress developed by the cells during culture, which leads to compaction. The collagen fiber prestress evaluated by fitting the experimentally measured compaction in an isotropic construct was used to predict the compaction which occurs in an anisotropic statically cultured tissue.

A least square optimization in the isotropic static case was used to determine the parameters $h_{1,c}$ and $h_{2,c}$ (Eq. 10), used to describe the biaxial tensile mechanical behavior of the collagen fibers. The same parameters were used to simulate the tensile mechanical behavior of an anisotropic static and the cyclic constructs. In the simulations a static strain of equivalent magnitude to the maximum amplitude of the applied cyclic strain (10%) was used to simulate an applied cyclic strain. All the microstructural mechanical constants used to simulate scaffold and collagen and the Young moduli E assigned to the linear elastic matrix are reported in Table 3.2.

3.4   Results

3.4.1   Structural characterization of engineered constructs

The Confocal Laser Scanning Microscopy of the samples from the bottom shows that the collagen is deposited mainly on the scaffold fibers and in the scaffold direction more than in between, independently of the applied strain (Fig. 3.5). As most adherent cells seeded onto a microfibrous substrate are known to elongate along the fiber direction (Fioretta et al., 2013) and produce bundles of collagen fibers in their main direction (Wang et al., 2003b, Canty et al., 2004, Richardson et al., 2007), it seems reasonable to assume that the collagen fibers are deposited along the direction of the scaffold fibers. Surprisingly, the Confocal Laser Scanning Microscopy from the top shows the presence of a dense collagen layer on top of the scaffold.

Surprisingly, the Confocal Laser Scanning Microscopy from the top shows the presence of a dense collagen layer on top of the scaffold. In particular, the scaffold anisotropy does not influence the collagen orientation in the top tissue layer neither for static and cyclic strain applied. In all cases, the collagen orientation is variable at different scanning depths throughout the thickness of this layer (Fig. 3.6). However, this study does not focus on understanding and quantifying the phenomena that drive the collagen orientation in the absence of scaffold. The collagen in the top layer assumes a different orientation at different depths. It is assumed that the differently oriented collagen fibers in the top layer globally contribute to the mechanical properties of the construct as an isotropic layer. Therefore the top layer is modeled as an isotropic layer in the simulations.

The collagen volume fractions calculated with Chloramin-T assay for each construct are reported in Table 3.3. Although not statistically tested, higher scaffold anisotropy seems to enhance the production of collagen. In the computations, for each construct 1/3 of the evaluated collagen volume fraction is considered to belong to the thickness of the scaffold, 2/3 to the top tissue layer, which is here assumed to be isotropic. Since it is not possible to split the samples to quantify the amount of collagen belonging to the top layer, these values are not based on experimental measurement. However they have been chosen in order to assign a higher collagen volume fraction to the top layer, which images show

TABLE 3.3: Collagen volume fraction in the engineered tissues.

construct	collagen volume fraction
Isotropic static	3.9%
Anisotropic static	6%
Isotropic cyclic 10%	5.5%
Anisotropic cyclic 10%	6.9%

to be denser than the collagen network formed within the scaffold fibers (Fig. 3.5 and 3.6).

The bare scaffolds, imaged after the culture period, do not show loss of structural anisotropy.

3.4.2 Mechanical behavior

The evaluated structural parameters were used to build a micro-scale model of the two scaffolds. The optimal parameters that characterize the mechanical behavior of the PCL-bisurea scaffold fibers $h_{1,s}$ and $h_{2,s}$ were estimated with reference to the biaxial mechanical behavior of the anisotropic scaffold (Table 3.2). The values were used to predict with good accuracy the mechanical properties of the isotropic scaffold (Fig. 3.7).

The micro-structural features of the scaffold and the collagen networks were used to build the computational model of the isotropic and anisotropic tissue engineered constructs.

In the isotropic statically loaded construct, the model is able to capture a quasi-isotropic compaction (Fig. 3.8), and evaluates an optimized cell prestress associated to each collagen fiber of 116.84 kPa (Table 3.2). The optimized cell prestress was used to model compaction in the anisotropic construct. In the anisotropic static construct, compaction is bigger in the direction parallel to the scaffold fiber main orientation (Fig. 3.8).

Taking into account a top isotropic collagen layer, the simulation at 30% equibiaxial strain of the isotropic scaffold after compaction desribes correctly the isotropic mechanical properties of the construct. This allowed the estimation of
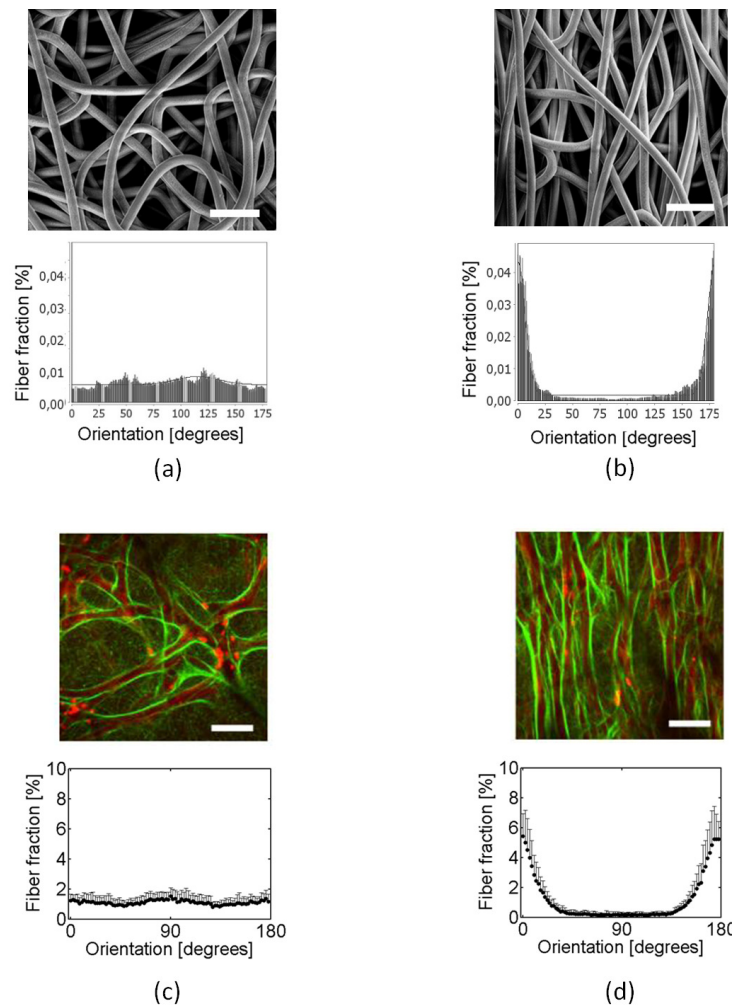
FIGURE 3.5: Representative SEM pictures of the isotropic (a) and anisotropic (b) scaffold, with respective fiber distribution. Representative confocal microscopy images of tissue engineered constructs cultured in isotropic (c) and anisotropic (d) scaffold, with respective collagen fiber distribution, imaged from the bottom of the construct. In figures (c) and (d) the collagen is represented in green, and the scaffold fibers are represented in red. The scale bar represents 50 µm.

the collagen material properties $h_{1,c}$ and $h_{2,c}$ (Table 3.2). With these parameters, the equibiaxial strain of the anisotropic construct and of the cyclically strained constructs could be predicted. All the constructs show an exponential-like stress-strain curve, and a higher stiffness than the bare scaffolds, implying the formation of tissue . The isotropic statically loaded construct shows isotropic mechanical properties, while the isotropic cyclically loaded construct shows a slightly higher stiffness in the direction of the applied stress, due to strain protection from degradation. All the simulations of constructs cultured in the
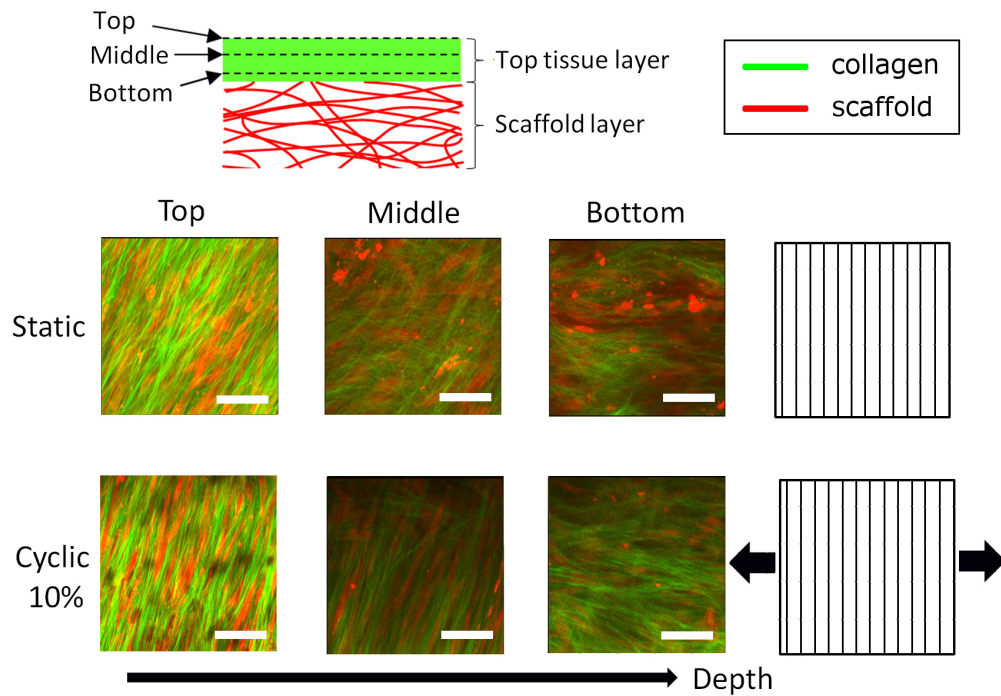
FIGURE 3.6: Pictures of the top collagen layer throughout the thickness of the layer. On the first row a tissue engineered construct cultured on an anisotropic scaffold in static conditions is represented, on the second row a construct cultured in cyclic conditions with the strain perpendicular to the fiber direction is represented. The scale bar represents 50 µm.
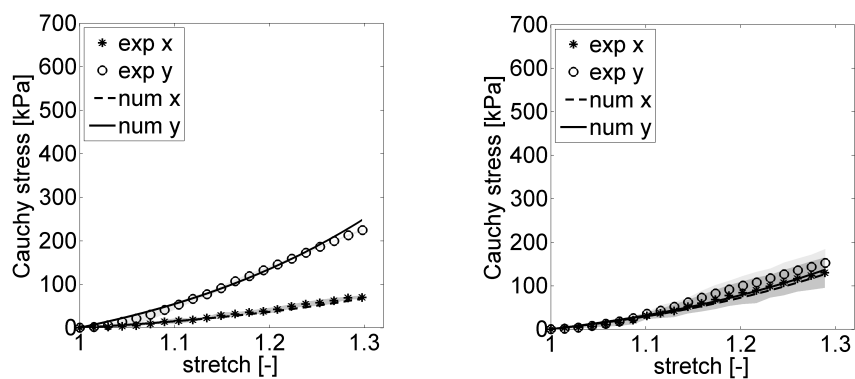
FIGURE 3.7: Fit of the experimental equibiaxial mechanical behavior for the anisotropic scaffold (left). Predicted biaxial mechanical behavior of the isotropic scaffold (right) by using the optimal material parameters of the anisotropic scaffold.
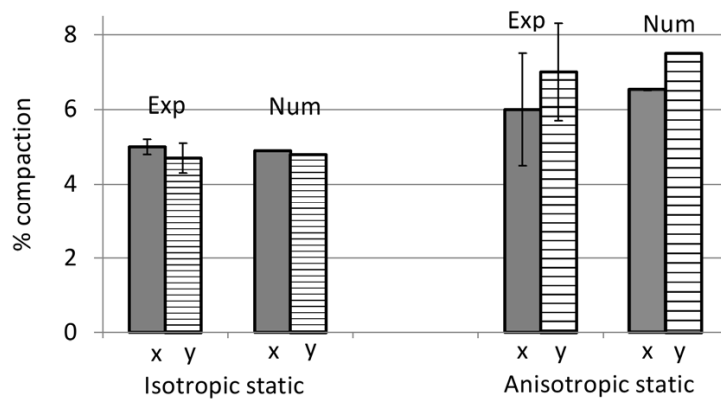
FIGURE 3.8: Compaction in tissue engineered constructs cultured on isotropic and anisotropic scaffold in static conditions. In the anisotropic case the y direction indicates the direction of main fiber orientation. The experimental data are averaged from two samples.

presence of cyclic strain show a slight underestimation of the stiffness in the strain direction. The tissue engineered constructs cultured on anisotropic scaffold with strain perpendicular to the fibers shows an isotropic mechanical behavior, while the predicted mechanical behavior is more anisotropic, probably due to a dominant orientation in the collagen top layer (Fig. 3.9).

All the tissue engineered constructs cultured with an anisotropic scaffold show a decrease of the anisotropy of the initial scaffold and a more isotropic behavior. This is the consequence of the presence of a dense collagen layer with variable collagen orientation throughout the layer thickness above and below the scaffold. When the contribution of the top layer is neglected in the simulations, the constructs show structural and mechanical anisotropy (Fig. 3.10).

3.5   Discussion

The present study investigated the possibility of relating the structural properties of engineered constructs to their mechanical behavior. For this, a mathematical model of collagen turnover was formulated. The model was implemented in a FE micro-scale model of a tissue engineered construct, accounting for the contribution of the scaffold and of the collagen network. The parameters that define the mechanical properties of PCL-bisurea scaffold fibers and collagen fibers were estimated. Two scaffolds, one isotropic and one anisotropic, were used to test
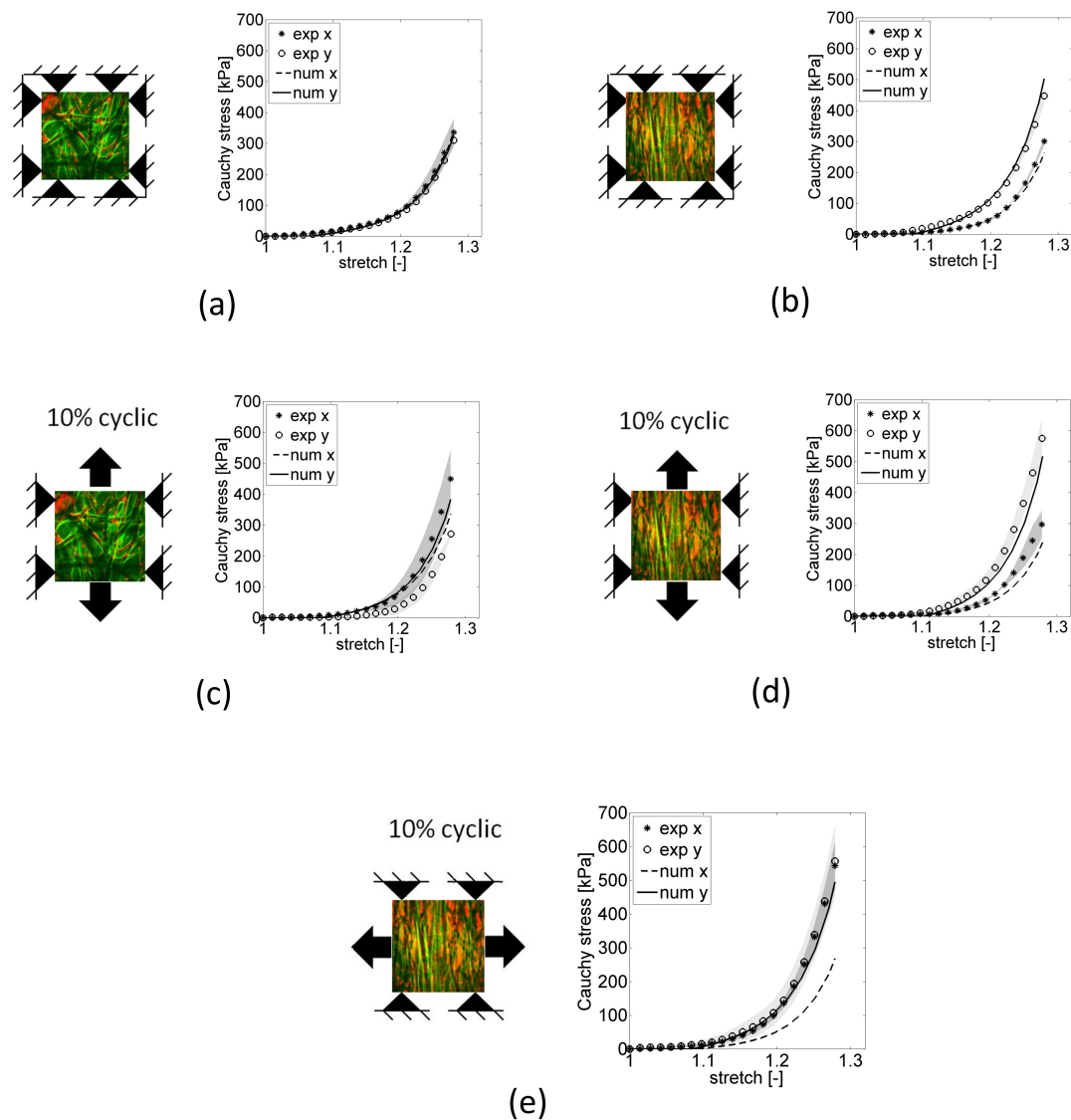
FIGURE 3.9: Fit of the experimental equibiaxial mechanical behavior of the isotropic static tissue engineered construct (a). The material parameters estimated in (a) are used to predict the equibiaxial mechanical behavior of tissue engineered constructs characterized by anisotropic scaffold with static strain applied (b), isotropic scaffold with cyclic strain applied (c) and anisotropic scaffold with cyclic 10% strain applied parallel (e) and perpendicular (e) to scaffold fibers.
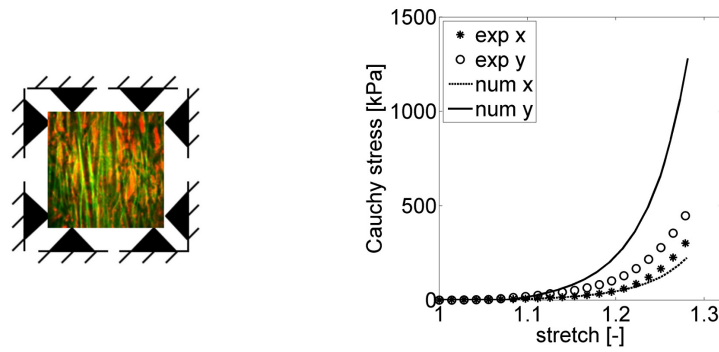
FIGURE 3.10: Predicted biaxial mechanical behavior of an anisotropic static tissue engineered construct, when it is assumed that the entire collagen volume fraction estimated follows the rules for collagen turnover within the scaffold fibers.

the approach. The structural properties of the scaffolds and the total volume fraction of the collagen network were used to evaluate the collagen distribution after two weeks of culture under different loading conditions. The model was used to simulate the biaxial mechanics of engineered constructs cultured over isotropic and anisotropic scaffold in static and cyclic loading conditions. The formation of top tissue layers with variable collagen distribution was taken into account in the simulations. Finally, the model was used to describe the mechanics of a tissue engineered construct without any top tissue layer. Its mechanical behavior resembles the anisotropy that characterizes cardiovascular tissues, as it is described by Driessen et al. (2007).

The presented model accounts for a number of phenomena that have been described in previous studies, like contact guidance by the scaffold fibers (Niklason et al., 2010, de Jonge, 2013), enhanced collagen deposition due to scaffold anisotropy (Lee and al, 2005, Teh et al., 2013) or use of cyclic load (Boerboom et al., 2008, Rubbens et al., 2009b), and load protection from enzymatic degradation (Huang and Yannas, 1977, Wyatt et al., 2009). It should be noticed that the described phenomena only occur when microfibrous scaffolds are used. In contrast, cells seeded on nanofibrous scaffolds have been shown to spread over more fibers, following the fibrous pattern and responding to the applied strain (Erisken and al, 2013, Subramony et al., 2013). At these conditions, the model is able to predict collagen distributions in agreement with experimental findings (Niklason et al., 2010, de Jonge, 2013).

For isotropic and anisotropic constructs with static and cyclic strain the model

successfully describes that the collagen mainly aligns along the scaffold fibers, accounting for the dominant effect of contact guidance. In addition, the model captures the phenomenon that extensional strain protects the collagen fibers against degradation.

However, the collagen layer that grows on top of the scaffold is, for simplicity, described as isotropic. The developed model does not intend to describe the phenomena that drive the collagen turnover in absence of scaffold. Moreover, images through the thickness of the top layer do not show a clear trend in the collagen orientation, but highly oriented collagen in different direction at different image depths. Therefore, in this layer the complex load driven phenomena that have been shown to drive collagen orientation in 3D constructs (Foolen et al., 2012) are not accounted for. For these reasons, the surface layers are not quantified but approximately hypothesized to be isotropic, as sum of the contribution of fibers in different directions. In particular, the lack of strain protection of collagen in this layer might be considered partly responsible for an underestimation of the mechanical performance in the strain direction in all the loaded constructs.

In the presence of a scaffold, the deposited collagen follows the surface of the scaffold fibers. Images of the tissue taken with confocal microscopy do not clearly show whether the collagen is deposited on and around the fibers or along them (de Jonge, 2013). However, Niklason et al. (2010) report nonlinear optical microscopic (NLOM) images of engineered tissues showing bundles of collagen fibers aligned with scaffold fibers. Therefore, it is more reasonable to hypothesize that the cells that elongate by contact guidance in the fiber direction (Fioretta et al., 2013, de Jonge, 2013) produce bundles of fibers coaxial with the scaffold fiber, more than around it (Wang et al., 2003b, Canty et al., 2004, Richardson et al., 2007). This might indicate that, in case of an aligned scaffold, the prevalence of collagen along the main direction of the scaffold fibers should increase the anisotropic mechanical properties of the constructs. Nevertheless, the constructs that are cultured on anisotropic scaffold substrates show a lower anisotropy than their initially bare scaffold. By imaging the scaffold after culture, it was verified that the scaffold does not lose its structural integrity after two weeks of culture, thus losing the characteristic anisotropy. Furthermore, the amount of compaction was investigated to verify whether different compaction in the two straining direction might cause a different initial straining point. Nevertheless, the measured compaction, between 5% and 8%, cannot explain alone the decrease of an initially

pronounced anisotropy. Finally, the presence of the top layer with variable collagen orientation and thickness comparable to the scaffold thickness was observed. This was considered to be the main responsible factor for the poorly anisotropic response of the constructs.

In conclusion, the developed model can successfully describe the collagen distribution and the mechanical properties of an engineered tissue cultured on an isotropic electrospun scaffold in static conditions, when the total collagen content of the construct is given. Furthermore it can predict the collagen distribution and the mechanical properties of the engineered constructs resulting from isotropic and anisotropic scaffolds when static and cyclic loading conditions are applied.

The dominance of contact guidance over strain suggests that the mechanical anisotropy that characterizes cardiovascular tissue can be mimicked when an anisotropic scaffold is used. However, it is necessary to verify that cells penetrate well into the scaffold, and avoid the formation of superficial collagen layers, whose architecture might decrease the mechanical anisotropy of the construct.

Chapter 4

Influence of substrate geometry on cell contact guidance

4.1   Abstract

Contact guidance originating from topographical cues is a powerful mechanism to align cells on substrates and in three dimensional fibrous environments, and even has been shown to overrule cyclic strain cues. The mechanism of contact guidance is still unclear and a better understanding is necessary in order to control cell and collagen orientation in engineered tissues. This study aims at understanding the intracellular mechanisms that occur when the cells respond by contact guidance to the topology of the substrate electrospun fibers. In this study, we use a recently developed computational framework to model the tension-driven development of stress fibers in cells spread over a flat substrate and on electrospun fibers with different diameters in the micrometer range. An order parameter is defined to indicate the degree of alignment of the actin stress fibers with the substrate. Simulations show that cells are better able to develop high stresses and aligned bundles of stress fibers when they are spread on the substrate than when they maintain a more spherical shape. The order parameter correlates well with experimental observations on cell spreading and alignment with small diameter fibers. A high order parameter is associated to spread and aligned cells that are generally observed in in vitro experiments.

4.2   Introduction

In vitro culture systems have shown that cells are able to respond to mechanical cues such as strain, flow and substrate stiffness. 2D cyclically cultured cells orient perpendicularly to the direction of an applied cyclic strain. The tendency of the cells to orient perpendicularly to the applied strain is called strain avoidance (Wang and Grood, 2000, Wang et al., 2003a, Loesberg et al., 2005, Lam et al., 2008, Yeong et al., 2010). This behavior is lost when the Rho-associated protein kinase (ROCK), that regulates the polymerization of the stress fibers, is inhibited (Kaunas et al., 2005). In uniaxially constrained 3D microtissues and 3D gels cells orient along the direction of an applied static or cyclic strain (de Jonge et al., 2013, Foolen et al., 2012). However, when a biaxial constraint is used and cyclic strain is applied in one direction, cells show strain avoidance unless the collagen network is too dense to allow for cellular reorientation (Foolen et al., 2012).

The phenomenon of contact guidance can be clearly observed when cells are exposed to a micro-scale patterned substrate. In this case the cell behavior is dominated by the substrate topography. Fibroblast cells orient in the direction of the 2D microgrooves where they are cultured, independently of the externally applied strain (Loesberg et al., 2005). Similarly, in 3D tissue engineered constructs using microfibrous electrospun substrates, the cells clearly orient along the fiber direction or spread at the intersection of two fibers (Fig. 4.1) (Bashur et al., 2009, Lowery et al., 2010, Fioretta et al., 2013). Fibroblast cells are able to feel the guidance of substrate grooves having a width of 5-10 µm, and the depth of the grooves plays a significant role in cell alignment (Loesberg et al., 2005). This size is comparable to the size of the fibroblast cells (Freitas, 1999). In this case the substrate micro-architecture overrules the applied strain. In addition, the organization of the stress fibers has been found to vary depending on the type of cells. Fioretta et al. (2013) showed that, on fibers with diameter above 5 µm, Endothelial Colony Forming Cells (ECFCs) elongate and develop long stress fibers in the direction of the scaffold fiber (Fig. 4.1), while Human Umbilical Vein Endothelial Cells (HUVECs) wrap around the fiber and develop fibers aligned circumferentially to the scaffold fiber (Fig. 4.1). Furthermore, cell nuclei present a more flat geometry in ECFCs and a more spherical geometry in HUVECs.

This principle does not hold in exactly the same way when the architecture of the substrate is in the nanometer range. In that case the size of fibroblast cells is considerably bigger than the size of the substrate structure. Cells can spread over more nanogrooves or nanofibers, being able to feel the substrate texture, but spreading more uniformly over the substrate (He et al., 2005, Ma et al., 2005, Badami et al., 2006, Fioretta et al., 2013).

Understanding the response of the cells to substrate topology and the ability to control the cell distribution and orientation is essential in tissue engineering applications. From previous studies it is clear that the cells are able to reorient the collagen (Stopak and Harris, 1982), and produce collagen in their main direction (Birk and Trelstad, 1984, Trelstad and Birk, 1985, Wang et al., 2003b, Canty et al., 2004, Richardson et al., 2007). The collagen is the main load bearing component of a soft tissue, and therefore its architecture determines the mechanical properties of the tissue (Billiar and Sacks, 2000a, Driessen et al., 2005a). Although the behavior of the cells with respect to their environment is currently broadly studied, it is not fully understood what are the mechanisms that cause the cells to align over a
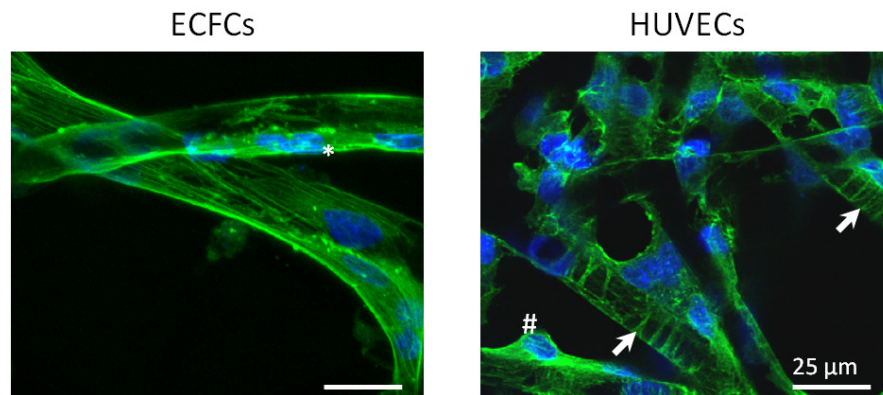
FIGURE 4.1: Immunofluorescent images of ECFCs and HUVECs cultured on PCL electrospun scaffolds with an average fiber diameter of 11 µm. Cell cytoskeleton is stained in green (phalloidin) and nuclei in blue (DAPI). ECFCs cytoskeleton is aligned along the scaffold fiber, with the nucleus flattened on the fiber (*). HUVECs, instead, displayed cytoskeleton filaments organized around the scaffold fiber (white arrows) and a rounded nucleus (#) (Fioretta et al., 2013).

patterned substrate. In particular, in the last decades fibrous scaffolds substrates have been largely used for cardiovascular tissue engineering applications (Mol, 2005, Courtney et al., 2006, Niklason et al., 2010, van Vlimmeren et al., 2011, Ionescu and Mauck, 2012, Chainani et al., 2013). Therefore, in order better control the development of cardiovascular replacement tissues, it is necessary to understand the mechanical principles that govern the interaction between the cells and their fibrous substrate.

A number of models have been proposed (Deshpande et al., 2007, Vernerey and Farsad, 2011, Obbink-Huizer et al., 2013) to predict the stress fiber evolution in response to external mechanical stimuli. Here we investigate if the model developed by Obbink-Huizer et al. (2013) can shed light on the interaction between a single cell and surface topology, by using a geometrically realistic representation of the cell and the substrate. These models are characterized by an evolution law for the actin stress fiber. High fiber tension induces either low stress fiber dissociation (Deshpande et al., 2007) or high stress fiber synthesis (Vernerey and Farsad, 2011, Obbink-Huizer et al., 2013), leading to a large amount of stress fibers in directions with high fiber tension. The model by Deshpande et al. predicts strain avoidance in response to cyclic strain, but cannot capture the increased strain avoidance for increased strain amplitude at a constant strain rate. On the other hand, the model proposed by Obbink-Huizer et al. (2013) independently

sense strain and strain rate. Moreover, this model has been used to describe that the cells are able to respond to the substrate anisotropy by orienting preferentially in the stiffest direction, and this effect increases with a decreased cell matrix stiffness.

The interaction between cells and their environment depends on the relative dimensions of the cell and the substrate topology. Fibroblasts, which are very often used for tissue engineering purposes (Merryman et al., 2007, Bourget et al., 2012, van Geemen et al., 2012, van Vlimmeren et al., 2012, Weidenhamer and Tranquillo, 2013) have a diameter of approximately 10-15 µm with a nucleus of approximately 5-6 µm, when they are observed in their rounded configuration (Freitas, 1999, Swanson et al., 1991, Webster et al., 2009). On electrospun microfibrous substrates, with fiber diameters of 5 µm and larger cells have been shown to elongate along single fiber, and may achieve lengths up to 100 µm (Fioretta et al., 2013).

We question (1) what is the architecture that stress fiber develops when a cell keeps a spherical geometry or assumes a spread geometry on a flat substrate, (2) what is the architecture that stress fiber develops when cells with different shapes orient their main axis parallel or perpendicular to a fiber substrate and whether it is influenced by the substrate diameter. To answer these questions, we design cells with rounded and flattened shapes on flat and fibrous substrates, and we define an orientation principle to characterize and compare different cell geometries.

4.3 Materials and Methods

4.3.1 Mathematical model

The computational model developed by (Obbink-Huizer et al., 2013) was used to decribe the formation of stress fibers. The total cell stress $\boldsymbol{\sigma}^{\text{cell}}$ is evaluated by summing the contribution of the stress fibers in a number of discrete directions. In each direction $\vec{e}_\theta$ the stress associated with the stress fibers σ_θ^p is weighted by the fiber volume fraction Φ_θ^p in that direction

$$\boldsymbol{\sigma}^{\text{cell}} = \sum_{\theta} w_{\theta} \, \Phi_{\theta}^{p} \, \sigma_{\theta}^{p} \, \vec{e}_{\theta} \vec{e}_{\theta} \tag{4.1}$$

The fiber stress is based on a Hill-type muscle model. According to this model, the cell fibers apply stress to their environment as a function of the strain ε (function $f(\varepsilon)$) and of the strain rate $\dot{\varepsilon}$ (function $g(\dot{\varepsilon})$) (Fig. 4.2).

$$\sigma_{\theta}^{p} = \sigma_{\max} f(\varepsilon) g(\dot{\varepsilon}) \tag{4.2}$$
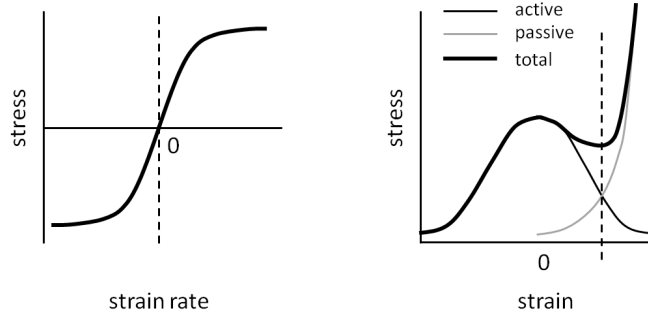
FIGURE 4.2: Dependence of the fiber tension on the strain rate (left) and on the strain (right) as described by Obbink-Huizer et al. (2013)

The length-tension relationship $f(\varepsilon)$ is characterized by an active component $f(\varepsilon)_a$, describing that active acto-myosin contraction decreases when the absolute strain in a contractile unit differs from zero. Next to this there is a passive component $f(\varepsilon)_p$ modeling a strain hardening response in extension

$$f(\varepsilon) = f(\varepsilon)_a + f(\varepsilon)_p \tag{4.3}$$

$$f(\varepsilon)_a = \exp^{-\left(\frac{\varepsilon_{\theta}}{\varepsilon_0}\right)^2} \tag{4.4}$$

$$f(\varepsilon)_p = \begin{cases} 0 & \text{if } \varepsilon_\theta < 0 \\ (\frac{\varepsilon_\theta}{\varepsilon_1})^2 & \text{if } \varepsilon_\theta \geq 0 \end{cases} \qquad (4.5)$$

where ε_0 describes how quickly contraction reduces as strain differs from zero and ε_1 describes passive strain hardening. ε_θ represents the Green-Lagrange strain $\varepsilon_\theta = \frac{1}{2}(\lambda_\theta^2 - 1)$, with λ_θ oriented in the direction θ. The length-velocity relationship $g_{\dot{\varepsilon}}$ indicates increased strain avoidance when strain rate is increased

$$g(\dot{\varepsilon}) = \frac{1}{1 + \frac{2}{\sqrt{5}}} \left(1 + \frac{k_v \dot{\varepsilon}_\theta + 2}{\sqrt{(k_v \dot{\varepsilon}_\theta + 2)^2 + 1}} \right) \qquad (4.6)$$

where k_v describes how quickly contraction reduces as the rate of shortening increases. A fiber stress in a certain direction leads to an increased stress fiber volume fraction in this direction, according to:

$$\frac{d\Phi_\theta^p}{dt} = (k_0^f + k_1^f \sigma_{\max} f_{\varepsilon,a} g_{\dot{\varepsilon}}) \Phi^m - k_d \Phi_\theta^p \qquad (4.7)$$

where k_0^f, k_1^f are stress fiber formation constants and k_d is a stress fiber dissociation constant. Furthermore actin mass conservation is assumed, accounting for the actin that is present as either monomer (Φ^m) or fiber (Φ_θ^p for angle θ)

$$\Phi^{\text{tot}} = \Phi^m + \sum_\theta w_\theta \, \Phi_\theta^p \qquad (4.8)$$

The 3D discrete fiber directions, are chosen with orientations and corresponding weighting factors determined by Lebedev quadrature points (Lebedev and Laikov, 1999). Since every Lebedev point has a 'partner' with the same orientation but opposite direction, only half of the Lebedev grid points are used, in this case 25 orientations, while the weighting factors of both directions are summed. The isotropic part, that comprises the isotropic plasma component, is modeled as a neo-Hookean material

TABLE 4.1: Material parameters.

parameter	description	value
$\sigma_{\max}$	maximal stress fiber stress	2.0^5 Pa
ε_0	how quickly contraction reduces as strain increasingly differs from 0	1.2^{-1}
ε_1	passive strain hardening	1.7^{-1}
k_v	how quickly contraction reduces as rate of shortening increases	5.0 s
k_0^f	basal stress fiber formation	1.5^{-9} s^{-1}
k_1^f	stress dependent stress fiber formation	7.0^{-10} s^{-1}Pa^{-1}
k_d	stress fiber dissociation	1.0^{-6} s^{-1}
Φ^{tot}	total actin volume fraction	5.0^{-2}

$$\boldsymbol{\sigma}^{\text{NH}} = \kappa\frac{ln(J)}{J}\boldsymbol{I} + \frac{G}{J}(\boldsymbol{F}\boldsymbol{F}^T - J^{2/3}\boldsymbol{I}) \tag{4.9}$$

where $\boldsymbol{\sigma}^{\text{NH}}$ is the substrate stress, $\boldsymbol{F}$ the deformation tensor J=det($\boldsymbol{F}$) and κ and G the bulk and the shear moduli respectively. The Young modulus of the New-Hookean material was set to E_{NH}=0.1 kPa, which is lower of a factor of 10^{-3} than the matrix stiffness used in previous simulations Obbink-Huizer et al. (2013), in order to allow the fibers to reorient when the cell develops stress and compacts. Such a value is in the same order of magnitude of the passive cytoplasm stiffness used in previous single cell studies by Ronan et al. (2012). The model parameters used in this work are listed in Table 4.1.

The cell nuclei was assumed to be composed of a linear elastic material, more than 10 times stiffer than the cytoplasm (Thoumine et al., 1999). The nucleus stiffness was set to E_n=4kPa (Ronan et al., 2012).

The described theoretical model was implemented in the commercial finite element package ABAQUS (SIMULIA, Providence, RI, USA).

4.3.2   Cell geometry

The 3D cell models were designed with the CAD software Autocad and Inventor Fusion. A reference spherical cell with 15 µm diameter and a concentric spherical nucleus of 6 µm diameter was assumed (Freitas, 1999). In all the cell geometries the volume of the cell and of the nucleus was kept constant.

Five different substrate shapes were simulated: flat substrate, and fibers with a diameter of 2 µm, 5 µm, 10 µm, 15 µm. Experimental studies show that, when the cells are seeded on these substrates, they deform assuming a flat geometry.

In particular, when fibroblast-like cells are seeded on a 2D flat substrate, they spread rather evenly in every direction and polymerize their actin filaments isotropically (Fardin et al., 2010). In order to investigate the stress fiber organization as a function of cell spreading, a rounded cell and spread cells with different aspect ratio (aspect ratio of 1 and 1.6), defined as the ratio between the long cell axis and the short cell axis, were modeled (Table 4.2 a, b and c).

ECFCs seeded on a fiber tend to elongate axis and form stress fibers along the fiber direction (Fioretta et al., 2013). The organization of the polymerized stress fibers in a cell with its main axis in the fiber direction was compared to the organization of the stress fibers in a cell with its main axis perpendicular to the fiber direction. To do that, an arc-shaped elongated cell along the fiber axis and a cell perpendicular to the fiber axis were modeled. This was done for a fiber substrate of 2, 5, 10 and 15 µm. For an easier comparison, the main axis of all the cells parallel to the fiber was set always equal to 100 µm (Table 4.2 e, g, j, k). In case of the cell perpendicular to the fiber main axis, the cell was modeled to be spherical, and the fiber shape was cut out of the cell volume (Table 4.2 d, f, i). The elongated arc shaped cell geometries refer to the topology of the ECFC cells observed by Fioretta et al. (2013). The cell geometries perpendicular to the scaffold fibers are not observed in experiments, and here included for comparison in contrast with the elongated geometry.
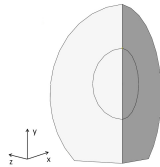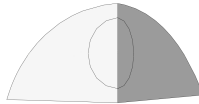
In contrast to the behavior of the ECFCs, HUVECs wrap around the fiber and form stress fibers predominantly in the circumferential direction of the fiber. When elongated, these cells present a nucleus that is more spherical than the ECFCs which are relatively ellipsoidal (Fioretta et al., 2013). We hypothesize that this behavior is due to the dominant polymerization of F-actin in cortical structures
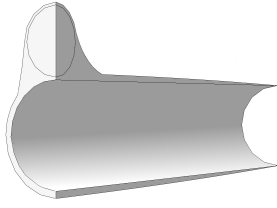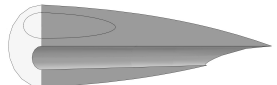
in HUVEC cells, that form close to the cell attachment at the fiber surface (Huot et al., 1997). This way the cell is able to wrap tightly around the fiber substrate and the nucleus. These geometrical features were used to model a HUVEC-like cell on a 10 µm fiber substrate (Table 4.2 h).

The nuclei of the cells on a flat substrate were modeled spherical. For the cells on a fiber substrate, the cell nucleus was modeled as an ellipsoid. We hypothesize that in ECFCs, the polymerized actin fibers form an actin cap that exerts tension on the nucleus and deform it (Khatau et al., 2009). The geometry of the ellipsoidal nucleus is represented by means of an aspect ratio (a.r. in Table 4.2), defined as ratio between the long and the short axis of the ellipsoid. For each cell geometry, the nucleus aspect ratio was chosen in order to keep the cell volume and the main axis constant, and allow a better comparison of the results of the different cells.

The surface of the cell in contact with the scaffold fiber was fully attached to the fiber. Symmetry was assumed, and 1/4 of the cell was modeled. On the external surface the cell was assumed to deform freely.

TABLE 4.2: Parameters for cell design.

id	substrate	cell shape	nucleus a. r.	cell geometry
a	flat	rounded	1	
b	flat	flat (a.r. 1)	1	
c	flat	flat (a.r. 1.6)	1	
d	15 µm fiber	⊥ to fiber	1.6	
e	15 µm fiber	∥ to fiber	2.6	

f	10 µm fiber	⊥ to fiber	1.7	
g	10 µm fiber	‖ to fiber	2.7	
h	10 µm fiber	‖ to fiber	1	
i	5 µm fiber	⊥ to fiber	1.2	
j	5 µm fiber	‖ to fiber	3.3	
k	2 µm fiber	⊥ to fiber	6.8	

4.3.3 Order parameter

An order parameter was defined to quantify the stress fiber orientation for the different cell geometry.

For every fiber direction the scalar product between the stress fiber direction $\vec{r}$ and the direction $\vec{i}$ is used to describe the angle θ_i between them (Fig. 4.3)

$$\left| \vec{i} \cdot \vec{r} \right| = |cos\theta_i| = \begin{cases} 1 & \text{if } \vec{r} \parallel \vec{i} \\ \geq 0 \;\; and \;\; < 1 & \text{otherwise} \end{cases}, \quad i = n, l, t \qquad (4.10)$$

where n is the normal direction to a flat substrate and l and t are the longitudinal and the tangential direction to a fiber substrate respectively.

For a flat susbtrate the order parameter ρ_n is described as an average over all the integration points of the finite element model by

$$\rho_n = \frac{\sum\limits_{i=1}^{n_{int}}(\sum\limits_{j=1}^{N}(1-|cos\theta_n|))}{n_{int}}. \tag{4.11}$$

For a fibrous substrate, the contact guidance in the longitudinal and circumferential fiber direction is distinguished with the use of a longitudinal (ρ_l) and a tangential (ρ_t) order parameter

$$\rho_l = \frac{\sum\limits_{i=1}^{n_{int}}(\sum\limits_{j=1}^{N}(|cos\theta_l|))}{n_{int}}, \qquad \rho_t = \frac{\sum\limits_{i=1}^{n_{int}}((\sum\limits_{j=1}^{N}(|cos\theta_t|))}{n_{int}} \tag{4.12}$$

where n_{int} is hte number of integration points in the model, and N is the number of stress fiber directions.
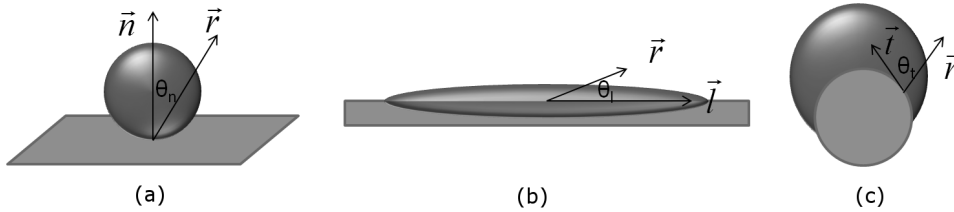
FIGURE 4.3: Schematic of the directions for the calculation of the order parameter. (a) On a flat substrate, n is the normal to the substrate, r is the local direction of the stress fibers, and θn is the angle between both directions. (b and c) On a fibrous substrate l is the longitudinal direction, t the tangential direction, r the local direction of the stress fibers. θ_l and θ_t are, respectively, the angles that they form

4.4   Results

The cells with a rounded shape on the flat substrate (Table 4.2 a) or with their main axis perpendicular to the fiber substrate (Table 4.2 d, f, i) develop high principal stresses, defined as the maximum eigenvalue of the stress tensor, at the cell basis and around the nucleus, while lower stresses characterize the rest of the cell body. In contrast, the spread cells on a flat substrate (Table 4.2 b, c), and the cells with a main axis parallel to the fiber direction (Table 4.2 e, g, h, j, k) overall show higher stresses throughout the cell body (Fig. 4.4 and Fig. 4.5).
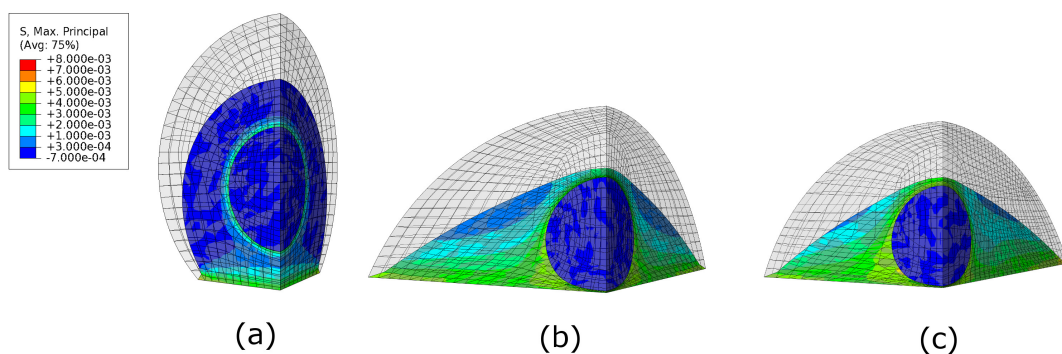
FIGURE 4.4: Principal stress distribution in (a) a rounded cell, (b) a spread cell with aspect ratio of 1, (c) a spread cell with aspect ratio of 1.6 onto a flat substrate

The fiber distribution shows that the cells that assume a flat configuration on the substrate (Table 4.2 b, c, e, g, h, j, k), recruit a high percentage of the available actin monomer to build up stress fibers. When the cell has a rounded shape a lower amount of monomer is polymerized in stress fibers (Fig. 4.6).

The spread and elongated cells (Table 4.2 b, c, e, g, h, j, k) develop bundels of fibers that run from the fixed boundary, at the substrate surface, to the nucleus. A difference can be observed between geometry g and h. In the first case the fibers preferentially run from the constraint boundary towards the nucleus, while in the second case the orientation in the longitudinal direction is less pronounced, and the development of a number of actin fibers in the circumferential direction can be observed.

In the rounded cell geometry (Table 4.2 a) and in those with main axis perpendicular to the fiber direction (Table 4.2 d, f, i), some stress fibers bundles can be observed at the cell basis, from the fixed surface toward the nucleus, and
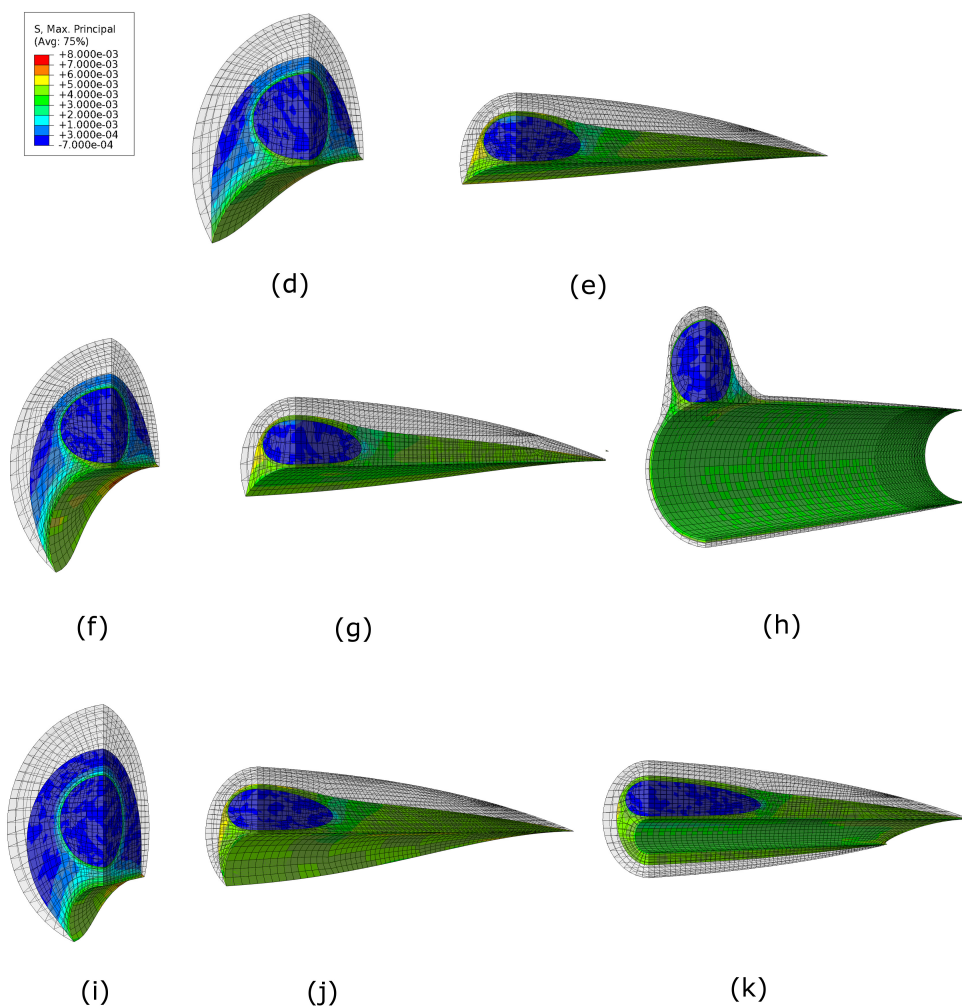
FIGURE 4.5: Principal stress distribution in a cell perpendicular (on the left) and parallel (on the right) to a fiber substrate. (d) and (e) 15 µm fibrous substrate, (f) and (g) and (h) 10 µm fibrous substrate, (i) and (j) 5 µm fibrous substrate, (k) 2 µm fibrous substrate.

around the nucleus. The rest of the cell body is characterized by a lower amount of fibers, that do not show any preferential orientation. No significant difference appears in the stress distribution and fibers pattern for different fiber diameter (Fig. 4.7 and Fig. 4.8).

The stress fiber distributions are represened by the global order parameter. In general, spread and elongated cell configurations show higher order parameters than their rounded counterparts. On a flat substrate an increased aspect ratio increases the order parameter (Table 4.2 b, c). Elongated cells (Table 4.2 b, d, g, h) show a much higher longitudinal order parameter than tangential. The two
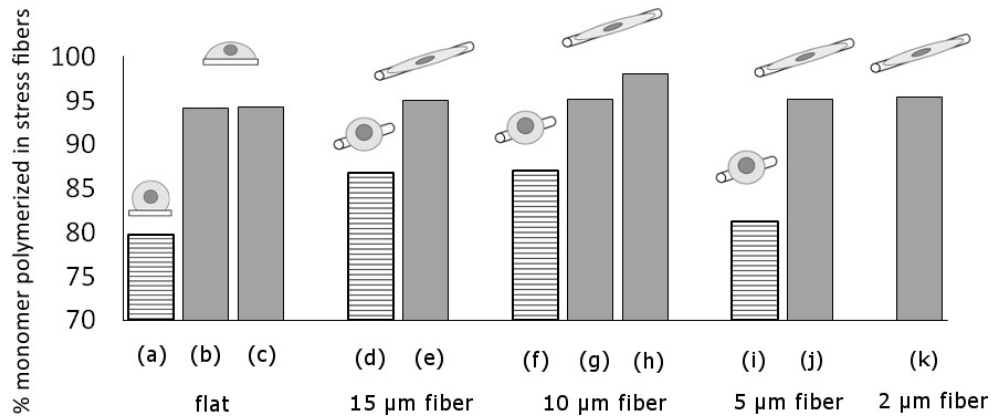
FIGURE 4.6: Percentage of the total monomer embedded in stress fibers over the whole cell model for different cell geometries
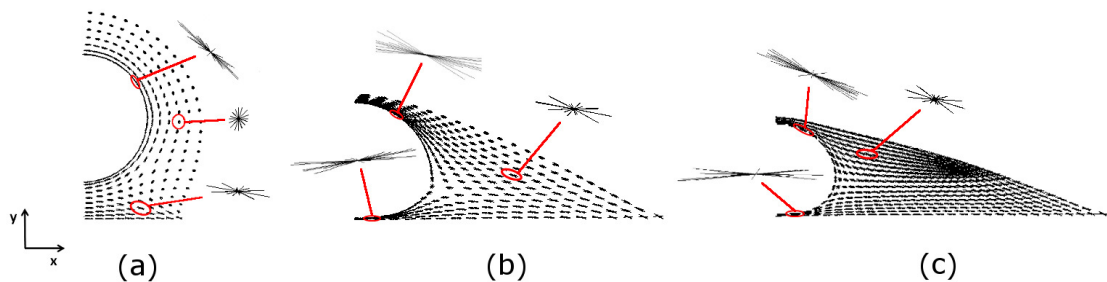
FIGURE 4.7: "Spider-like" cross-sectional representation of the stress fiber distribution for different cell geometries on flat substrate. (a) Rounded cell geometry, (b) spread cell geometry with aspect ratio of 1, (c) spread design with aspect ratio of 1.6 onto a flat substrate.

parameters are of comparable amplitude for the cell geometry Table 4.2 h wrapped around the fiber (Fig. 4.8).

A positive relation can be observed between order parameter and developed stress.

4.5   Discussion

The aim of the present study was to investigate the influence of the substrate fiber diameter on the polymerization and the orientation of stress fibers in the cell cytoplasm. For this purpose, a flat plane and a single fiber with different diameters (2 µm, 5 µm, 10 µm, 15 µm) were used as substrate for a single cell. In all the cases a more rounded cell configuration was compared to a spread configuration. Results show that spread and elongated cells have a more polymerized stress fibers
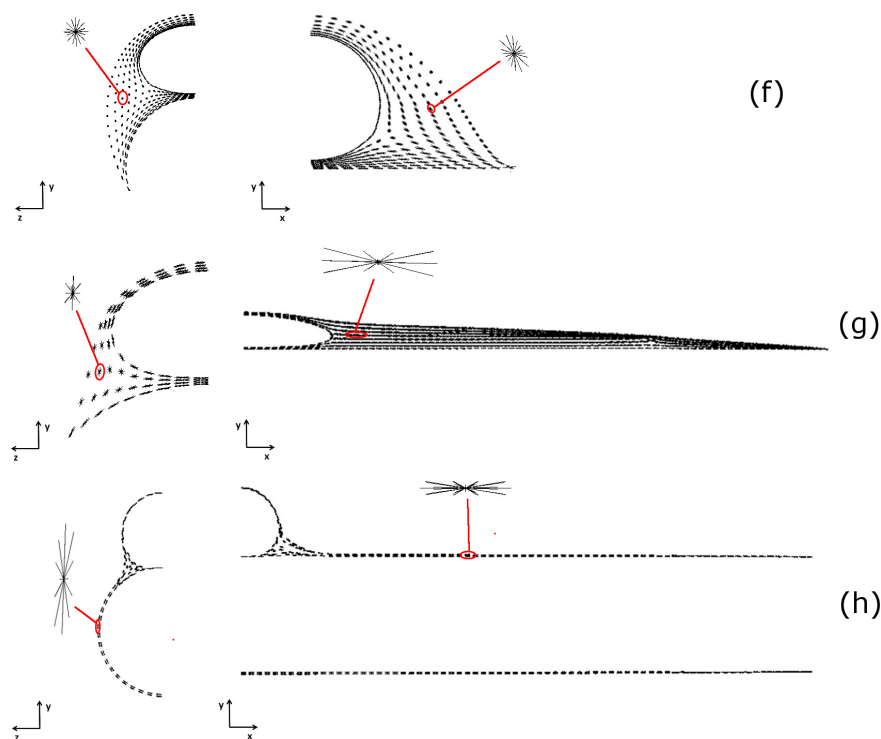
FIGURE 4.8: "Spider-like" cross-sectional representation of the stress fiber distribution for different cell geometries on fiber substrate. Circumferential (left) and longitudinal (right) view of a cell perpendicular to a 10µm fiber (geometry f). Circumferential (left) and longitudinal (right) view of an arc-shaped cell (geometry g) and a cell wrapped around a 10 µm fiber substrate (geometry h).
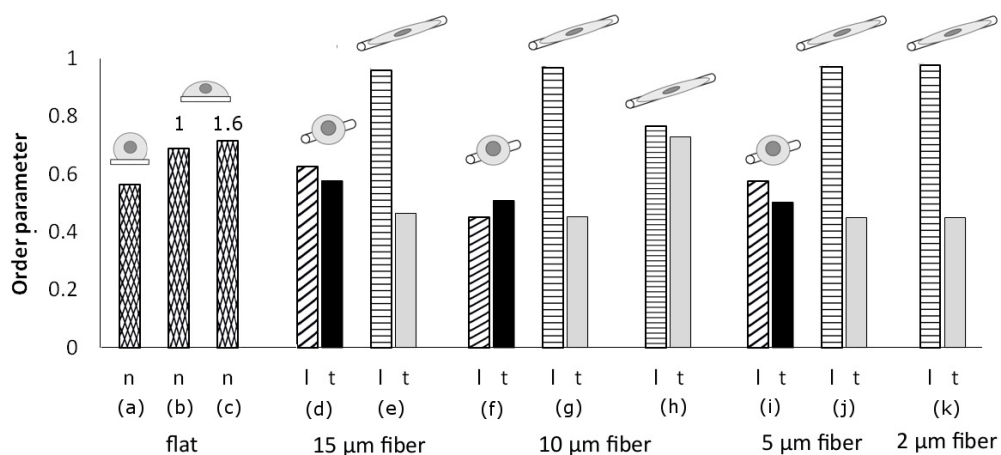
FIGURE 4.9: Order parameter for the different proposed cell design. The index "t" indicates the tangential order parameter and "l" the longitudinal order parameter for a fibrous substrate, the index "n" indicates the order parameter measured with respect to the normal to a flat substrate. The schematics on top of the graph indicate the type of cell design

in comparison with their spherical counterparts. A flattened cell configuration favours the formation of oriented bundles of stress fibers and a high tensional state. In addition, the order parameter increases with the cell elongation. Finally, a cell whose cytoplasm is tightly wrapped around the fiber substrate develops fibers that run in the circumferential direction.

In general, this study indicates that the shape of the substrate closely relates to the possibility of the cell to spread on it. Cell spreading is a complex mechanism based on the interaction of membrane-based integrins with their substrate (Cuvelier et al., 2007). When adhesion occurs, cells apply forces to their substrate and respond through cytoskeleton re-organization (Ladoux and Nicolas, 2012). Therefore the amount and the orientation of stress fibers that are built in the cell depends on the spatial organization of the attachments sites. Furthermore, the position and the shape of the nucleus are important for stress fibers formation, as the nucleus represents a stiff structure inside the cell body.

The presence of a more significant amount of actin fibers in a spread configuration than in a rounded configuration is in agreement with the work described by Ronan et al. (2012). In his work, the presence of a band of stress fibers running from the top of the nucleus to the cell periphery was predicted, while in the rounded cell stress fibers can be found mainly at the cell basis and around the nucleus. In the model of Ronan et al. (2012) a high tensional state is responsible for a reduced fiber dissociation, while in the model of Obbink-Huizer et al. (2013) a high tensional state causes high fiber formation. In both cases, an higher adhesion area guarantees an the development of a high stress and a net high amount of stress fibers.

Fibroblast cells on 5 and 10 µm fibers or oriented grooves comparable to the cell size orient longitudinally to the fibers and the grooves (Charest et al., 2007, Hwang et al., 2009, Fioretta et al., 2013). In contrast, when fiber diameters are in the nanometer range, cells (much smaller than the cell size) span a number of fibers and assume a more uniform configuration (Subramony et al., 2013). A high order parameter indicates that, in principle, an elongated cell on a small fiber (2 µm diameter in our case) might be a favourable cell configuration. However, scaffolds that are spun by conventional electrospinning have shown a direct relation between the fiber diameter and the scaffold porosity (Zhong et al., 2011). Therefore, a scaffold with small fiber diameter ($<$ 1-2 µm) will typically have a pore size that is too small for cells of 10-15 µm diameter to span only one or two fibers (Balguid

et al., 2009). In these cases cells encounter more than one fiber in their elongation process and start spreading over more fibers (Chaurey et al., 2012, Fioretta et al., 2013). At the scaffold surface, the cell can follow the orientation of the nanofibers when they create a clear orientation pattern (Baker and Mauck, 2007, Prabhakaran et al., 2013).

It has been observed that ECFCs cultured on electrospun substrates develop stress fibers mainly in the longitudinal direction, while HUVECs cultured over the same substrate develop stress fibers mainly in the circumferential direction (Fioretta et al., 2013). Fioretta et al. (2013) report that ECFCs cultured over a fibrous substrate (5-10 μm diameter fibers) show a clear actin cap over the nucleus. They hypothesize that this may cause higher intracellular tension in ECFCs, which may deform the nucleus. In contrast, the lack of an actin cap in HUVECs might be the reason for the presence in these cells of a more rounded nucleus. In addition, it has been found that HUVECs develop a significant amount of cortical actin, which locates at the periphery of the cell (Huot et al., 1997). These observations explain the rationale behind the modeling of an elongated and a wrapped cell around the scaffold fiber, modeled with an ellipsoidal and a spherical nucleus respectively. As results show, the different shape of the two cells leas to different stress fiber formation.

In conclusion, the use of a mechanical cell model on a single cell level allows us to observe the stress fiber architecture that develops within a cell on a flat (2D) and a fibrous substrate (3D) as function of the cell shape. The formation of a large amount of stress fibers in spread cells that relates to the tensional state in the cell can be considered as the underlying physical and mechanical mechanism for cell contact guidance both over 2D and 3D substrates. In turn, the cell shape is determined by the substrate geometry, which regulates the cell attachment, and the capability of the nucleus to deform within the cell. In vitro experiments performed using microcontact printing to constrain cells into predefined shapes have shown that cell survival is not determined by the total amount of available cell ligand, but rather its spatial distribution (Chen et al., 1997). The important condition to be satisfied is the possibility of the cell to spread over a large area on the substrate. In contrast, a small adhesion area leads the cell to apoptosis even when many ligands are available. More recently, it has also been shown that stem-cell differentiation depends on cell shape (Kilian et al., 2010). The formation of a large amount of stress fibers in spread cells relates to a high tensional state

in the cell. The maintenance of a high tensional state has been demonstrated to influence cell survival and differentiation (Cai et al., 1998, McBeath et al., 2004, Nelson et al., 2004, Müller et al., 2013). The possibility of achieving such a tensional state by adhering and spreading following the topology of the substrate surface and forming organized stress fibers can be considered as the underlying physical and mechanical mechanism for cell contact guidance both over 2D and 3D substrates.

Chapter 5

Cell-mediated compaction in soft tissues at the micro-scale

5.1 Abstract

The extracellular matrix that develops in engineered tissues is strongly influenced by the presence of a (fibrous) scaffold via the contact guidance mechanism. After degradation of the scaffold, however, remodeling of the tissue is frequently observed in response to external mechanical stimuli, internal cell mediated stresses, or combinations thereof. Here we explore effect of the cell traction on the collagen remodeling using a discrete representation of the collagen network. We compare this to a recently developed continuum model, and then we use the model to investigate the effect of tissue anisotropy and fiber interconnection on the compaction of tissue engineered strips. A good agreement is found between the discrete and continuum model. In addition, in our current model a pronounced tissue anisotropy does not influence the amount of tissue compaction, as instead fiber interconnection does. These results offer a first validation of the continuum model and indicate the possibility of modeling tissue compaction on a fine scale. Despite the continuum model, on a smaller scale a more realistic representation of the fiber network, comprehensive of the interaction of fibers oriented in different directions can be achieved.

5.2 Introduction

Living engineered tissues have the ability to remodel in response to mechanical stimuli. In particular the fibrous collagen network, which is the main load-bearing component of the extra-cellular matrix is susceptible to cell mediated remodeling. Cells not only synthesize the collagen and secrete collagen-degrading enzymes (Huang and Yannas, 1977, Canty et al., 2004, Bhole et al., 2009), but may also apply tension to the collagen fibers. In particular after degradation of the scaffold, cell tension driven remodeling of the collagen network may occur (Foolen et al., 2012). Prior to degradation of the scaffold, contact guidance may overrule any load induced remodeling of the collagen network (de Jonge, 2013, Chapter 3).

Cells respond to changes in mechanical stress by upregulating α-SMA (Rabkin-Aikawa et al., 2004), leading to a reorganization of the cytoskeletal structure with assembly of actomyosin units forming the stress fibers. When 3D tissue constructs are statically constrained in one direction only, cell tension

and cell alignment develops in this constrained direction and tissue compaction is observed in the orthogonal directions. In cyclically strained tissue constructs, cell orientation and tension depend on the boundary conditions applied to the construct (Wang and Grood, 2000, Foolen et al., 2012). If the tissue constructs are bi-axially constrained and cyclically strained in one direction, cells align in the direction perpendicular to the cyclic strain direction. If, on the other hand, the tissue is constrained uniaxially only, cells align in the direction of the cyclic strain direction (Foolen et al., 2012).

Understanding cell alignment and cell tension in response to mechanical stimuli is crucial because cells tend to preferentially secrete collagen in the direction of the main axis of the cells (Wang et al., 2003c, Canty et al., 2004, Gealy et al., 2009), while collagen degradation depends on the strain (stress) in the collagen fiber (Huang and Yannas, 1977, Ruberti and Hallab, 2005, Bhole et al., 2009, Wyatt et al., 2009).

Several models have been developed recently to describe and understand tissue remodeling. Usually it is assumed that collagen fibers align prefentially along or in between the principal stress or principal strain direction (Driessen et al., 2004, Baek et al., 2006, Hariton et al., 2007, Kuhl and Holzapfel, 2007, Driessen et al., 2008). These models successfully predict the helical collagen orientation in the arterial wall, and the pronounced circumferential collagen orientation in the valve leaflet. However, these models do not account for the cell-mediated compaction.

Recently, Loerakker et al. (2014) developed a physically motivated model for tissue remodeling, combining the strain dependent collagen degradation algorithm developed by Heck (2013), with the actin stress fiber model developed by Obbink-Huizer et al. (2013). The model accounts for irreversible tissue compaction, by accounting for inverse growth (permanent shortening) of the collagen fibers. For this purpose, the model assumes that the cell stress is in equilibrium with the stress in the collagen fibers.

The model developed by Loerakker et al. (2014) represents the tissue as a continuum mixture of cells, collagen fibers, and isotropic matrix components. In the present study, this model is adapted and applied to a discrete model developed previously (Argento et al., 2012). The collagen fibers are described by one-dimensional elements and the contribution of the active cell stress and the passive matrix components are separated. The key microstructural features of

a collagen network (fiber diameter, fiber orientation, fiber interconnection, fiber tissue porosity) can be represented. The collagen network is initially assumed to develop primarily in the direction of a fibrous scaffold (de Jonge, 2013). The architecture that the collagen has when the scaffold is completely degraded is considered to be the "initial" network for the cell-mediated tissue compaction. As the "initial" collagen configuration is function of the architecture of the electrospun scaffold, this kind of framework is suitable to evaluate the effect of the structural features of the initial collagen network and of the scaffold on the cell-mediated tissue compaction.

The predictions of the discrete model developed in this work are compared to the results of the continuum theory of Loerakker et al. (2014). We investigate the impact of the fiber interconnection density, and the initial collagen fiber distribution. In addition, the effect of the size of a tissue engineered strip, of the fiber interconnections and of the initial collagen fiber distribution is evaluated.

5.3 Materials and methods

5.3.1 Mechanics of tissue components

The computational model developed by Loerakker et al. (2014) was adapted to the discrete micro-scale tissue model developed by Argento et al. (2012) to simulate collagen remodeling. The discrete finite element tissue model is composed of a planar network of one-dimensional truss elements, representing collagen fibers. The key structural features of the fibrous network (fiber diameter, orientation, volume fraction, interconnection, material) can be adjusted in the model. This network is embedded in a three-dimensional continuum matrix, representing the proteoglycan gelatinous component of the matrix, and the cell passive component (Fig. 5.1).

5.3.1.1 Actin stress fibers

The computational model developed by Obbink-Huizer et al. (2013) was applied to the discrete model to describe the formation of stress fibers in the cell cytoplasm, in response to external mechanical stimuli. In the discrete model it is assumed
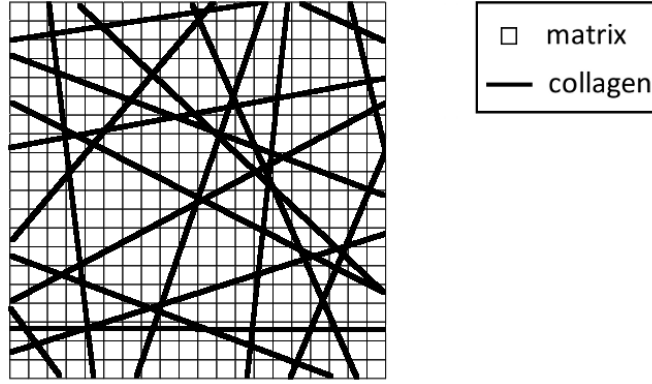
FIGURE 5.1: Schematic of the computational model developed by Argento et al. (2012). The one-dimensional fiber network is depicted in black color, while the continuum matrix is depicted in white color

that the stress fibers align with the collagen fibers. Briefly, a constant amount of actin monomer (ϕ^{tot}) is present in the cell, partly as free monomer (ϕ^m) and partly as stress fibers (ϕ^p).

$$\phi^{\text{tot}} = \phi^m + \phi^p \tag{5.1}$$

The cells apply forces to their environment through their stress fibers and associated integrins. The stress exerted by the stress fibers in the direction θ is defined as a function of the strain ε and the strain rate $\dot{\varepsilon}$

$$\sigma_\theta^p = \sigma_{\max} f(\varepsilon) g(\dot{\varepsilon}) \tag{5.2}$$

with

$$f(\varepsilon) = f(\varepsilon)_a + f(\varepsilon)_p \tag{5.3}$$

$$f(\varepsilon)_a = \exp^{-(\frac{\varepsilon_\theta}{\varepsilon_0})^2} \tag{5.4}$$

$$f(\varepsilon)_p = \begin{cases} 0 & \text{if } \varepsilon_\theta < 0 \\ (\frac{\varepsilon_\theta}{\varepsilon_1})^2 & \text{if } \varepsilon_\theta \geq 0 \end{cases} \tag{5.5}$$

where the subscript a indicates the active cell contraction, and p the passive strain hardening, and

$$g(\dot{\varepsilon}) = \frac{1}{1 + \frac{2}{\sqrt{5}}} \left(1 + \frac{k_v \dot{\varepsilon}_\theta + 2}{\sqrt{(k_v \dot{\varepsilon}_\theta + 2)^2 + 1}} \right) \tag{5.6}$$

where k_v describes how quickly contraction reduces as the rate of shortening increases.

The stress fiber volume fraction varies proportionally to the fiber stress

$$\frac{d\Phi_\theta^p}{dt} = (k_0^f + k_1^f \sigma_{\max} f_{\varepsilon,a} g_{\dot{\varepsilon}}) \Phi^m - k_d \Phi_\theta^p \tag{5.7}$$

ruled by the k_1^f, k_2^f and k_d constants.

5.3.1.2 Collagen fibers

The collagen fiber distribution is defined by a periodic function (Gasser et al., 2006, Driessen et al., 2008)

$$\phi_{cf}^\theta = A \exp\left[\frac{\cos(2(\gamma_\theta - \alpha)) + 1}{\beta} \right] \tag{5.8}$$

where the fiber volume fraction ϕ_f in each direction θ is defined by the the main fiber orientation α, the standard deviation β, and the scaling parameter A. As described by Argento et al. (2012) a sampling procedure of the volume fraction function is used to generate a discrete fiber network (Fig. 5.1). The fibers were spaced at intervals of 5° between 0 and 360°.

The irreversible collagen shortening caused by the tension the cells exert on the collagen fibers is modeled by the introduction of an inverse growth. To do this, the stretch associated with the collagen fibers λ is split into an elastic and a growth component

$$\lambda = \lambda_e \lambda_g. \tag{5.9}$$

The collagen fiber stress is defined by an exponential function of the elastic collagen stretch

$$\sigma_{cf} = \begin{cases} k_1 \lambda_e^2 \left(e^{k_2 \left(\lambda_e^2 - 1 \right)} - 1 \right), & \lambda_e > 0 \\ \frac{k_1 k_2}{k_3} \left(e^{k_2 \left(\lambda_e^2 - 1 \right)} - 1 \right), & \lambda_e \le 0 \end{cases} \tag{5.10}$$

where $k_3 >> k_1 k_2$ defines a small compressive stress, useful to prevent convergence issues due to function discontinuities.

5.3.1.3   Isotropic extracellular matrix component

The isotropic part of the extracellular matrix and the passive cell contribution, are lumped and described as a compressible Neo-Hookean material

$$\boldsymbol{\sigma}^{\text{NH}} = \phi_{mc} [\kappa \frac{ln(J)}{J} \boldsymbol{I} + \frac{G}{J} (\boldsymbol{F} \boldsymbol{F}^T - J^{2/3} \boldsymbol{I})] \tag{5.11}$$

where $J = \det(\boldsymbol{F})$ is the Jacobian matrix, G is the shear modulus and κ is the compression modulus. $\phi_{mc} = 1 - \sum_{i=1}^{N} \phi_{cf}^i - \phi_a$ is the matrix volume fraction, calculated as difference of the total volume fraction, and the total volume fraction assigned to the N collagen fibers and actin fibers.

5.3.2   Cell-mediated compaction

Tissue compaction is caused by the contractile stress (σ_{cf}) that cells apply to the collagen fibers. Collagen fibers are assumed to be in equilibrium with the cell stress

$$\sigma_{cf,p} = \sigma_{sf} \tag{5.12}$$

From this stress, the preferential $\lambda_{e,p}$ is calculated using Eq. (5.10). Next, the preferential collagen stretch $\lambda_{g,p}$ (which is ≤ 1) can be calculated using Eq. (5.9), and used to update the growth component of the collagen stretch according to

$$\frac{d\lambda_g}{dt} = \frac{1}{\tau_\lambda} \left(\lambda_{g,p} - \lambda_g\right) \tag{5.13}$$

where τ_λ is a time constant.

5.3.3   Collagen remodeling

The volume fraction of each collagen fiber depends on the production and degradation of collagen

$$\frac{d\varphi_{cf}}{dt} = \frac{d\varphi_{cf,prod}}{dt} + \frac{d\varphi_{cf,degr}}{dt} \tag{5.14}$$

The degradation law is based on the work of Wyatt et al. (2009)

$$\frac{d\varphi_{cf,degr}}{dt} = D_{min} + \frac{D_{max} - D_{min}}{1 + 10^{200(\varepsilon_e^t - \varepsilon_{trans})}} \frac{\varphi_{cf}}{\tau_\varphi} \tag{5.15}$$

where ε_{trans} is the transition strain and τ_φ is the remodeling time constant. The transition strain is chosen such that collagen degradation becomes minimal when

the collagen fiber stress equals the maximum stress fiber stress. The collagen production in a certain direction is assumed to be proportional to the amount of stress fibers that the cell develops in that direction (Wang et al., 2003c, Canty et al., 2004, Gealy et al., 2009)

$$\frac{d\varphi_{cf,prod}}{dt} = \frac{\varphi_{sf}}{\sum\limits_{1=1}^{N} \varphi_{sf}^{i}} \sum\limits_{i=1}^{N} \frac{d\varphi_{cf,degr}}{dt} \tag{5.16}$$

where N is the number of collagen fibers.

5.3.4 Numerical implementation

In the discrete model, the mechanical behavior of the collagen fibers and cells is assigned to the one-dimensional truss elements. At the $i - th$ integration point the variation of the collagen fiber volume fraction is described by the change in cross-sectional area $A_{cross,cf}$ of the fiber, according to

$$A_{cross,cf}^{i} = \frac{\varphi_{cf}^{i} V}{L^{i}} \tag{5.17}$$

where V is the volume of the discrete model, and L^i is the length of the truss to which the $i-th$ integration point belongs. The variation of the fiber cross sectional area is taken into account in the calculation of the fiber stress, as described in Eq. (5.10).

The isotropic Neo-Hookean material behavior described in Section 5.3.1.3 is assigned to the three-dimensional continuum material where the fibers are embedded.

5.3.5 Model parameters

The parameters used in the model are reported in Table 5.1. The parameters that refer to stress fibers were used as in Obbink-Huizer et al. (2013). The parameters

TABLE 5.1: Parameters used in the simulations.

Model component	Parameter	Value	Reference
Stress fibers	σ_{max}	2.0^5 Pa	Obbink-Huizer et al. (2013)
	ε_0	1.2^{-1}	Obbink-Huizer et al. (2013)
	ε_1	1.7^{-1}	Obbink-Huizer et al. (2013)
	k_v	5.0 s	Obbink-Huizer et al. (2013)
	k_0^f	1.5^{-9} s^{-1}	Obbink-Huizer et al. (2013)
	k_1^f	7.0^{-10} s^{-1}Pa^{-1}	Obbink-Huizer et al. (2013)
	k_d	1.0^{-6} s^{-1}	Obbink-Huizer et al. (2013)
	Φ^{tot}	5.0^{-2}	Obbink-Huizer et al. (2013)
Collagen fibers	σ_{cf}	0.5 [-]	Driessen et al. (2007)
	k_1	1689kPa	Driessen et al. (2007)
	k_2	1.93 [-]	Driessen et al. (2007)
	k_3	100MPa	Loerakker et al. (2014)
Isotropic component	φ_{mc}	0.45 [-]	Loerakker et al. (2014)
	E	10kPa	Driessen et al. (2007)
	ν	0.3 [-]	Driessen et al. (2007)
	G	$\frac{E}{2(1+\nu)}$	Loerakker et al. (2014)
	κ	$\frac{E}{3(1-2\nu)}$	Loerakker et al. (2014)
Remodeling	τ_λ	500 s	Loerakker et al. (2014)
	τ_φ	1000 s	Loerakker et al. (2014)
	D_{min}	0.5 [-]	Heck (2013)
	D_{max}	1 [-]	Heck (2013)
	$\varepsilon_{\mathrm{trans}}$	0.017 [-]	Loerakker et al. (2014)
	$\varepsilon_{\mathrm{e,p,max}}$	0.028 [-]	Loerakker et al. (2014)

that refer to collagen fibers were used as in Driessen et al. (2007). The parameters that refer to the collagen turnover were used as in Loerakker et al. (2014).

5.3.6 Simulations

The collagen network described by a distribution of truss elements and embedded in a three-dimensional continuum matrix is a planar network positioned in the xy-plane.

To validate the discrete model against the continuum model by Loerakker et al. (2014) a square sample of dimensions 1 mm $\times$ 1 mm $\times$ 0.01 mm was modeled,

and left free to compact at the boundaries (Fig. 5.2). A small amount of fiber interconnections was used (30%).

The difference between an isotropic fiber distribution ($\alpha = 0$, $\beta = 1000$) and an anisotropic distribution ($\alpha = 0$, $\beta = 0.2$) was investigated using strips of 1 mm $\times$ 0.5 mm $\times$ 0.01 mm constrained at the to ends in the x- and the y- direction (Fig. 5.2).

When using the strip geometry, the discrete fiber networks are considered to be fully interconnected, and at each intersection between two fibers of the network a node is defined (100% fiber interconnection).

To investigate the effect of the fiber crosslinks a strip of dimensions 1 mm $\times$ 0.5 mm $\times$ 0.01 mm with a 30% fiber interconnection was simulated.

All the described models are summarized in Fig. 5.2.

In all the simulations performed on strip geometries with the discrete model the displacement of the top and the bottom boundary nodes of the strip is fit to a parabolic function to evaluate the compaction in the middle of the sample. The collagen fiber volume fractions were fit to a Gaussian function.

In the continuum model the final collagen fiber orientation after remodeling was quantified by an order parameter O_{cf}. This parameters has value +1 when the fibers are aligned in the x direction, -1 when the fibers are aligned in the y direction, and 0 when the fibers are isotropically distributed

$$O_{cf} = \int_{\frac{-\pi}{2}}^{\frac{\pi}{2}} \frac{\varphi_{cf}\left(\gamma\right)}{\phi_{cf}} cos\left(2\gamma\right) \, \mathrm{d}\gamma \tag{5.18}$$

where γ is the angle that the collagen fiber forms with the x direction.

5.4   Results

After tissue remodeling of the square tissue both the continuum and the discrete model reveal a compaction of 24% in the x and in the y direction, and an isotropic
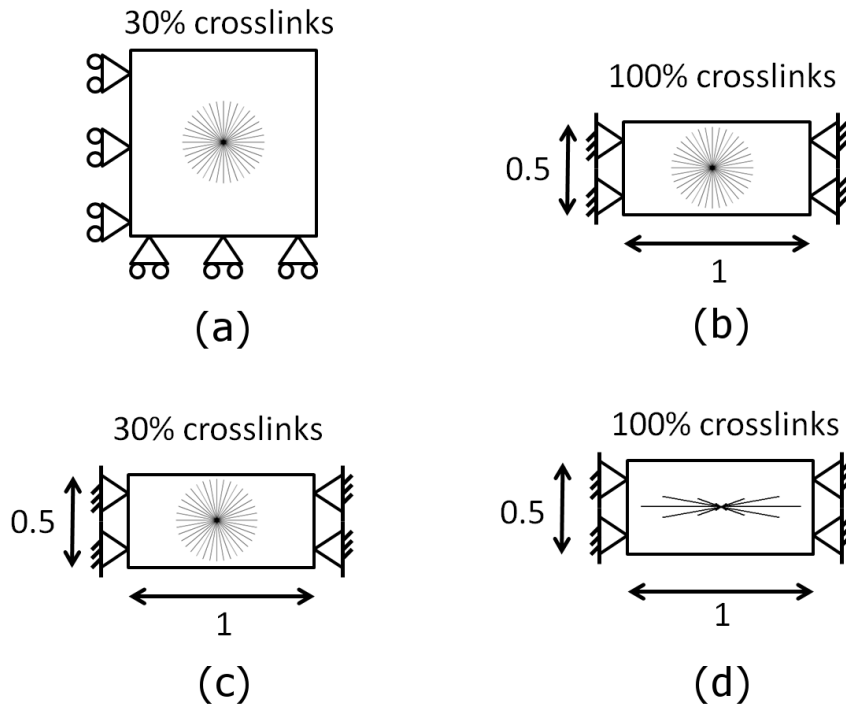
FIGURE 5.2: Geometries used in the simulations. The "spider diagram" represents the initial distribution of collagen fibers used for each simulation. a) Schematic of the squared model with boundary conditions used to validate the discrete model, b) schematic of a strip with initially isotropic collagen distribution and fully interconnected collagen network, c) schematic of a strip with initially isotropic collagen distribution and low percentage of crosslinks , d) schematic of a strip with initially anisotropic collagen distribution.

fiber distribution. The collagen distribution predicted by the discrete model is in agreement with the one predicted by the continuum model (Fig. 5.3).

For the the strip geometries with fully interconnected fiber network (100% interconnected nodes) the compaction in the middle of the strip varies between 38% and 40%, against 34% compaction evaluated by the continuum model. In all the discrete models the collagen fiber distribution is Gaussian. When remodeling occurs, the fibers in the direction of the applied strain, are protected from degradation, and degrade almost completely in the direction perpendicular to it. This effect determines, both in the continuum and in the discrete model a collagen distribution that is mainly oriented in the direction of the constraint (Fig. 5.4). The parameters α and β that characterize the fitted Gaussian fiber distributions for all the simulations, compared to the fiber distribution predicted by the continuum model are reported in Table 5.2.
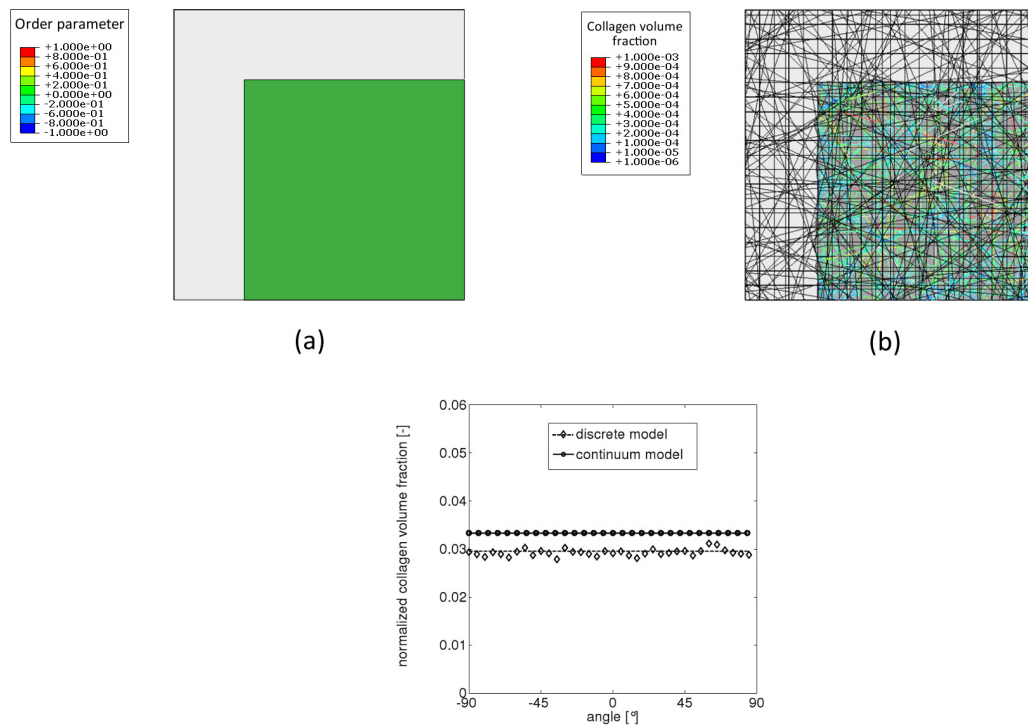
FIGURE 5.3: a) Order parameter of the collagen distribution in a continuum square geometry, b) collagen volume fraction distribution in a discrete square. Below comparison of the normalized collagen volume fractions after remodeling.

The strips with isotropic (b) and anisotropic (d) initial collagen distribution, characterized by the same dimensions, show a compaction of 38% and 39% in the middle of the strip, respectively (Table 5.2). However, the strip with initially anisotropic collagen distribution compacts faster than the strip with isotropic collagen distribution.

The strips b and c, characterized by the same dimensions but different amount of fiber interconnections, show a compaction of 38% and 43% in the middle of the strip, respectively (Table 5.2).

5.5   Discussion

A discrete micro-scale model of cell-tension mediated collagen remodeling has been developed based on the continuum theory of Loerakker et al. (2014). We modeled tissue synthesis and degradation on a single collagen fiber. First, the ability of
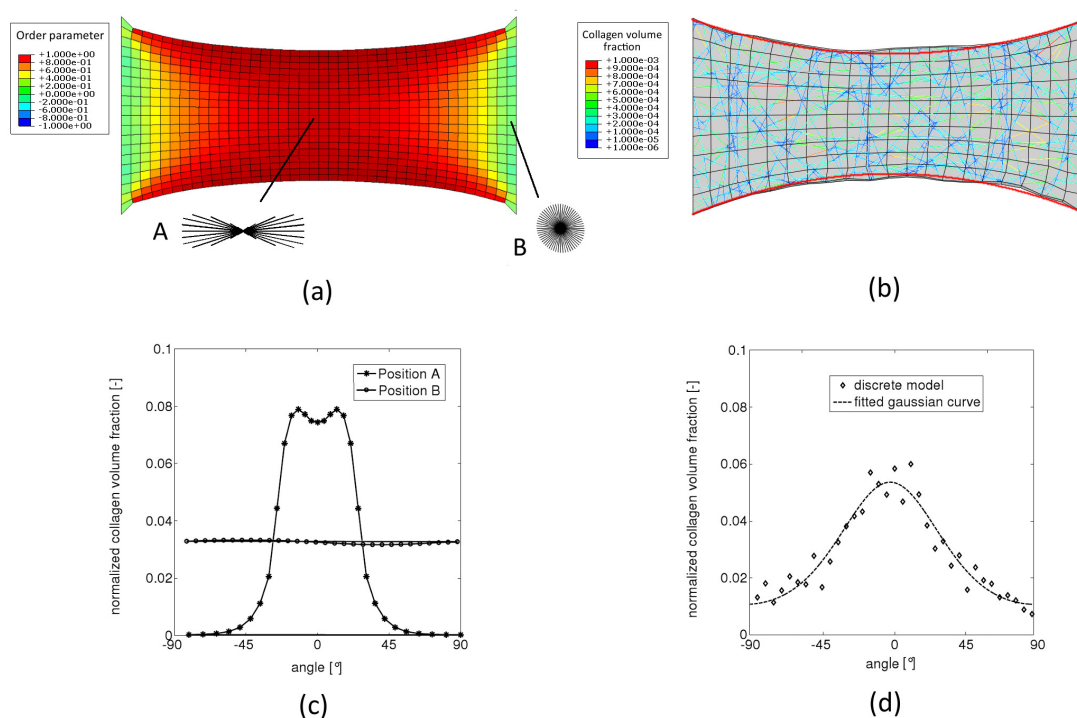
FIGURE 5.4: a) Order parameter of the collagen distribution in a continuum strip. b) collagen volume fraction distribution in a discrete strip, the red curves indicate the parabolic fit used to evaluate tissue compaction, c) normalized collagen volume fraction distribution in the center and at the boundary of the continuum model, d) normalized collagen volume fraction distribution overall the discrete strip.

TABLE 5.2: Parameters of the collagen distributions of the different models. For each discrete model, initial and final parameters α and β of the Gaussian distributions that fits the collagen volume fraction distribution and the compaction (C) at the free boundary are reported. For the continuum models the parameters α and β in the middle of the strip and the compaction (C) at the free boundary are reported.

id	Crosslinks	Initial distribution		Discrete			Continuum		
		α	β	α	β	C	α	β	C
a	30%	0	1e+4	0	1e+4	0.24	0	1e+4	0.24
b	100%	0	1e+4	0	1.2	0.38	0	0.5	0.34
c	30%	0	1e+4	0	1.7	0 .43	-	-	-
d	100%	0	0.2	0	1	0.39	-	-	-

the discrete model to describe tissue compaction and collagen distribution was tested on a squared geometry. The results of the discrete model resemble well the results obtained with the continuum model. Next, the discrete model was applied to uniaxially constrained strips to evaluate the effect of the initial collagen distribution and fiber interconnection. The initial collagen distribution does not influence tissue compaction, and an increased interconnection of the fiber network decreases the compaction of the tissue.

Although continuum-level models (Barocas and Tranquillo, 1997, Obbink-Huizer et al., 2013, Loerakker et al., 2014) are important for understanding the interactions between the cells and the surrounding matrix, they do not provide insight into the contribution of detailed structural features such as fiber interconnectivity and fiber dimensions. The discrete distribution of the collagen fibers is described as a macro-scale network describing the collagen distribution in small-scale tissues (Legant et al., 2009, Foolen et al., 2012). Therefore, the collagen fiber distribution in the discrete model cannot be evaluated on a very local level (i.e. at the center and at the boundary of the sample), but only globally over the small-scale tissue. This explains the different collagen fiber distributions observed for the continuum and the discrete model in Figure 5.4 c and d: in the continuum model the distributions are local in the center and the boundary of the sample, while in the discrete model the distribution is evaluated over the whole tissue.

The discrete model and the continuum model predict the same amount of tissue compaction when a squared geometry is used, and the boundary conditions do not affect the calculations. Using the uniaxially constrained strip, the continuum model predicts a compaction at the center of 34%, while the discrete model (with 30% fiber interconnection) predicts a compactions of 43%. Therefore the boundary conditions affect the continuum model more than they do in the discrete model. When using a strip with an increased length/width aspect ratio (up to aspect ratio = 3.6), Loerakker et al. (2014) did find a compaction of 43%. The discrete model can reproduce collagen distribution patterns that are consistent with those described by the continuum model. Experimental validation would be necessary to assess the actual boundary effect in small-sized tissues.

The predicted alignment of the fibers in the constrained direction is in agreement with previous experimental studies on tissue strips or engineered valves circumferentially constrained (Neidert and Tranquillo, 2006, Rubbens et al., 2009a, Foolen et al., 2012).

Furthermore, the effect of the collagen architecture, and in particular collagen orientation, was investigated. Surprisingly, an initially anisotropic collagen network ($\beta = 0.2$) induces the same compaction that is induced by an initially isotropic collagen network ($\beta = 1000$). This is probably due to the fact that in both cases the cells still develop some of their traction forces in the direction perpendicular to the constrained direction.

Furthermore, in the presented model, the cell stress influences the collagen orientation, but the capability of the collagen fibers to guide cell orientation (contact guidance of the collagen over cells) (Foolen et al., 2012) is not accounted for. A deeper investigation of this phenomenon and its inclusion in the model might provide a more realistic representation of the effect of the initial collagen orientation.

The lower compaction observed in strips with a small amount of fiber interconnections in the discrete model (30%, as in strip c) than in those with a high degree of fiber interconnection (100%, as in strip b) indicates that the interaction of the fibers in different directions might play a role in the tissue compaction, and should be taken into account in the evaluation of the tissue remodeling behavior.

The interaction between different fiber orientations is a local phenomenon that can be captured by the discrete fiber model. In the continuum model no interaction between fibers can be described, and each direction is assumed to be independent from the others.

Consistent with the continuum model (Loerakker et al., 2014), it is assumed that the total amount of collagen degraded equals the total amount of collagen that is synthesized. A combination of the remodeling algorithm described in this work and of the algorithm for collagen growth described in Chapter 3 might enable a deeper investigation of the dynamics of collagen remodeling.

Chapter 6

Discussion

The potential of the described approach to couple the microstructure of the scaffold and the construct to their macroscopic mechanical behavior will be evaluated. Lastly, an overview of the questions opened by this work and possible strategies to address them will be discussed.

6.1   Problem statement and main findings

The successful development of an *in situ* engineered tissue from porous fibrous scaffolds would constitute a breakthrough in heart valve tissue engineering. While the traditional tissue engineering approach requires an expensive and time consuming tissue culture, the *in situ* approach would provide an off-the-shelf scaffold product, attractive for clinical use. However, for safe and long-term use, the off-the-shelf scaffold and the evolving tissue within should be mechanically functional. Hence, it must be ensured that:

- the heart valve scaffold is hemodynamically functional;

- the construct remains functional during *in vivo* tissue development;

- the *in vivo* synthesized extracellular matrix is able to sustain the hemodynamic loads and can maintain hemodynamic function also after scaffold degradation.

During *in situ* tissue engineering the load bearing capacity of the valve is gradually transferred from the scaffold to the de novo synthesized extracellular matrix. The initial organization of the extracellular matrix is largely affected by the scaffold architecture. Once the scaffold has degraded the extracellular matrix remodels in response to hemodynamic loads and cell-mediated tension in the valve, possibly resulting in an altered matrix organization. Computational models are useful tools to understand the relationship between microstructural parameters of the scaffold, the extracellular matrix and the macroscopic mechanical behavior of the evolving heart valve replacement.

In the current thesis the mechanical challenges of *in situ* tissue engineering have been addressed. The results can be summarized as follows:

- *Fibrous scaffold alignment significantly influences macroscopic scaffold mechanics and hemodynamic function of the heart valve replacement.*

  To evaluate the mechanical performance of electrospun scaffolds for tissue engineering we developed a multi-scale model of the scaffold that incorporates the key design parameters of the scaffold (fiber diameter, orientation, material and interconnections) (Chapter 2). The macromechanical properties of electrospun scaffolds with varying microstructures were studied with this model. Among all the design parameters, the variation of fiber orientation had the largest influence on the ultimate scaffold mechanics. In particular, we found that in engineered heart valve leaflets a significant degree of fiber alignment in the circumferential direction is needed to assure leaflet coaptation and strain distributions comparable to native valves during diastole.

- *A computational model can predict tissue macroscopic mechanical behavior from scaffold structural properties and collagen remodeling mechanisms.*

  A model of tissue turnover in the presence of a scaffold was developed (Chapter 3). Prior to degradation of the scaffold, sufficient extracellular matrix, and in particular collagen, needs to be synthesized to carry the hemodynamic loads during and after degradation of the scaffold. In the presence of a microfibrous scaffold, contact guidance is a powerful mechanism responsible for the alignment of the synthesized collagen along the scaffold fibers. It was previously shown that contact guidance even dominates over strain-induced collagen alignment mechanisms (de Jonge, 2013). A combination of contact guidance and strain-induced synthesis and degradation was shown to predict experimentally observed tissue mechanics (Chapter 3). The model successfully captured the transformation of the typical nearly linear stress-strain behavior of the scaffold into an exponential stress-strain curve representative of neo-tissue.

- *Cell shape relates to the formation of stress fibers in the cell cytoplasm.*
  To further understand contact guidance, a recently developed model that describes actin stress fiber remodeling was used to analyze actin orientation in cells in relation to the cell geometry on microfibers. Cells elongated along the fiber direction polymerize more oriented bundles of stress fibers and develop a higher tension state than cells having their main axis perpendicular to the fiber. In addition, the shape assumed by a cell on a scaffold

fiber (elongated in the fiber direction or tightly wrapped around the fiber) influences the direction of the polymerized stress fibers.

- *Cell tension mediates collagen remodeling after scaffold degradation.* The cell-mediated collagen remodeling after scaffold degradation was investigated using a discrete microstructural model. A previously developed model for collagen remodeling (Loerakker et al., 2014) was adapted for application at the micro-scale (Chapter 5). According to this model, the stress developed by the cells is responsible for tissue compaction. It was shown that the discrete model is able to reproduce the compaction described in tissue engineered strips by a continuum model. The predicted remodeled collagen architecture caused by cell tension, described as the result of synthesis and degradation of the collagen fibers, reproduce the collagen distribution described by the continuum framework. Tissue compaction is not influenced by the initial collagen network while it is affected by the amount of fiber interconnections.

6.2   Tools for scaffold design: discussion and limitations

The micro-scale model developed in this thesis describes scaffold networks and collagen networks as composed of one-dimensional interconnected elements, where each element represents one single fiber. This approach offers the possibility of controlling and varying the topological features of the network, and therefore represent a large variety of different structures.

A similar approach has been adopted by Stylianopoulos and Barocas (2007). In their approach, the network is composed of segments growing in opposite directions from nucleation sites that are generated randomly inside a cubic volume. In contrast, the approach presented in this thesis builds the network from a fiber distribution function. The parameters of the fiber distribution are derived from SEM images. However, the SEM images are characterized in terms of main fiber orientation and standard deviation, whereas the model represents a family of networks with those properties, and not one specific network. Stylianopoulos and Barocas (2007) adopt a volume-average technique, that requires a finite element model at the macro-scale and the construction of a RVE at the micro-scale around each Gauss point. Our approach, on the other end,

defines a micro-scale finite element problem coupled to a closed-form constitutive model at the macro-scale. This approach is computationally less expensive than the volume-average approach.

As observed also by Stylianopoulos et al. (2008), a microscopic discrete model is suitable to describe and evaluate the mechanical properties of a fiber network with different structural properties that can be controlled by electrospinning: fiber diameter, orientation, volume fraction, interconnections, material. Moreover, in a micro-scale approach the tissue growth, degradation and remodeling are evaluated on a single-fiber level. The description of these phenomena on a very local scale enables the description of interaction between different fibers (e.g. growth of collagen fibers along the scaffold fibers due to contact guidance). These parameters can only partially be included in continuum models (Driessen et al., 2005b, 2004, Holzapfel et al., 2000).

Despite these benefits, the computational tools described in this thesis show a number of limitations, and there is room for improvement.

To account for contact guidance, the collagen was assumed to align in the direction of the scaffold fibers a priori (Chapter 3). Although the predicted collagen fiber architecture and mechanical behavior agree with experimental observations (de Jonge, 2013), a more mechanistic explanation is needed. Experimental studies conducted by Canty et al. (2006) demonstrate that the cell cytoskeleton is involved in the collagen co-alignment with the cell main direction, which in presence of a scaffold coincide with the fibers' orientation (Fioretta et al., 2013). Furthermore, previous studies have demonstrated the influence of biochemical factors, such as specific growth factors (Laato et al., 1987, Frazier et al., 1996) to enhance or inhibit collagen synthesis. Currently, the biochemical phenomena that rule collagen production are not included in the computational model. Nevertheless, a combination of the mechanical aspects together with the mechanosensitive processes that guide collagen synthesis might be desirable, as they would provide a better insight in the mechanisms of tissue development than purely mechanical models do.

The discrete scaffold and tissue model described in the thesis is a 2D model. In reality, however, the electrospun scaffold is a 3D layered structure. The use of a 2D model limits the possibility of modeling the thickness effect in relatively thick scaffolds. However, the micro-scale model presented in this thesis can be converted

in layered 3D structures. In a multi-layer model, the properties of the fiber network can be defined independently in each layer and intersections between the fibers in the different layers can be defined in the space between the layers (Ippel et al., 2012). Layered scaffolds with structural properties varying throughout their thickness might be suitable to mimic the layered architectures of native tissues (Wang et al., 2013, Soo Kim et al., 2014). Bi-layered electrospun tubes with variable orientation per layer have been designed as blood vessel replacement to mimic the media and adventitia layers of the vessel (Kim, 2008, Vaz et al., 2005). Furthermore, the use of multiple layers with different porosity and fiber diameter might be used as a strategy to induce good cell infiltration on one side with high porosities while providing strength to the construct with denser and thicker fibers on the other side (Knight et al., 2013). A 3D layered microstructural model would allow the description of all these different microstructures and a good control of the mechanical properties of these substitutes.

Biaxial mechanical tests have been used in Chapter 2 and Chapter 3 as a validation tool to evaluate the mechanical properties of electrospun meshes. However, taken alone, biaxial mechanical tests are not sufficient to assess the functionality of a scaffold as tissue substitute. An overall characterization of scaffolds subjected to an *in vivo*-like cyclic load requires fatigue testing (Shimko and Nauman, 2007) in order to understand whether the structure can withstand the physiological cyclic load. The strain examined in this thesis did not exceed 30%, while physiological strains may reach up to 60% in a heart valve in aortic position (Driessen et al., 2005b).

The biaxial tests performed in this thesis use incrementally increasing strain levels, from 10% up to to 40% (Chapter 3). When strain is increased, the stress-strain curve at the new strain amplitude shows a hysteresis behavior. In addition, the stress-strain curves are shifted because of micro-damage that develops in the extracellular matrix (Fig. 6.1 right). This behavior is not observed in the biaxial testing of bare electrospun scaffolds (Fig. 6.1 left). The mechanical behavior shown by engineered tissues is most likely due to a disruption of fiber crosslinks when a certain strain amplitude is applied, thereby softening the material mechanical behavior. For rubber-like materials this effect has been labeled as the Mullins effect (Mullins, 1948). This micro-damage that induces softening of the tissues has not been described in this thesis. The Mullins effect might be included in our micro-scale model by defining criteria that induce disruption of the fiber

interconnections. This would allow a more comprehensive representation of the microstructural phenomena occurring in the scaffold with applied strain and of the macromechanical material behavior.
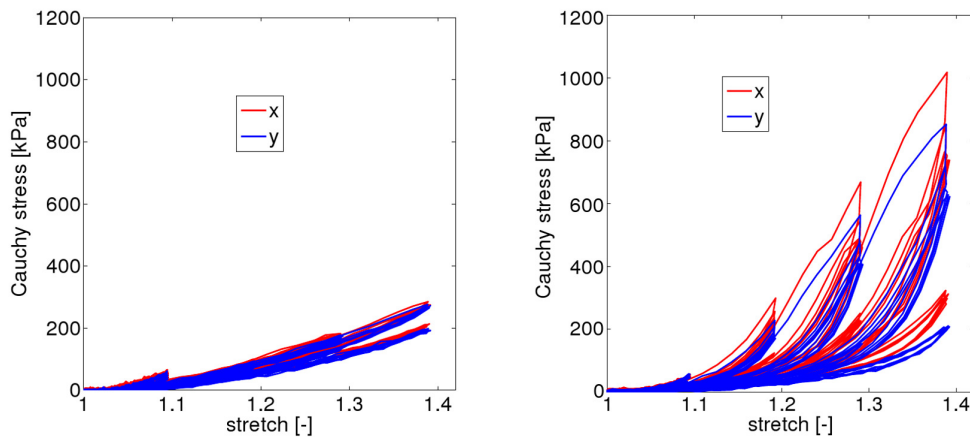
FIGURE 6.1: Cauchy stress-stretch curves of a biaxial mechanical test performed on isotropic PCL bisurea scaffold and a tissue engineered tissue cultured on an isotropic electrospun scaffold in static conditions for two weeks. In turn, 10%, 20%, 30% and 40% uniaxial and biaxial cyclic strain are applied. At each strain amplitude, the construct is cyclically strained for five times.

6.3 Future perspectives

The theory and the computational tools developed in this thesis can be used to optimize the mechanical design of scaffolds for *in situ* tissue engineering. The main design indication highlighted by this study is a pronounced anisotropy of the scaffold as a means to achieve higher radial stretches in engineered valve leaflets, a better leaflet coaptation and a more native-like collagen distribution. This represents an important step forward toward functional engineered heart valves, as it might help in reducing leaflet retraction and valve regurgitation *in vivo* (Mol, 2005).

It has been suggested that, compared to microfibrous scaffold, nanofibrous scaffolds can better resemble the natural cell environment created by the ECM (Li et al., 2008, Stankus et al., 2008). However, in the conventional electrospinning technique the use of nano-diamter fibers relates to very small pore sizes. Therefore, new techniques like low temperature electrospinning or scaffolds with sacrificial fibers have been proposed to enhance cell infiltration that otherwise would be

limited (Simonet et al., 2007, Guimarães et al., 2010). Despite an improved cell infiltration and proliferation, the use of nanofibers or bigger pore sizes results in reduced mechanical stiffness and resilience of the scaffold. By varying the fiber diameter, the described computational model might be used to explore the mechanical properties of nanofibrous scaffold.

Moreover, the presence of crosslinks in the proposed computational model allows for the possibility of modeling ruptures of the fiber interconnections (Beex et al., 2014). This might help in understanding softnening mechanisms and non-linear mechanical behavior observed in the engineered tissues.

The impact of scaffold degradation on the mechanical properties of the construct was neglected in our models (Chapter 5). An extension of the developed computational framework with scaffold fiber content decreasing with time, might provide a tool for the design of a scaffold with an optimal degradation rate.

Although a homogenization procedure is used to extract macroscopic data from the micro-scale analysis, there is no feedback between the micro-scale and the macro-scale as required in a true multi-scale computational analysis Smit et al. (1998), Breuls et al. (2002). Such analysis requires that changes in the micro-scale properties directly influence the macro-scale behavior and vice versa. The disadvantage of the use of coupled micro-macro computational homogenization strategies (Kouznetsova, 2002, Stylianopoulos and Barocas, 2007), is of course a significantly larger computation time compared to the solution time required by a macroscopic problem with closed-form homogenized constitutive equations.

Heart valves are subject to cyclic hemodynamic loads, which have a significant impact on cell orientation and cell tension and therefore may affect collagen remodeling (Foolen et al., 2012). The time scales for cells to respond to (changes) in cyclic deformations is of order hours, while the time scale associated with tissue remodeling is of the order weeks to months. A direct simulation of the cyclic strains in a heart valve, cell response and associated remodeling is not feasible. Special algorithms are required to account for the dynamic strains and the remodeling consequences.

In conclusion, the present work has achieved the objectives to predict macroscopic mechanical properties of (electrospun) scaffolds and tissue constructs based on the micro-scale architecture and mechanical properties. The models developed in

this thesis form the basis for a rational design of scaffolds for the *in situ* tissue engineering of cardiovascular tissues.

Bibliography

Alberts, B., 2000. Molecular biology of the cell. Garland Science.

Amoroso, N.J., D'Amore, A., Hong, Y., Wagner, W.R., Sacks, M.S., 2011. Elastomeric electrospun polyurethane scaffolds: the interrelationship between fabrication conditions, fiber topology, and mechanical properties. Advanced Materials 23, 106–11.

Argento, G., Simonet, M., Oomens, C.W.J., Baaijens, F.P.T., 2012. Multi-scale mechanical characterization of scaffolds for heart valve tissue engineering. Journal of Biomechanics 45, 2893–2898.

Badami, A.S., Kreke, M.R., Thompson, M.S., Riffle, J.S., Goldstein, A.S., 2006. Effect of fiber diameter on spreading, proliferation, and differentiation of osteoblastic cells on electrospun poly (lactic acid) substrates. Biomaterials 27, 596–606.

Baek, S., Rajagopal, K., Humphrey, J., 2006. A theoretical model of enlarging intracranial fusiform aneurysms. Transactions-American Society Mechanical Engineers Journal of Biomechanical Engineering 128, 142–149.

Baker, B.M., Mauck, R.L., 2007. The effect of nanofiber alignment on the maturation of engineered meniscus constructs. Biomaterials 28, 1967–1977.

Balguid, A., Mol, A., van Marion, M.H., Bank, R.A., Bouten, C.V.C., Baaijens, F.P.T., 2009. Tailoring fiber diameter in electrospun poly(epsilon-caprolactone) scaffolds for optimal cellular infiltration in cardiovascular tissue engineering. Tissue Engineering Part A 15, 437–44.

Balguid, A., Rubbens, M.P., Mol, A., Bank, R.A., Bogers, A.J., Van Kats, J.P., De Mol, B.A., Baaijens, F.P., Bouten, C.V., 2007. The role of collagen cross-links in biomechanical behavior of human aortic heart valve leaflets-relevance for tissue engineering. Tissue engineering 13, 1501–1511.

Barocas, V.H., Tranquillo, R.T., 1997. An anisotropic biphasic theory of tissue-equivalent mechanics: the interplay among cell traction, fibrillar network deformation, fibril alignment, and cell contact guidance. Journal of Biomechanical Engineering 119, 137–145.

Bashur, C.A., Shaffer, R.D., Dahlgren, L.A., Guelcher, S.A., Goldstein, A.S., 2009. Effect of fiber diameter and alignment of electrospun polyurethane meshes on mesenchymal progenitor cells. Tissue Engineering Part A 15, 2435–2445.

Beachley, V., Wen, X., 2009. Effect of electrospinning parameters on the nanofiber diameter and length. Materials Science and Engineering: C 29, 663–668.

Beex, L., Peerlings, R., Geers, M., 2014. A multiscale quasicontinuum method for lattice models with bond failure and fiber sliding. Computer Methods in Applied Mechanics and Engineering 269, 108–122.

Bhole, A.P., Flynn, B.P., Liles, M., Saeidi, N., Dimarzio, C.A., Ruberti, J.W., 2009. Mechanical strain enhances survivability of collagen micronetworks in the presence of collagenase: implications for load-bearing matrix growth and stability. Philosophical Transactions. Series A, Mathematical, Physical, and Engineering Sciences 367, 3339–3362.

Billiar, K., Sacks, M., 2000a. Biaxial mechanical properties of the natural and glutaraldehyde treated aortic valve cusp - part I: Experimental results. Journal of Biomechanical Engineering 122, 23–30.

Billiar, K.L., Sacks, M.S., 2000b. Biaxial mechanical properties of the native and glutaraldehyde-treated aortic valve cusp - part II: A structural constitutive model. Journal of Biomechanical Engineering 122, 327–335.

Birk, D.E., Trelstad, R.L., 1984. Extracellular compartments in matrix morphogenesis: collagen fibril, bundle, and lamellar formation by corneal fibroblasts. The Journal of Cell Biology 99, 2024–2033.

Boerboom, R.A., Rubbens, M.P., Driessen, N.J.B., Bouten, C.V.C., Baaijens, F.P.T., 2008. Effect of strain magnitude on the tissue properties of engineered cardiovascular constructs. Annals of Biomedical Engineering 36, 244–53.

Bourget, J.M., Gauvin, R., Larouche, D., Lavoie, A., Labbé, R., Auger, F.A., Germain, L., 2012. Human fibroblast-derived ecm as a scaffold for vascular tissue engineering. Biomaterials 33, 9205–9213.

Breuls, R.G., Sengers, B.G., Oomens, C.W.J., Bouten, C.V.C., Baaijens, F.P.T., 2002. Predicting local cell deformations in engineered tissue constructs: a multilevel finite element approach. Journal of Biomechanical Engineering 124, 198–207.

Brown, R., Prajapati, R., McGrouther, D., Yannas, I., Eastwood, M., 1998. Tensional homeostasis in dermal fibroblasts: Mechanical responses to mechanical loading in three-dimensional substrates. Journal of Cellular Physiology 175, 323–332.

Cai, S., Pestic-Dragovich, L., ODonnell, M.E., Wang, N., Ingber, D., Elson, E., De Lanerolle, P., 1998. Regulation of cytoskeletal mechanics and cell growth by myosin light chain phosphorylation. American Journal of Physiology-Cell Physiology 275, C1349–C1356.

Canty, E.G., Lu, Y., Meadows, R.S., Shaw, M.K., Holmes, D.F., Kadler, K.E., 2004. Coalignment of plasma membrane channels and protrusions (fibripositors) specifies the parallelism of tendon. The Journal of cell biology 165, 553–563.

Canty, E.G., Starborg, T., Lu, Y., Humphries, S.M., Holmes, D.F., Meadows, R.S., Huffman, A., O'Toole, E.T., Kadler, K.E., 2006. Actin filaments are required for fibripositor-mediated collagen fibril alignment in tendon. Journal of Biological Chemistry 281, 38592–38598.

Chainani, A., Hippensteel, K.J., Kishan, A., Garrigues, N.W., Ruch, D.S., Guilak, F., Little, D., 2013. Multi-layered electrospun scaffolds for tendon tissue engineering. Tissue Engineering Part A 19, 2594–2604.

Charest, J.L., García, A.J., King, W.P., 2007. Myoblast alignment and differentiation on cell culture substrates with microscale topography and model chemistries. Biomaterials 28, 2202–2210.

Chaurey, V., Block, F., Su, Y.H., Chiang, P.C., Botchwey, E., Chou, C.F., Swami, N.S., 2012. Nanofiber size-dependent sensitivity of fibroblast directionality to alignment methodology of scaffold. Acta Biomaterialia 8, 3982–3990.

Chen, C.S., Alonso, J.L., Ostuni, E., Whitesides, G.M., Ingber, D.E., 2003. Cell shape provides global control of focal adhesion assembly. Biochemical and Biophysical Research Communications 307, 355–361.

Chen, C.S., Mrksich, M., Huang, S., Whitesides, G.M., Ingber, D.E., 1997. Geometric control of cell life and death. Science 276, 1425–1428.

Chen, M., Patra, P.K., Warner, S.B., Bhowmick, S., 2007. Role of fiber diameter in adhesion and proliferation of nih 3t3 fibroblast on electrospun polycaprolactone scaffolds. Tissue Engineering 13, 579–87.

Chowdhury, M., Stylios, G., 2010. Effect of experimental parameters on the morphology of electrospun nylon 6 fibres. International Journal of Basic & Applied Sciences 10, 116–131.

Cooley, J.F., 1902. Apparatus for electrically dispersing fluids.

Courtney, T., Sacks, M.S., Stankus, J., Guan, J., Wagner, W.R., 2006. Design and analysis of tissue engineering scaffolds that mimic soft tissue mechanical anisotropy. Biomaterials 27, 3631–3638.

Culav, E.M., Clark, C.H., Merrilees, M.J., 1999. Connective tissues: matrix composition and its relevance to physical therapy. Physical Therapy 79, 308–319.

Cuvelier, D., Théry, M., Chu, Y.S., Dufour, S., Thiéry, J.P., Bornens, M., Nassoy, P., Mahadevan, L., 2007. The universal dynamics of cell spreading. Current biology 17, 694–699.

Dahl, S.L., Vaughn, M.E., Hu, J.J., Driessen, N.J., Baaijens, F.P.T., Humphrey, J.D., Niklason, L.E., 2008. A microstructurally motivated model of the mechanical behavior of tissue engineered blood vessels. Annals of Biomedical Engineering 36, 1782–1792.

Dasi, L.P., Simon, H.A., Sucosky, P., Yoganathan, A.P., 2009. Fluid mechanics of artificial heart valves. Clinical and Experimental Pharmacology and Physiology 36, 225–237.

Deshpande, V.S., McMeeking, R.M., Evans, A.G., 2007. A model for the contractility of the cytoskeleton including the effects of stress-fibre formation and dissociation. Proceedings of the Royal Society A: Mathematical, Physical and Engineering Science 463, 787–815.

Driessen, N., Bouten, C., Baaijens, F., 2005a. Improved prediction of the collagen fiber architecture in the aortic heart valve. Journal of Biomechanical Engineering 127, 329–36.

Driessen, N., Bouten, C., Baaijens, F., 2005b. A structural constitutive model for collagenous cardiovascular tissues incorporating the angular fiber distribution. Journal of Biomechanical Engineering 127, 494–503.

Driessen, N., Wilson, W., Bouten, C., Baaijens, F., 2004. A computational model for collagen fibre remodelling in the arterial wall. Journal of Theoretical Biology 226, 53–64.

Driessen, N.J.B., Boerboom, R.A., Huyghe, J.M.R.J., Bouten, C.V.C., Baaijens, F.P.T., 2003. Computational analyses of mechanically induced collagen fiber remodeling in the aortic heart valve. Journal of Biomechanical Engineering 125, 549–557.

Driessen, N.J.B., Bouten, C.V.C., Baaijens, F.P.T., 2005c. Improved prediction of the collagen fiber architecture in the aortic heart valve. Journal of Biomechanical Engineering 127, 329–336.

Driessen, N.J.B., Cox, M.A.J., Bouten, C.V.C., Baaijens, F.P.T., 2008. Remodeling of the angular collagen fiber distribution in cardiovascular tissues. Biomechanics and Modeling in Mechanobiology 7, 93–103.

Driessen, N.J.B., Mol, A., Bouten, C.V.C., Baaijens, F.P.T., 2007. Modeling the mechanics of tissue-engineered human heart valve leaflets. Journal of Biomechanics 40, 325–334.

Driessen-Mol, A., Bouten, C., Zund, G., Guenter, C., Visjager, J., Turina, M., Baaijens, F., Hoerstrup, S., 2003. The relevance of large strains in functional tissue engineering of heart valves. The Journal of Thoracic and Cardiovascular Surgery 51, 78–83.

Driessen-Mol, A., Driessen, N.J.B., Rutten, M.C.M., Hoerstrup, S.P., Bouten, C.V.C., Baaijens, F.P.T., 2005. Tissue engineering of human heart valve leaflets: a novel bioreactor for a strain-based conditioning approach. Annals of Biomedical Engineering 33, 1778–1788.

Eckert, C.E., Mikulis, B.T., Gottlieb, D., Gerneke, D., LeGrice, I., Padera, R.F., Mayer, J.E., Schoen, F.J., Sacks, M.S., 2011. Three-dimensional quantitative micromorphology of pre- and post-implanted engineered heart valve tissues. Annals of Biomedical Engineering 29, 205–222.

Erisken, C., al, 2013. Scaffold fiber diameter regulates human tendon fibroblast growth and differentiation. Tissue Engineering Part A 19(3-4), 519–28.

Fardin, M., Rossier, O., Rangamani, P., Avigan, P., Gauthier, N., Vonnegut, W., Mathur, A., Hone, J., Iyengar, R., Sheetz, M., 2010. Cell spreading as a hydrodynamic process. Soft Matter 6, 4788–4799.

Fioretta, E., Simonet, M., Smits, A., Baaijens, F.P.T., Bouten, C.V.C., 2013. Differential response of endothelial and endothelial colony forming cells on electrospun scaffolds with distinct micro-fiber diameters. Biomacromolecules doi: 10.1021/bm4016418.

Flanagan, T.C., Sachweh, J.S., Frese, J., Schnöring, H., Gronloh, N., Koch, S., Tolba, R.H., Schmitz-Rode, T., Jockenhoevel, S., 2009. In vivo remodeling and structural characterization of fibrin-based tissue-engineered heart valves in the adult sheep model. Tissue Engineering Part A 15, 2965–2976.

Foolen, J., Deshpande, V.S., Kanters, F.M., Baaijens, F., 2012. The influence of matrix integrity on stress-fiber remodeling in 3D. Biomaterials 33, 7508–7518.

Frazier, K., Williams, S., Kothapalli, D., Klapper, H., Grotendorst, G.R., 1996. Stimulation of fibroblast cell growth, matrix production, and granulation tissue formation by connective tissue growth factor. Journal of Investigative Dermatology 107, 404–411.

Freitas, R.A.J., 1999. Nanomedicine, Volume I: Basic Capabilities. Landes Bioscience.

Fridez, P., Zulliger, M., Bobard, F., Montorzi, G., Miyazaki, H., Hayashi, K., Stergiopulos, N., 2003. Geometrical, functional, and histomorphometric adaptation of rat carotid artery in induced hypertension. Journal of biomechanics 36, 671–680.

Fridrikh, S.V., Yu, J.H., Brenner, M.P., Rutledge, G.C., et al., 2003. Controlling the fiber diameter during electrospinning. Physical Review Letters 90, 144502–1–144502–4.

Gasser, T.C., Ogden, R.W., Holzapfel, G.A., 2006. Hyperelastic modelling of arterial layers with distributed collagen fibre orientations. Journal of The Royal Society Interface 3, 15–35.

Gealy, C., Hayes, A.J., Buckwell, R., Young, R.D., Caterson, B., Quantock, A.J., Ralphs, J.R., 2009. Actin and type i collagen propeptide distribution in the developing chick cornea. Investigative Ophthalmology & Visual Science 50, 1653–1658.

van Geemen, D., Driessen-Mol, A., Grootzwagers, L.G., Soekhradj-Soechit, R.S., Vis, P.W.R., Baaijens, F.P., Bouten, C.V., 2012. Variation in tissue outcome of ovine and human engineered heart valve constructs: relevance for tissue engineering. Regenerative Medicine 7, 117–126.

Gottlieb, D., Kunal, T., Emani, S., Aikawa, E., Brown, D.W., Powell, A.J., Nedder, A., Engelmayr Jr, G.C., Melero-Martin, J.M., Sacks, M.S., et al., 2010. In vivo monitoring of function of autologous engineered pulmonary valve. The Journal of Thoracic and Cardiovascular Surgery 139, 723–731.

Graham, H.K., Holmes, D.F., Watson, R.B., Kadler, K.E., 2000. Identification of collagen fibril fusion during vertebrate tendon morphogenesis. the process relies on unipolar fibrils and is regulated by collagen-proteoglycan interaction. Journal of Molecular Biology 295, 891–902.

Greiner, A.M., Chen, H., Spatz, J.P., Kemkemer, R., 2013. Cyclic tensile strain controls cell shape and directs actin stress fiber formation and focal adhesion alignment in spreading cells. PloS one 8, e77328.

Guimarães, A., Martins, A., Pinho, E.D., Faria, S., Reis, R.L., Neves, N.M., 2010. Solving cell infiltration limitations of electrospun nanofiber meshes for tissue engineering applications. Nanomedicine 5, 539–554.

Hadi, M., Sander, E., Ruberti, J., Barocas, V., 2012. Simulated remodeling of loaded collagen networks via strain-dependent enzymatic degradation and constant-rate fiber growth. Mechanics of Materials 44, 72–82.

Hariton, I., Gasser, T., Holzapfel, G., et al., 2007. Stress-driven collagen fiber remodeling in arterial walls. Biomechanics and Modeling in Mechanobiology 6, 163–175.

He, W., Yong, T., Teo, W.E., Ma, Z., Ramakrishna, S., 2005. Fabrication and endothelialization of collagen-blended biodegradable polymer nanofibers: potential vascular graft for blood vessel tissue engineering. Tissue Engineering 11, 1574–1588.

Heath, D.E., Lannutti, J.J., Cooper, S.L., 2010. Electrospun scaffold topography affects endothelial cell proliferation, metabolic activity, and morphology. Journal of Biomedical Material Research Part A 94, 1195–1204.

Heck, T.A.M., 2013. Cell traction and strain dependent collagen degradation predict tissue adaptation. Master's thesis. Eindhoven University of Technology.

Henry, J.A., Simonet, M., Pandit, A., Neuenschwander, P., 2007. Characterization of a slowly degrading biodegradable polyesterurethane for tissue engineering scaffolds. Journal of Biomedical Materials Research Part A 82, 669–679.

Hill, R., 1963. Elastic properties of reinforced solids: some theoretical principles. Journal of the Mechanics and Physics of Solids 11, 357–372.

Hill, R., 1984. On macroscopic effects of heterogeneity in elastoplastic media at finite strain. Mathematical Proceedings of the Cambridge Philosophical Society 95, 481–494.

Hoerstrup, S.P., Sodian, R., Daebritz, S., Wang, J., Bacha, E.A., Martin, D.P., Moran, A.M., Guleserian, K.J., Sperling, J.S., Kaushal, S., et al., 2000. Functional living trileaflet heart valves grown in vitro. Circulation 102, Iii–44–Iii–49.

Holmes, D.F., Lowe, M.P., Chapman, J.A., 1994. Vertebrate (chick) collagen fibrils formed in vivo can exhibit a reversal in molecular polarity. Journal of Molecular Biology 235, 80–83.

Holzapfel, G.A., Gasser, T.C., Ogden, R.W., 2000. A new constitutive framework for arterial wall mechanics and a comparative study of material models. Journal of Elasticity and the Physical Science of Solids 61, 1–48.

Hong, Y., Guan, J., Fujimoto, K.L., Hashizume, R., Pelinescu, A.L., Wagner, W.R., 2010. Tailoring the degradation kinetics of poly (ester carbonate urethane) urea thermoplastic elastomers for tissue engineering scaffolds. Biomaterials 31, 4249–4258.

Huang, C., Yannas, I.V., 1977. Mechanochemical studies of enzymatic degradation of insoluble collagen fibers. Journal of Biomedical Material Research 11, 137–154.

Humphrey, J., 1999. Remodeling of a collagenous tissue at fixed lengths. Journal of Biomechanical Engineering 121, 591–597.

Huot, J., Houle, F., Marceau, F., Landry, J., 1997. Oxidative stress–induced actin reorganization mediated by the p38 mitogen-activated protein kinase/heat shock protein 27 pathway in vascular endothelial cells. Circulation Research 80, 383–392.

Huszar, G., Maiocco, J., Naftolin, F., 1980. Monitoring of collagen and collagen fragments in chromatography of protein mixtures. Analiytical Biochemestry 105, 494–9.

Hwang, C., Park, Y., Park, J., Lee, K., Sun, K., Khademhosseini, A., Lee, S., 2009. Controlled cellular orientation on plga microfibers with defined diameters. Biomedical Microdevices 11, 739–746.

Ionescu, L.C., Mauck, R.L., 2012. Porosity and cell preseeding influence electrospun scaffold maturation and meniscus integration in vitro. Tissue Engineering Part A 19, 538–547.

Ippel, B.A., Argento, G., Oomens, C.W.J., 2012. Multi-scale analysis of 3D electrospun scaffold for tissue engineering.

de Jonge, N., 2013. Guiding collagen orientation at the micro-level in engineered cardiovascular tissues. Ph.D. thesis. Eindhoven University of Technology.

de Jonge, N., Kanters, F.M., Baaijens, F.P., Bouten, C.V., 2013. Strain-induced collagen organization at the micro-level in fibrin-based engineered tissue constructs. Annals of Biomedical Engineering 41, 763–774.

Kadler, K.E., Holmes, D.F., Graham, H., Starborg, T., 2000. Tip-mediated fusion involving unipolar collagen fibrils accounts for rapid fibril elongation, the occurrence of fibrillar branched networks in skin and the paucity of collagen fibril ends in vertebrates. Matrix Biology 19, 359–365.

Kai, D., Prabhakaran, M.P., Jin, G., Ramakrishna, S., 2011. Guided orientation of cardiomyocytes on electrospun aligned nanofibers for cardiac tissue engineering. Journal of Biomedical Material Research Part B Applied Biomaterials 98, 379–386.

Kaunas, R., Nguyen, P., Usami, S., Chien, S., 2005. Cooperative effects of rho and mechanical stretch on stress fiber organization. Proceedings of the National Academy of Sciences of the United States of America 102, 15895–15900.

Khatau, S.B., Hale, C.M., Stewart-Hutchinson, P., Patel, M.S., Stewart, C.L., Searson, P.C., Hodzic, D., Wirtz, D., 2009. A perinuclear actin cap regulates nuclear shape. Proceedings of the National Academy of Sciences 106, 19017–19022.

Kilian, K.A., Bugarija, B., Lahn, B.T., Mrksich, M., 2010. Geometric cues for directing the differentiation of mesenchymal stem cells. Proceedings of the National Academy of Sciences 107, 4872–4877.

Kim, G.H., 2008. Electrospun pcl nanofibers with anisotropic mechanical properties as a biomedical scaffold. Biomedical Materials 3, 025010.

Kim, W., Cho, S., Kang, M., Lee, T., Park, J., 2001. Tissue-engineered heart valve leaflets: an animal study. The International Journal of Artificial Organs 24, 642–648.

Knight, R., Booth, C., Wilcox, H., Fisher, J., Ingham, E., 2005. Tissue engineering of cardiac valves: re-seeding of acellular porcine aortic valve matrices with human mesenchymal progenitor cells. The Journal of Heart Valve Disease 14, 806–813.

Knight, T., Basu, J., Rivera, E.A., Spencer, T., Jain, D., Payne, R., 2013. Fabrication of a multi-layer three-dimensional scaffold with controlled porous micro-architecture for application in small intestine tissue engineering. Cell Adhesion & Migration 7, 267–274.

Kouznetsova, V., 2002. Computational homogenization for the multi-scale analysis of multi-phase materials. Ph.D. thesis. Eindhoven University of Technology.

Kouznetsova, V., Brekelmans, W.A.M., Baaijens, F.P.T., 2001. An approach to micro-macro modeling of heterogeneous materials. Computational Mechanics 27, 37–48.

Krahn, K.N., C, B.C.V., van Tuijl, S., van Zandvoort, M.A., M, M., 2006. Fluorescently labeled collagen binding proteins allow specific visualization of collagen in tissues and live cell culture. Analytical Biochemestry 350, 177–185.

Kuhl, E., Holzapfel, G.A., 2007. A continuum model for remodeling in living structures. Journal of Materials Science 42, 8811–8823.

La Carrubba, V., Pavia, F.C., Brucato, V., Piccarolo, S., 2008. Plla/pla scaffolds prepared via thermally induced phase separation (tips): tuning of properties and biodegradability. International Journal of Material Forming 1, 619–622.

Laato, M., Kahari, V., Niinikoski, J., Vuorio, E., 1987. Epidermal growth factor increases collagen production in granulation tissue by stimulation of fibroblast proliferation and not by activation of procollagen genes. Biochemical Journal 247, 385–388.

Ladoux, B., Nicolas, A., 2012. Physically based principles of cell adhesion mechanosensitivity in tissues. Reports on Progress in Physics 75, 116601.

Lam, M.T., Clem, W.C., Takayama, S., 2008. Reversible on-demand cell alignment using reconfigurable microtopography. Biomaterials 29, 1705–1712.

Langer, R., Vacanti, J.P., 1993. Tissue engineering. Science 260, 920–926.

Lebedev, V., Laikov, D., 1999. A quadrature formula for the sphere of the 131st algebraic order of accuracy. Doklady Mathematics 59, 477–481.

Lee, C.H., al, 2005. Nanofiber alignment and direction of mechanical strain affect the ecm production of human acl fibroblast. Biomaterials 26(11), 1261–70.

Lee, T.C., Midura, R.J., Hascall, V.C., Vesely, I., 2001. The effect of elastin damage on the mechanics of the aortic valve. Journal of Biomechanics 34, 203–210.

Legant, W.R., Pathak, A., Yang, M.T., Deshpande, V.S., McMeeking, R.M., Chen, C.S., 2009. Microfabricated tissue gauges to measure and manipulate forces from 3D microtissues. Proceedings of the National Academy of Sciences 106, 10097–10102.

Li, D., Xia, Y., 2004. Electrospinning of nanofibers: reinventing the wheel? Advanced Materials 16, 1151–1170.

Li, X.T., Zhang, Y., Chen, G.Q., 2008. Nanofibrous polyhydroxyalkanoate matrices as cell growth supporting materials. Biomaterials 29, 3720–3728.

Loerakker, S., Obbink-Huizer, C., Baaijens, F.P.T., 2014. A physically-motivated constitutive model for cell-mediated compaction and collagen remodeling in soft tissues. Biomechanics and Modeling in Mechanobiology doi: 10.1007/s10237-013-0549-1.

Loesberg, W., Walboomers, X., Van Loon, J., Jansen, J., 2005. The effect of combined cyclic mechanical stretching and microgrooved surface topography on the behavior of fibroblasts. Journal of Biomedical Materials Research Part A 75, 723–732.

Lowery, J.L., Datta, N., Rutledge, G.C., 2010. Effect of fiber diameter, pore size and seeding method on growth of human dermal fibroblasts in electrospun poly (e-caprolactone) fibrous mats. Biomaterials 31, 491–504.

Ma, Z., He, W., Yong, T., Ramakrishna, S., 2005. Grafting of gelatin on electrospun poly (caprolactone) nanofibers to improve endothelial cell spreading and proliferation and to control cell orientation. Tissue Engineering 11, 1149–1158.

Matsumoto, T., Hayashi, K., 1994. Mechanical and dimensional adaptation of rat aorta to hypertension. Journal of Biomechanical Engineering 116, 278–283.

McBeath, R., Pirone, D.M., Nelson, C.M., Bhadriraju, K., Chen, C.S., 2004. Cell shape, cytoskeletal tension, and rhoa regulate stem cell lineage commitment. Developmental cell 6, 483–495.

Menten, L., Michaelis, M.I., 1913. Die kinetik der invertinwirkung. Biochemische Zeitschrift 49, 333–369.

Merryman, W.D., Liao, J., Parekh, A., Candiello, J.E., Lin, H., Sacks, M.S., 2007. Differences in tissue-remodeling potential of aortic and pulmonary heart valve interstitial cells. Tissue Engineering 13, 2281–2289.

Meuwissen, M.H., Oomens, C.W.J., Veldpaus, F.E., Janssen, J.D., 1996. Identification of errors in constitutive models by sensitivity analysis. Computer Aided Design in Composite Material Technology V, 61 –70.

Milleret, V., Simona, B., Neuenschwander, P., Hall, H., 2011. Tuning electrospinning parameters for production of 3D-fiber-fleeces with increased porosity for soft tissue engineering applications. Journal of European Cells and Materials 21, 286–303.

Mol, A., 2005. Functional tissue engineering of human heart valve leaflets. Ph.D. thesis. Eindhoven University of Technology.

Mol, A., Rutten, M.C., Driessen, N.J., Bouten, C.V., Zünd, G., Baaijens, F.P., Hoerstrup, S.P., 2006. Autologous human tissue-engineered heart valves prospects for systemic application. Circulation 114, I–152.

Mol, A., Smits, A.I., Bouten, C.V., Baaijens, F.P., 2009. Tissue engineering of heart valves: advances and current challenges. Expert Reviews Medical Devices 6, 259–275.

Müller, P., Langenbach, A., Kaminski, A., Rychly, J., 2013. Modulating the actin cytoskeleton affects mechanically induced signal transduction and differentiation in mesenchymal stem cells. PloS one 8, e71283.

Mullins, L., 1948. Effect of stretching on the properties of rubber. Rubber Chemistry and Technology 21, 281–300.

Neidert, M.R., Tranquillo, R.T., 2006. Tissue-engineered valves with commissural alignment. Tissue Engineering 12, 891–903.

Nelson, C.M., Pirone, D.M., Tan, J.L., Chen, C.S., 2004. Vascular endothelial-cadherin regulates cytoskeletal tension, cell spreading, and focal adhesions by stimulating rhoa. Molecular biology of the cell 15, 2943–2953.

Nemat-Nasser, S., 1999. Averaging theorems in finite deformation plasticity. Mechanics of Materials 31, 493–523.

Niklason, L.E., Abbott, W., Gao, J., Klagges, B., Hirschi, K.K., Ulubayram, K., Conroy, N., Jones, R., Vasanawala, A., Sanzgiri, S., et al., 2001. Morphologic and mechanical characteristics of engineered bovine arteries. Journal of Vascular Surgery 33, 628–638.

Niklason, L.E., Yeh, A.T., Calle, E.A., Bai, Y., Valentin, A., Humphrey, J.D., 2010. Enabling tools for engineering collagenous tissues integrating bioreactors, intravital imaging, and biomechanical modeling. Proceedings of the National Academy of Sciences 107, 3335–3339.

Obbink-Huizer, C., Oomens, C.W., Loerakker, S., Foolen, J., Bouten, C.V., Baaijens, F.P., 2013. Computational model predicts cell orientation in response to a range of mechanical stimuli. Biomechanics and Modeling in Mechanobiology 13, 227–236.

Patience, C., Takeuchi, Y., Weiss, R.A., 1998. Zoonosis in xenotransplantation. Current Opinion in Immunology 10, 539–542.

Paul, R.G., Bailey, A.J., 2003. Chemical stabilisation of collagen as a biomimetic. The Scientific World Journal 3, 138–155.

Perrino, A.C., Reeves, S.T., 2008. A practical approach to transesophageal echocardiography. Wolters Kluwer Health.

Pibarot, P., Dumesnil, J.G., 2009. Prosthetic heart valves selection of the optimal prosthesis and long-term management. Circulation 119, 1034–1048.

Prabhakaran, M.P., Vatankhah, E., Ramakrishna, S., 2013. Electrospun aligned phbv/collagen nanofibers as substrates for nerve tissue engineering. Biotechnology and Bioengineering 110, 2775–2784.

Rabkin-Aikawa, E., Farber, M., Aikawa, M., Schoen, F.J., 2004. Dynamic and reversible changes of interstitial cell phenotype during remodeling of cardiac valves. Journal of Heart Valve Disease 13, 841–847.

Raghavan, B.K., Coffin, D.W., 2011. Control of inter-fiber fusing for nanofiber webs via electrospinning. Journal of Engineered Fibers and Fabrics 6, 1–5.

Richardson, S.H., Starborg, T., Lu, Y., Humphries, S.M., Meadows, R.S., Kadler, K.E., 2007. Tendon development requires regulation of cell condensation and cell shape via cadherin-11-mediated cell-cell junctions. Molecular and Cellular Biology 27, 6218–6228.

Roh, J.D., Sawh-Martinez, R., Brennan, M.P., Jay, S.M., Devine, L., Rao, D.A., Yi, T., Mirensky, T.L., Nalbandian, A., Udelsman, B., et al., 2010. Tissue-engineered vascular grafts transform into mature blood vessels via an inflammation-mediated process of vascular remodeling. Proceedings of the National Academy of Sciences 107, 4669–4674.

Ronan, W., Deshpande, V.S., McMeeking, R.M., McGarry, J.P., 2012. Numerical investigation of the active role of the actin cytoskeleton in the compression resistance of cells. Journal of the Mechanical Behavior of Biomedical Materials 14, 143–157.

Rubbens, M.P., Driessen-Mol, A., Boerboom, R.A., Koppert, M.M., van Assen, H.C., Romeny, B.M.T., Baaijens, F.P., Bouten, C.V., 2009a. Quantification of the temporal evolution of collagen orientation in mechanically conditioned engineered cardiovascular tissues. Annals of Biomedical Engineering 37, 1263–1272.

Rubbens, M.P., Mol, A., Boerboom, R.A., Bank, R.A., Baaijens, F.P.T., Bouten, C.V.C., 2009b. Intermittent straining accelerates the development of tissue properties in engineered heart valve tissue. Tissue Engineering Part A 15, 999–1008.

Ruberti, J.W., Hallab, N.J., 2005. Strain-controlled enzymatic cleavage of collagen in loaded matrix. Biochemical and Biophysical Research Communications 336, 483–489.

Sauren, 1981. The mechanical behaviour of the aortic valve. Ph.D. thesis. Technische Hogeschool Eindhoven.

Schenke-Layland, K., Opitz, F., Gross, M., Döring, C., Halbhuber, K., Schirrmeister, F., Wahlers, T., Stock, U., 2003. Complete dynamic repopulation of decellularized heart valves by application of defined physical signals: an in vitro study. Cardiovascular Research 60, 497–509.

Schmidt, D., Dijkman, P.E., Driessen-Mol, A., Stenger, R., Mariani, C., Puolakka, A., Rissanen, M., Deichmann, T., Odermatt, B., Weber, B., et al., 2010. Minimally-invasive implantation of living tissue engineered heart valvesa comprehensive approach from autologous vascular cells to stem cells. Journal of the American College of Cardiology 56, 510–520.

Schoen, F.J., Levy, R.J., 1999. Tissue heart valves: current challenges and future research perspectives. Journal of Biomedical Material Research 47, 439–465.

Schwarz, U.S., Safran, S.A., 2013. Physics of adherent cells. Reviews of Modern Physics 85, 1327–1381.

Scott, M., Vesely, I., 1995. Aortic valve cusp microstructure: the role of elastin. The Annals of thoracic surgery 60, S391–S394.

Segal, A., 1984. SEPRAN User Manual, Standard Problems and Programmers Guide. Ingenieursbureau SEPRA, Leidschendam, The Netherlands.

Senthilnathan, V., Treasure, T., Grunkemeier, G., Starr, A., 1999. Heart valves: which is the best choice? Cardiovascular Surgery 7, 393–397.

Shimko, D.A., Nauman, E.A., 2007. Development and characterization of a porous poly (methyl methacrylate) scaffold with controllable modulus and permeability. Journal of Biomedical Materials Research Part B: Applied Biomaterials 80, 360–369.

Shinoka, T., Breuer, C.K., Tanel, R.E., Zund, G., Miura, T., Ma, P.X., Langer, R., Vacanti, J.P., Mayer Jr, J.E., 1995. Tissue engineering heart valves: valve leaflet replacement study in a lamb model. The Annals of Thoracic Surgery 60, S513–S516.

Siddiqui, R.F., Abraham, J.R., Butany, J., 2009. Bioprosthetic heart valves: modes of failure. Histopathology 55, 135–144.

Silverthorn, D.U., Garrison, C.W., 2004. Human Physiology: An Integrated Approach. 3rd edition. Benjamin-Cummings Publishing Company.

Simonet, M., Schneider, O.D., Neuenschwander, P., Stark, W.J., 2007. Ultraporous 3d polymer meshes by low-temperature electrospinning: use of ice crystals as a removable void template. Polymer Engineering & Science 47, 2020–2026.

Smit, R., Brekelmans, W., Meijer, H., 1998. Prediction of the mechanical behavior of nonlinear heterogeneous systems by multi-level finite element modeling. Computer Methods in Applied Mechanics and Engineering 155, 181–192.

Soares, A., Oomens, C., Baaijens, F., 2012. A computational model to describe the collagen orientation in statically cultured engineered tissues. Computer Methods in Biomechanics and Biomedical Engineering 17, 251–262.

Soares, A.L.F., Stekelenburg, M., Baaijens, F.P.T., 2011. Remodeling of the collagen fiber architecture due to compaction in small vessels under tissue engineered conditions. Journal of Biomechanical Engineering 133, 071002.

Sodian, R., Loebe, M., Hein, A., Martin, D.P., Hoerstrup, S.P., Potapov, E.V., Hausmann, H., Lueth, T., Hetzer, R., 2002. Application of stereolithography for scaffold fabrication for tissue engineered heart valves. Asaio Journal 48, 12–16.

Soliman, S., Sant, S., Nichol, J.W., Khabiry, M., Traversa, E., Khademhosseini, A., 2011. Controlling the porosity of fibrous scaffolds by modulating the fiber diameter and packing density. Journal of Biomedical Materials Research Part A 96, 566–574.

Soo Kim, B., Ji Kim, E., Suk Choi, J., Hoon Jeong, J., Hyunchul Jo, C., Woo Cho, Y., 2014. Human collagen-based multilayer scaffolds for tendon-to-bone interface tissue engineering. Journal of Biomedical Materials Research Part A doi: 10.1002/jbm.a.35057.

Stankus, J.J., Freytes, D.O., Badylak, S.F., Wagner, W.R., 2008. Hybrid nanofibrous scaffolds from electrospinning of a synthetic biodegradable elastomer and urinary bladder matrix. Journal of Biomaterials Science, Polymer Edition 19, 635–652.

Stella, J.A., Wagner, W.R., Sacks, M.S., 2010. Scale-dependent fiber kinematics of elastomeric electrospun scaffolds for soft tissue engineering. Journal of Biomedical Material Research Part A 93, 1032–42.

Stock, U.A., Nagashima, M., Khalil, P.N., Nollert, G.D., Herdena, T., Sperling, J.S., Moran, A., Lien, J., Martin, D.P., Schoen, F.J., et al., 2000. Tissue-engineered valved conduits in the pulmonary circulation. The Journal of Thoracic and Cardiovascular Surgery 119, 732–740.

Stopak, D., Harris, A.K., 1982. Connective tissue morphogenesis by fibroblast traction: I. tissue culture observations. Developmental Biology 90, 383–398.

Stylianopoulos, T., Barocas, V., 2007. Volume-averaging theory for the study of the mechanics of collagen networks. Computer Methods in Applied Mechanics and Engineering 196, 2981–2990.

Stylianopoulos, T., Bashur, C.A., Goldstein, A.S., Guelcher, S.A., Barocas, V.H., 2008. Computational predictions of the tensile properties of electrospun fibre meshes: effect of fibre diameter and fibre orientation. Journal of the Mechanical Behavior of Biomedical Materials 1, 326–335.

Subramony, S.D., Dargis, B.R., Castillo, M., EU, A., Tracey, M.S., Su, A., Lu, H.H., 2013. The guidance of stem cell differentiation by substrate alignment and mechanical stimulation. Biomaterials 34, 1942–1953.

Sutherland, F.W., Perry, T.E., Yu, Y., Sherwood, M.C., Rabkin, E., Masuda, Y., Garcia, G.A., McLellan, D.L., Engelmayr, G.C., Sacks, M.S., et al., 2005. From stem cells to viable autologous semilunar heart valve. Circulation 111, 2783–2791.

Swanson, J.A., Lee, M., Knapp, P.E., 1991. Cellular dimensions affecting the nucleocytoplasmic volume ratio. The Journal of Cell Biology 115, 941–948.

Teh, T.K., Toh, S.L., Goh, J.C., 2013. Aligned fibrous scaffolds for enhanced mechanoresponse and tenogenesis of mesenchymal stem cells. Tissue Engineering Part A 19, 1360–1372.

Thoumine, O., Cardoso, O., Meister, J.J., 1999. Changes in the mechanical properties of fibroblasts during spreading: a micromanipulation study. European Biophysics Journal 28, 222–234.

Thubrikar, M., Aouad, J., Nolan, S., 1986. Comparison of the in vivo and in vitro mechanical properties of aortic valve leaflets. The Journal of Thoracic and Cardiovascular Surgery 92, 29–36.

Trelstad, R.L., Birk, D.E., 1985. The fibroblast in morphogenesis and fibrosis: Cell topography and surface-related functions. Ciba Foundation Symposium 114, 4–19.

Trelstad, R.L., Hayashi, K., Gross, J., 1976. Collagen fibrillogenesis: intermediate aggregates and suprafibrillar order. Proceedings of the National Academy of Sciences 73, 4027–4031.

Van Lieshout, M., Vaz, C., Rutten, M., Peters, G., Baaijens, F., 2006. Electrospinning versus knitting: two scaffolds for tissue engineering of the aortic valve. Journal of Biomaterials Science, Polymer Edition 17, 77–89.

Vaz, C., Van Tuijl, S., Bouten, C., Baaijens, F., 2005. Design of scaffolds for blood vessel tissue engineering using a multi-layering electrospinning technique. Acta Biomaterialia 1, 575–582.

Venugopal, J., Low, S., Choon, A.T., Ramakrishna, S., 2008. Interaction of cells and nanofiber scaffolds in tissue engineering. Journal of Biomedical Material Research Part B: Applied Biomaterials 84, 34–48.

Vernerey, F.J., Farsad, M., 2011. A constrained mixture approach to mechano-sensing and force generation in contractile cells. Journal of the Mechanical Behavior of Biomedical Materials 4, 1683–1699.

Vesely, I., 1997. The role of elastin in aortic valve mechanics. Journal of Biomechanics 31, 115–123.

van Vlimmeren, M., Driessen-Mol, A., Oomens, C., Baaijens, F., 2012. Passive and active contributions to generated force and retraction in heart valve tissue engineering. Biomechanics and Modeling in Mechanobiology 11, 1015–27.

van Vlimmeren, M.A., Driessen-Mol, A., van den Broek, M., Bouten, C.V., Baaijens, F.P., 2010. Controlling matrix formation and cross-linking by

hypoxia in cardiovascular tissue engineering. Journal of Applied Physiology 109, 1483–1491.

van Vlimmeren, M.A., Driessen-Mol, A., Oomens, C.W., Baaijens, F.P., 2011. An in vitro model system to quantify stress generation, compaction, and retraction in engineered heart valve tissue. Tissue Engineering Part C: Methods 17, 983–991.

van Vlimmeren, M.A.A., 2011. The contribution of matrix and cells to leaflet retraction in heart valve tissue engineering. Ph.D. thesis. Eindhoven University of Technology.

Walters, B.D., Stegemann, J.P., 2013. Strategies for directing the structure and function of 3D collagen biomaterials across length scales. Acta Biomaterialia S1742-7061, 430–433.

Wang, H., Layton, B., Sastry, A., 2003a. Nerve collagens from diabetic and nondiabetic sprague–dawley and biobreeding rats: an atomic force microscopy study. Diabetes/Metabolism Research and Reviews 19, 288–298.

Wang, J., Chen, H., Seth, A., McCulloch, C.A., 2003b. Mechanical force regulation of myofibroblast differentiation in cardiac fibroblasts. American Journal of Physiology-Heart and Circulatory Physiology 285, H1871–H1881.

Wang, J.H., Grood, E.S., 2000. The strain magnitude and contact guidance determine orientation response of fibroblasts to cyclic substrate strains. Connective Tissue Research 41, 29–36.

Wang, J.H., Jia, F., Gilbert, T.W., Woo, S.L., 2003c. Cell orientation determines the alignment of cell-produced collagenous matrix. Journal of Biomechanics 36, 97–102.

Wang, Y.f., Guo, H.f., Ying, D.j., 2013. Multilayer scaffold of electrospun pla–pcl–collagen nanofibers as a dural substitute. Journal of Biomedical Materials Research Part B: Applied Biomaterials 101, 1359–1366.

Webster, M., Witkin, K.L., Cohen-Fix, O., 2009. Sizing up the nucleus: nuclear shape, size and nuclear-envelope assembly. Journal of Cell Science 122, 1477–1486.

Weidenhamer, N.K., Tranquillo, R.T., 2013. Influence of cyclic mechanical stretch and tissue constraints on cellular and collagen alignment in fibroblast-derived cell sheets. Tissue Engineering Part C: Methods 19, 386–395.

Wisse, E., Spiering, A., van Leeuwen, E., Renken, R., Dankers, P., Brouwer, L., van Luyn, M., Harmsen, M., Sommerdijk, N., Meijer, E., 2006. Molecular recognition in poly(epsilon-caprolactone)-based thermoplastic elastomers. Biomacromolecules 7, 3385–95.

Wyatt, K.E., Bourne, J.W., Torzilli, P.A., 2009. Deformation-dependent enzyme mechanokinetic cleavage of type i collagen. Journal of Biomechanical Engineering 131, 051004.

Yacoub, M.H., Takkenberg, J.J.M., 2005. Will heart valve tissue engineering change the world? Nature Clinical Practice Cardiovascular Medicine 2, 60–1.

Yeong, W.Y., Yu, H., Lim, K.P., Ng, K.L.G., Boey, Y.C.F., Subbu, V.S., Tan, L.P., 2010. Multiscale topological guidance for cell alignment via direct laser writing on biodegradable polymer. Tissue Engineering Part C: Methods 16, 1011–1021.

Zhong, S., Zhang, Y., Lim, C.T., 2011. Fabrication of large pores in electrospun nanofibrous scaffolds for cellular infiltration: a review. Tissue Engineering Part B: Reviews 18, 77–87.

Zilla, P., Brink, J., Human, P., Bezuidenhout, D., 2008. Prosthetic heart valves: catering for the few. Biomaterials 29, 385–406.

Acknowledgements

Time for writing these few lines has finally come. A lot of people have contributed to make these four years a unique experience, that has thaught me much, both from a professional and from a personal point of view.

Frank, your enthusiasm for science and breakthrough technologies for life science has been for me a source of inspiration during these years. Carlijn, your passion, sharp scientific observations, patience and attention for the details was crucial to achieve this booklet as a result. Cees, thank you for being always available to listen to my "modeling dilemmas", always encouraging me to keep up the good work and never give up.

I would like to thank Prof. Liesbet Geris, Prof. Keita Ito, Prof. Nico Verdonschot, Prof. Franz van de Vosse for the careful evaluation of my thesis and for taking part in my defence committee.

Special thanks goes to Chen-Ket, Marc, Agnese, Tina, Emanuela, Ginny, Sandra, Christine, Anthal, Samaneh, Arianna, Tommaso, Inge and all the other colleagues that every day worked with me and and thaught me about cells, computations and electrospinning with their experience and their enthusiasm for science. Even more important memories are all the nice lunch times, coffees, parties, beers and conferences we have shared during these years.

Thank you to all the people that have shared these years with me in the great office 4.13. I will miss alle praatjes in het Nederlands, the courses at the sportcentrum, (maybe) even the fights for the control of the heater.

One of the most important treasures I found in Eindhoven that made these four years very special are my international friends. Fanzy and papa Andrea the parties with you are always memorable, Ceylan you are one of the nicest and caring people I have met, Massimiliano and Sahel you are the cutest pic-nic company, Lusia and David you spoiled me with muffins and kindness. Luca, Elena, Mahdiar, Samuele, Elena, Lorenzo, Stephanie and Andrea party and dinners with you that always end up with playing guitar and singing till late are just the very best.

Thanks to my flatmates Davit, Vanessa, Francesca, Chiara...you made my time at home funny and pleasant with dinners, parties and a lot of chatter!

Although they are currently somewhere around Europe my BEST friends are just the most amazing company to travel around Europe, start the year in the best way and visit Napoli...we "Rock the Europe"!

Mamma e papà grazie per aver sempre appoggiato le mie scelte, pur a costo di avermi così lontana, di avermi fatto compagnia con il vostro sorriso e le vostre parole di incoraggiamento attraverso uno schermo nei momenti difficili. I vostri baci da lontano tutte le sere sono la mia linfa, vi voglio bene!

Francesca e Giacomo le nostre tradizionali settimane bianche sono state tra i momenti più divertenti e rilassanti di questi anni nonostante le cadute in snowboard!

Michele, ti devo davvero tanto perchè senza di te neanche una parola di questo libricino sarebbe mai esistita. Sei stato il mio sostegno sin dal giorno in cui mi hai incoraggiato a trasferirmi fin quassù e la mia paziente guida e miglior completamento in tutti i giorni successivi, nei momenti più divertenti, più pazzi e più difficili. Grazie per l'amore che mi dimostri ogni giorno, incoraggiandomi sempre a fare le scelte migliori per me. Abbiamo già scritto tante pagine, e ne abbiamo ancora da scrivere almeno trentamila altrettanto belle.

Hartelijk bedankt voor deze gezellige ervaring in Eindhoven!

Giulia

Curriculum vitae

Giulia was born in Potenza, Italy, on 24th May 1985. In 2003 she obtained her diploma at the Scientific High School "Galileo Galilei" in Potenza. She studied Biomedical Engineering at "Università degli Studi di Napoli Federico II", where she obtained her Bachelor degree in 2006 and her Master degree in 2008. She, thereafter, moved to Milan to work as research fellow. At Politecnico di Milano she developed first a surgical user interface for Computer Assisted Neurosurgery and later an algorithms for the reconstruction of the ventricular wall from imaging data. In these years she developed her passion for research in the biomedical field, aiming at improving the health conditions of patients with diseases. This enthusiasm made her move to Eindhoven, the Netherlands, in January 2010, to work at Eindhoven University of Technology in the Soft tissue and Biomechanics group at the Biomedical Engineering Department. Here she carried out her PhD under the supervision of Prof. Frank Baaijens, Prof. Carlijn Bouten and Dr. Cees Oomens that brought to the results illustrated in this thesis. The aim of her PhD project was to investigate the relation betweeen the microstructural architecture and the global mechanical properties of scaffolds for cardiovascular tissue engineering and engineered constructs, in order to improve their mechanical performance. Since March 2014 Giulia is working as Function Developer at Phlips.

List of publications

Argento G., Simonet M., Oomens C.W.J., Baaijens F.P.T., 2012. Multi-scale mechanical characterization of scaffolds for heart valve tissue engineering. Journal of Biomechanics 45(16), 2893–8.

Loerakker S., **Argento G.**, Oomens C. W.J., Baaijens F. P.T., 2013. Effects of valve geometry and tissue anisotropy on the radial stretch and coaptation area of tissue-engineered heart. Journal of Biomechanics 46(11), 1792-800.

I. van Loosdregt, **Argento G**, Driessen-Mol A., Oomens C.W.J., Baaijens F.P.T., 2013. Cell-mediated retraction versus hemodynamic loading - A delicate balance in tissue-engineered heart valves. Journal of Biomechanics doi: 10.1016/j.jbiomech.2013.10.049J

Argento G., de Jonge N., Söntjens S.H.M., Oomens C.W.J., Bouten C.V.C., Baaijens F.P.T.. Modeling the impact of scaffold architecture and mechanical loading on collagen turnover in engineered cardiovascular tissues. Submitted.

Argento G., Obbink-Huizer C., Fioretta E., Oomens C.W.J., Bouten C.V.C., Baaijens F.P.T.. Influence of substrate geometry on cell contact guidance. Submitted.